Catalytic Substrate Oxidations by Iron/Hydrogen Peroxide: Generation of High-valent Iron-oxo Intermediates by Proton-Induced O–O Bond Cleavage

A DISSERTATION
SUBMITTED TO THE FACULTY OF THE GRADUATE SCHOOL OF THE
UNIVERSITY OF MINNESOTA
BY

Partha Pratim Das

IN PARTIAL FULFILLMENT OF THE REQUIREMENTS
FOR THE DEGREE OF
DOCTOR OF PHILOSOPHY

Prof. Lawrence Que Jr., Advisor

August 2011

© Partha Pratim Das 2011

ACKNOWLEDGEMENTS

My stay at the University of Minnesota towards earning a PhD degree would not be possible without the help and support of some people. These people contributed one way or other and supported me professionally or personally to make this possible.

I want to thank first my advisor Prof. Lawrence Que Jr. for his support and direction throughout my time in his laboratory. I sincerely appreciate his training and efforts to make myself an independent scientist. The thing that I most enjoyed in his lab was the flexibility of the working hours. It was also great that I had the liberty to explore science beyond my regular projects. Larry was always supportive with the new experiments that I performed just out of curiosity. I also had the pleasure to take the course on 'Interpretation of Organic Spectroscopy' from him in my first semester. It was a great pleasure for me to work with one of the best chemical minds of the current time who taught me to design and perform experiments, interpret the data, think out of the box, see the big picture and ultimately tell a complete and compelling story to the audience or to the readers.

I also want to thank my committee members as well for their time and support. I have known all of them for almost five years if not more. I was extremely fortunate that I could take classes from almost all of them. Prof. Kent Mann's course on 'Physical Inorganic Chemistry' was one of the best courses I have taken in the University of Minnesota. Kent is an excellent teacher and I really enjoyed the discussions with him in the class. I also had the privilege to take the kinetics course from Prof. John Lipscomb. Besides the class, John was always available for discussion whenever I had trouble understanding kinetics or in need to discuss reaction mechanism. I also want to thank Prof. Bill Tolman for teaching the course on 'Bio-inorganic Chemistry'. This class was a great motivation for me and I was reassured that I really wanted to study bio-inorganic chemistry in my PhD.

I am also appreciative of my collaborator at the Tufts University, Prof. Elenea V. Rybak-Akimova and her graduate student Ms. Olga V. Makhlynets. I have been engaged with them for a long time and it was a great experience. I also want to thank Prof. Eckard Münck and his post-doc Dr. Sebastian A. Stoian at the Carnegie Mellon University for running Mössbauer experiments for my samples.

I am also thankful to the present and past members of the 'ever-evolving' Que group. I have been helped by almost all of them at one point or other during my stay in the group. I started my work in the group with a former post-doc Dr. Rubén Mas-Ballesté. Rubén was the person who taught me (a P. Chemist at that point) important lessons in synthetic inorganic chemistry and catalysis. It was also great pleasure to work with my collaborators in the group Drs. Katherine M. Van Heuvlen and Matthew A. Cranswick, who helped me with the resonance Raman. Kathy was also extremely supportive and one of the few persons that I could talk to even in the bad times. Dr. Gen-Qiang Xue helped me with scientific discussion and suggestions. Drs. Kallol Ray and Iweta Pryjomska-Ray were also very inspirational to me during their stay in the lab. Iweta was the person who taught me driving in Minnesota. My special thanks go to my colleagues at the catalysis lab Drs. Paul D. Oldenburg and Praneeth Vijayendran and Mr. Yan Feng for their help and support. Praneeth was my one-stop help for the organic synthesis and my companion in the numerous trips to Starbucks, Mesa-Pizza and other eateries. Yan was always available for help, especially when our GC and GC-MS were not very cooperative. I have always enjoyed my conversations with both Praneeth and Yan both on science and on life-style.

The staff at the Chemistry Department was also extremely helpful and supportive during my entire stay at the department. Both Mr. Chuck Tomlinson and Ms. Nancy Thao at the Chemistry graduate office helped me greatly in navigating through the graduate school. Messrs. Bruce Moe, Mike Casey, and Eric Schultz of the electronic shop will also be remembered for their kind help and support and counseling with the computers and software. Mss. Patti Combs and Suzanne McColley of the Chemistry accounting office

were also very patient and supportive with the purchasing and processing. Especially the kind help of Suzanne made this process painless and super smooth.

I have also been involved for almost four years or more with the Chemistry graduate student workshop committee (GSWC). It was a great experience to work with the other graduate students and more importantly to work for the grad students. This was a great place for me to meet and network with the fellow graduate students and to get the feeling "Hey! You are not alone". I want to thank all the people of GSWC that I have worked with who made this experience enjoyable.

The person who I owe a lot is Ms. Anusree Mukherjee, my best friend and also a colleague in the Que lab. It is simply impossible for me to reach at this point without her support, in rain or shine. We learned a lot (both Chemistry and other stuffs) from each other and often got amazed by the fact that two people with contrasting personalities could be so indispensable to each other.

Finally I want to thank my parents and family for their outright support to me throughout my graduate career. You are my eternal source of inspiration and ambition. It is your belief in me that helps me reach this point. I am fortunate and blessed to have both of you for the important lessons you taught me about honesty, integrity and hard work that make me who I am. I want to dedicate this thesis to you.

Abstract

Non-heme iron enzymes are responsible for various stereospecific hydroxylations under ambient conditions. Pterin-dependent hydroxylases hydroxylate the aromatic rings of aromatic amino acids while Rieske dioxygenases perform *cis*-dihydroxylation of aromatic double bonds. The most important step in the functioning of these enzymes is the cleavage of the O–O bond. The goal of this research is to investigate the reactivity of synthetic model complexes with H_2O_2 towards selective oxidative transformations.

Iron complexes with tetradentate ligands (TPA, BPMEN where TPA = tris(2-pyridylmethyl)amine and BPMEN = *N,N´*-bis(2-pyridylmethyl)-*N,N´*-dimethyl-1,2-diaminoethane)) are synthesized and tested in the acid-catalyzed oxidation reactions with H_2O_2 as the oxidant. The addition of aliphatic acids is found to increase the yield of both alkane and olefin oxidations. Interestingly, the use of benzoic acids, instead, leads to the hydroxylation of the aromatic ring, which is found to be in competition with olefin oxidation. Further investigation reveals FeTPA/H_2O_2-catalyzed regioselective *ortho*-(producing salicylates) and *ipso*-hydroxylation (producing phenolates) of benzoates. Detailed kinetic studies of these reactions – to get a better understanding of the reaction mechanism – show an acid-induced H/D kinetic isotope effect, suggesting the involvement of proton in the rate limiting O–O bond heterolysis of iron(III)-peroxos towards the formation of the high-valent Fe^{V}=O species (postulated as the active oxidant). The tuning of ligand (TPA and BPMEN) electronics, by introducing electron-donating substituents in the backbone, exerts a 'push-effect' and increases the rate of O–O bond cleavage and affords a higher yield of catalytic oxidation products.

Table of Contents

List of Tables

List of Figures

List of Schemes

Abbreviations

α-KG	α-ketoglutarate
TauD	Taurine/α-ketoglutarate dioxygenase
DAOCS	Deacetoxycephalosporin C synthase
NDO	Naphthalene dioxygenase
PheH	Phenylalanine hydroxylase
TyrH	Tyrosine hydroxylase
TrpH	Tryptophan hydroxylase
TPA	Tris(2-pyridylmethyl)amine
SR-TPA	Tris(4-methoxy-3,5-dimethylpyridyl-2-methyl)amine
EW-TPA	Tris-(5-methoxycarbonylpyridyl-2-methyl)amine
3-Me_3TPA	Tris(3-methylpyridyl-2-methyl)amine
5-Me_3TPA	Tris(5-methylpyridyl-2-methyl)amine
6-Me_2TPA	Bis(6-methylpyridyl-2-methyl)amine
6-Me_3TPA	Tris(6-methylpyridyl-2-methyl)amine
6-Ph-TPA	(6-Phenyl-2-pyridylmethyl)bis(2-pyridylmethyl)amine
BPMEN	*N,N*´-bis(2-pyridylmethyl)-*N,N*´-dimethyl-1,2-diaminoethane
SR-BPMEN	*N,N*´-bis(4-methoxy-3,5-dimethylpyridyl-2-methyl)-*N,N*´-dimethyl-1,2-diaminoethane
6-Me_2BPMEN	*N,N*´-bis(6-methylpyridyl-2-methyl)-*N,N*´-dimethyl-1,2-diaminoethane
N4Py	*N,N*-bis(2-pyridylmethyl)bis(2-pyridyl)methylamine)

TMC	1,4,8,11-Tetramethyl-1,4,8,11-tetraaza-cyclotetradecane
PCA	Pyrazine-2-carboxylate
Tp^{Ph2}	Hydrotris(3,5-diphenylpyrazol-1-yl)borate
BF	Benzoylformate
KIE	Kinetic isotope effect
TON	Turn over number
NIH	National Institutes of Health
TBHP	*tert*-butyl hydroperoxide
MPPH	2-methyl-1-phenyl-2-propyl hydroperoxide
*m*CPBA	*meta*-chloroperbenzoic acid
NMR	Nuclear magnetic resonance
ESI-MS	Electrospray ionization Mass spectrometry
EPR	Electron paramagnetic resonance
EXAFS	Extend X-ray absorption fine structure
GC	Gas chromatography
GC-MS	Gas chromatography mass spectrometry
ORTEP	Oak Ridge thermal ellipsoid plot
DFT	Density functional theory
PyO	Pyridine *N*-oxide
ToMOH	Toluene/*o*-xylene monooxygenase hydroxylase
MMOH	Methane monooxygenase hydroxylase

Chapter 1

Bio-mimetic Oxidation Catalysis by Non-heme Iron Complexes

1.1 Introduction

Dioxygen activation catalyzed by a variety of metalloenzymes is one of the most important chemical reactions in Nature.[1,2] Interestingly, the triplet ground state of O_2 – due to the presence of two unpaired electrons in the two degenerate highest occupied molecular orbitals – inhibits its spontaneous reaction with the spin-paired singlet state of organic substrates.[1,3,4] The low one-electron oxidation potential of O_2 also contributes to its sluggish kinetic reactivity.[5] On a positive note, this prevents the spontaneous combustion of the bio-molecules to carbon dioxide and water and helps sustain life on Earth. However, the question that has intrigued chemists and biochemists for the half century since the first demonstration of incorporation of O_2 into a biological molecule[6] is how O_2 can react at ambient temperature and pressure. Nature's response to this spin mismatch generally involves either a transition metal (*e.g.* iron or copper) or an organic co-factor (*e.g.* flavin or pterin) or both, as in the case of heme systems. It is also important to mention that in all biological oxidations O_2 is reductively activated, as the simple inversion of the electron spin to form singlet O_2 is highly endothermic.[4] Oxidases and oxygenases activate dioxygen from the triplet state to the reactive singlet or doublet (radical) species.

The activation of dioxygen at a transition metal center typically requires the availability of multiple metal oxidation states (as in iron and copper). A wide variety of mono- and

multinuclear iron and copper enzymes has been discovered that can carry out diverse biological transformations.[7] The iron-containing enzymes can be classified as heme- and non-heme, based on the active site structures. Heme-containing iron enzymes have been extensively studied, with cytochrome P450 as a prototypical example.[2,8] Non-heme iron enzymes, on the other hand, can be divided into two classes: mononuclear and dinuclear. Methane monooxygenase is perhaps the best example of the latter class that selectively oxidize the most difficult of hydrocarbon substrates *i.e.* methane to methanol.[9,10]

Mononuclear non-heme iron enzymes, on the other hand, can carry out a wide array of oxidation reactions including *cis*-dihydroxylation of C=C bonds and hydroxylation and halogenation of C–H bond.[3,11,12] Interestingly, these enzymes share a common motif in their active sites – the so-called 2-His-1-carboxylate facial triad (Figure 1.1).[13,14] This arrangement of ligands leaves at least two *cis* labile sites at the iron center available for the activation of O_2, a notion best illustrated by the crystal structure of the enzyme-substrate-O_2 adduct of naphthalene dioxygenase featuring a side-on bound dioxygen moiety (Figure 1.1).[15] *cis*-Dihydroxylation of carbon–carbon double bonds in Nature is carried out by Rieske dioxygenases, which convert arenes into *cis*-dihydrodiol derivatives in the first step of arene biodegradation by soil bacteria.[16,17] On the other hand, C–H bond hydroxylation is carried out by α-ketoglutarate (α-KG)-dependent iron enzymes[11] TauD,[18-24] prolyl-4-hydroxylase,[25,26] and AlkB.[27-29] Apart from hydroxylation, another subclass of the Fe/α-KG-dependent enzymes (halogenases, namely SyrB2 and CytC3) is

shown to catalyze the halogenation of C–H bonds.[30-33] Interestingly, the reported crystal structure of the enzyme SyrB2,[31] which catalyzes the chlorination of threonine in syringomycin E biosynthesis, demonstrates the replacement of the carboxylate ligand with a halide ion in the 2-His-1-carboxylate facial triad.[34] Halogenases have also been shown to perform bromination of the C–H bonds.[35] A high-valent iron-oxo species was proposed as the active oxidant in the Fe/α-KG-dependent enzymes.[18] Interestingly, a Fe^{IV}=O species is trapped and spectroscopically characterized for each of TauD[19] and its mutant,[36] prolyl-4-hydroxylase,[37] and CytC3.[33] Pterin-dependent hydroxylases constitute another class of non-heme iron enzymes[5,12,38-40] that activate dioxygen in the presence of a tetrahydrobiopterin co-factor and generate an iron(IV)-oxo intermediate[41] that hydroxylates the aromatic rings of their namesake amino acids. Phenylalanine hydroxylase (PheH)[42-44] catalyzes phenylalanine (Phe) catabolism in liver, while tryptophan-[45] and tyrosine hydroxylases[46] function in the central and peripheral nervous systems and catalyze the rate limiting formation of neurotransmitters like dopamine, epinephrine and norepinephrine.[12,38] The remarkable scope of oxidative transformations catalyzed by non-heme iron enzymes seems to be even broader than their heme counterparts.[3,8]

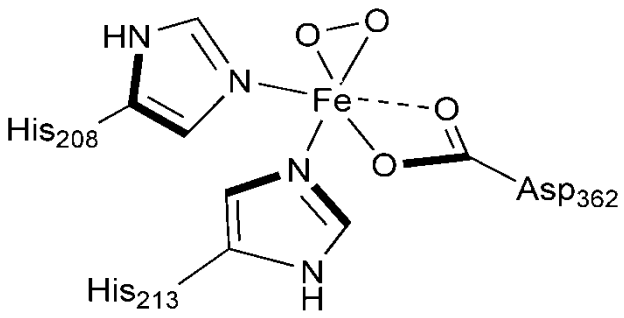

Figure 1.1: Structure of mononuclear iron active site of naphthalene dioxygenase containing 2-His-1-carboxylate facial triad with bound dioxygen (PDB 107N).

Inspired by Nature and with the goal of making efficient catalysts for industrial purposes, bio-inspired catalysts have been developed over the years to carry out similar transformations.[47] Moreover, the bio-inspired catalysts can have an edge over the metalloenzymes. For example, the synthetic catalysts could increase the scope of the substrates and could be used for scaling up the reactions or tuning the selectivity of the reactions performed.[48] Interestingly, iron complexes hold special promise for oxidative catalysis since iron is cheap, abundant and relatively non-toxic (compared to the second- or third-row transition metals) and it has access to multiple oxidation states.[49] Bio-inspired iron catalysts have been developed for the oxidation reactions with tridentate[50,51] and tetradentate[52-56] ligand sets that provide two *cis*-labile sites[47] (Figure 1.2) where the oxidants can be activated to carry out hydrocarbon oxidation. Hydrogen peroxide was chosen as the oxidant in this bio-inspired catalysis study, because it is abundant,

relatively cheap, and easy to handle and the byproduct is water. The accumulated data over the last few years point towards a common mechanistic landscape, where alkanes,[52,57] olefins,[50,51,53,55,58,59] and aromatics[60-62] are oxidized, often in competition with each other.[63]

1.2 Alkane Hydroxylation

Non-heme iron catalysts can carry out the hydroxylation of a C–H bond using a redox active iron center and using either peroxide (H_2O_2, *tert*-butyl hydroperoxide) or dioxygen as the oxidant.[64] In many cases, metal-based oxidants are proposed to be involved rather than hydroxyl radicals (like Fenton chemistry[65]) in the selective oxidative transformations catalyzed by non-heme iron complexes and H_2O_2.[64] Although it is often difficult in the catalytic systems to observe the actual oxidants that carry out the transformations, indirect probes (kinetic isotopic effect, regioselectivity, alcohol-to-ketone ratio, and substrate-based probes of radical lifetime) have been devised to understand the reaction mechanisms.[64] The kinetic isotope effect is essentially a competitive oxidation between protio- and deuteroalkanes based on the difference in the strengths of C–H and C–D bonds (~1.7 kcal mol^{-1}). In the case of oxidations by the highly reactive and therefore unselective oxidant HO•, a KIE value of 1-2 is observed.[66] On the contrary, metal-based oxidants are more selective and yield KIE values greater than the theoretical maximum of 7 in both enzymatic reactions[18,67,68] and model complexes.[69,70] The determination of regioselectivity (3°/2° ratio) in adamantane oxidation is another measure to check

whether the reaction is proceeding via a metal-based oxidant.[64] A high 3°/2° ratio of 15 or more usually suggests the involvement of a metal-based oxidant, while HO• typically yields a value of 2.[66,71,72] An alcohol-to-ketone (A/K) ratio is also another simple indicator used for distinguishing between metal-based oxidations and radical (HO•)-assisted pathways. When the alkyl radicals are generated in the course of oxidation of secondary alkanes (cyclohexane), O_2 is trapped in a diffusion-controlled rate to form an alkylperoxyl radical,[73] which results in a Russell-type termination step leading to the formation of equimolar amounts of alcohol and ketone.[74] In the case of metal-based oxidants, however, the generated alkyl radicals react with the metal center in a very fast 'oxygen rebound' step to generate the alcohol product, although some ketones could be formed due to the further oxidation of the alcohol product. Consequently higher A/K values were observed for metal-based oxidations.[64] Substrate-based radical probes are also available that can distinguish metal-based oxidations from radical-induced reactions. One type involves the *cis* isomer of 1,2-dimethylcyclohexane and decalin. The main competition in these two substrates is between epimerization of the putative tertiary alkyl radical and the subsequent C–O bond formation. Reactions that generate long-lived alkyl radicals afford both *cis* and *trans* alcohols with a *cis*-to-*trans* ratio of 1.2 in the oxidation of *cis*-1,2-dimethylcyclohexane.[72] In the case of metal-based oxidants, however, where the C–O bond formation or the so-called 'oxygen rebound' step is extremely fast, only that tertiary alcohol is formed whose original configuration is retained .[67,75]

Complexes **1** and **2** (Figure 1.2), non-heme iron catalysts based on the tetradentate pyridylamine ligands, were shown to oxidize alkanes to alcohols using H_2O_2 as an oxidant. C–H bonds as strong as 99 kcal mol^{-1} (in cyclohexane) have been activated by the oxidants generated with both **1**/H_2O_2 and **2**/H_2O_2.[52,57] A family of iron complexes of the synthetically modified TPA and BPMEN ligands has also been developed by a systematic introduction of the substituents at the various positions of the pyridine rings.[52] Depending on the positions of the substituents on the pyridine rings, two different classes of iron catalysts have emerged. One class has low-spin iron(II) centers (Class A), while the other has high-spin iron(II) centers (Class B). The Class A catalysts consist of the parent TPA and BPMEN ligands and their 5- and 3-substituted variants (Figure 1.3).[52,53] On the other hand, Class B catalysts involve the iron complexes of the ligands where at least two of the pyridine rings are substituted at the 6-positions. Class A catalysts differ from Class B catalysts with respect to the incorporation of O atom from water into cyclohexanol and the relatively shorter life time of the formed alkyl radical.[52]

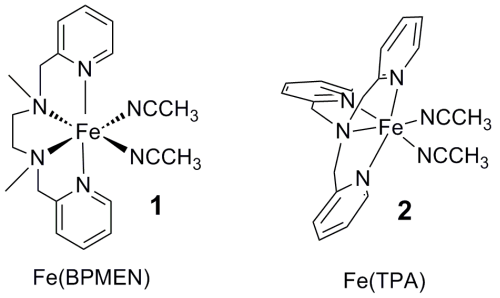

Figure 1.2: The flagship bio-mimetic non-heme iron complexes that carry out the oxidation of alkane, olefin and aromatics using H_2O_2 as oxidant.

In terms of C–H bond hydroxylation, **1** was shown to be more effective as a catalyst with over 60% conversion (based on oxidant), while **2** had half of the total conversion efficiency (including cyclohexanol and cyclohexanone).[57] Cyclohexanol accounted for >80% of the products in the oxidation of cyclohexane in both cases. The observed alcohol-to-ketone (A/K) ratios were unperturbed even under aerobic atmosphere, which suggested that C–H bond cleavage did not generate a long-lived alkyl radical susceptible to radical chain autoxidation. Furthermore, the results of the competitive experiments between cyclohexane and cyclohexane-d_{12} showed an intermolecular kinetic isotope effect (KIE) of 3.3-4.3 (Table 1.1), suggesting the involvement of a selective oxidant.[52] The observed 3°/2° ratio of 15-27 in the oxidation of tertiary and secondary C–H bonds of adamantane supported the involvement of a metal-based oxidant. The oxidants involved in these transformations were proposed to be high-valent iron-oxo species based on studies with isotopically labeled water and hydrogen peroxide, which showed a 20-40% incorporation of ^{18}O from water into the cyclohexanol product.[52] The O atom from water could be exchanged at the high-valent iron-oxo center leading to its incorporation into the alkane oxidation products (Scheme 1.1). The iron complexes of β-substituted TPA ligands (such as $[Fe^{II}(5\text{-}Me_3\text{-}TPA)]^{2+}$ and $[Fe^{II}(3\text{-}Me_3\text{-}TPA)]^{2+}$) also showed a similar reactivity feature as of **2**.

Class B catalysts, consisting of high-spin iron complexes of the α-substituted TPA ligands (**8**, **9**, **21**, and **22** in Figure 1.3), exhibited a different reactivity pattern from the parent TPA ligand or its β-substituted derivatives (Figure 1.3). The A/K ratio in the cyclohexane oxidation decreased significantly for the catalysts with more than one α-substituent. In the extreme case of **9**, almost equal amounts of alcohol and ketone products were observed (Table 1.1).[52] Moreover, O_2 had an important role in these oxidation reactions unlike in the case of Class A catalysts. When labeling studies were performed under $^{18}O_2$ atmosphere with the catalysts **8**, **9**, **21**, and **22**, an increased (25–80%) ^{18}O-incorporation into cyclohexanol were observed.[52] The difference in the reactivity pattern for the Class B catalysts from their low-spin counterparts was further demonstrated by the formation of the epimeric tertiary alcohol products in the oxidation of *cis*-1,2-dimethylcyclohexane. Interestingly, a linear correlation between the increasing amount of ^{18}O-incorporation from $^{18}O_2$ into the cyclohexanol and the loss of stereoselectivity in the oxidation of *cis*-1,2-dimethylcyclohexane could be drawn, which indicated that alkane oxidations by **8**, **9**, **21**, and **22** involved alkyl radicals of longer lifetime than those that might be produced in the case of **1**, **2**, and **4**.[52] However, KIE values of 3-4 in the hydroxylation of cyclohexane / cyclohexane-d_{12} and the high 3°/2° ratios of >15 in adamantane oxidation (Table 1.1) in the case of Class B catalysts were comparable to that of Class A. Therefore, it was concluded that rather selective metal-based oxidants were involved in the oxidation of C–H bonds by α-substituted Fe^{II}TPA catalysts.[52]

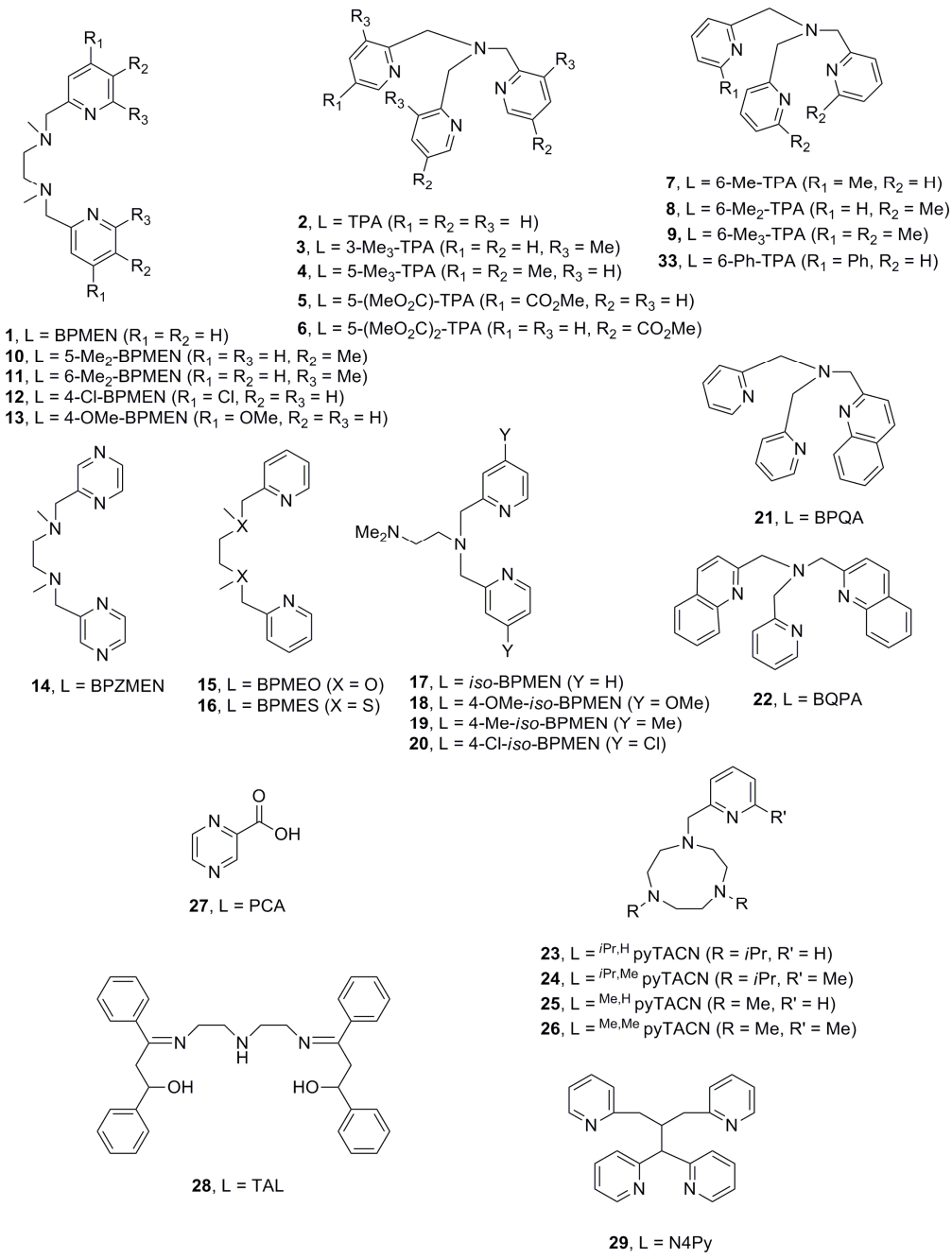

Figure 1.3: Ligands of iron complexes (represented by the numbers) used for the hydroxylation, desaturation, and halogenation of alkanes using H_2O_2 or O_2 as the oxidant.

Scheme 1.1: Proposed mechanism of alkane and olefin oxidations catalyzed by Class A and Class B catalysts using H_2O_2 as an oxidant

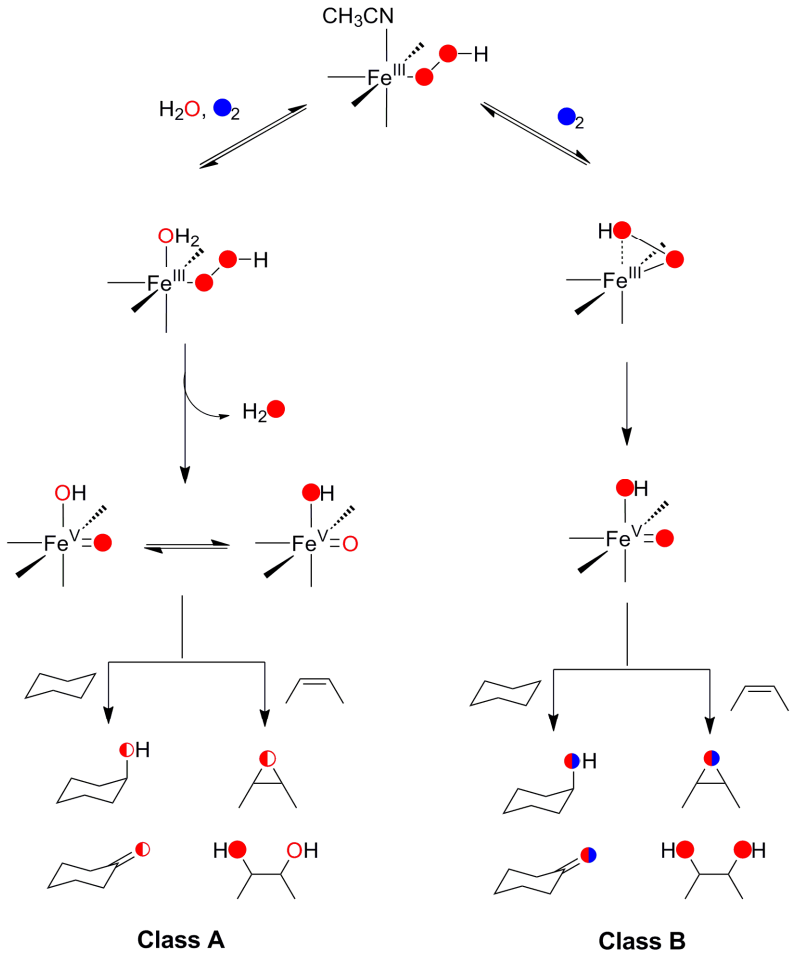

In subsequent years, other research groups have also explored the area of alkane oxidation by non-heme iron complexes. Most notable was the work of Costas and coworkers, where they used iron complexes of methylpyridine derivatized triazacyclononane (**23** – **26** in Figure 1.3) with H_2O_2 as the oxidant to effect the oxidation of cyclohexane.[56] A 60-70% conversion to the cyclohexanol product was observed with a high A/K ratio of 10-12 (Table 1.1). These complexes also showed a high degree (>90%) of retention of configuration in the case of *cis*-1,2-dimethylcyclohexane oxidation and a high-value of 3°/2° ratio in adamantane oxidation. These observations together with the ^{18}O-incorporation from water into cyclohexanol suggested the involvement of the high-valent iron-oxo species in this selective transformation.

Britovsek and co-workers also explored the reactivity of the iron complexes with a modified BPMEN ligand framework (**14** – **20** in Figure 1.3) towards cyclohexane oxidation (Table 1.1).[76] However, the introduction of the substituents at the pyridine rings of the BPMEN or the replacement of the pyridines with pyrazines did not improve the conversion of cyclohexane to the products. The replacement of the amine nitrogens in the BPMEN framework with either O or S atoms led to the iron complexes prone to ligand displacement and catalyst decomposition. The S-containing ligand, in fact, was more prone to the oxidation to form sulfoxides. Changing the orientation of the ethylenediamine backbone of BPMEN (*iso*-BPMEN) also reduced the yield of the oxidation products. Interestingly a control experiment reported in this study with

$[Fe(OTf)_2(CH_3CN)_2]/H_2O_2$ showed a very poor conversion (4% based on added oxidant) in the cyclohexane oxidation and a low A/K ratio of 1.6, which further pointed out the importance of bio-mimetic *N*-based ligand frameworks to effect the catalytic C–H bond oxidation of alkanes.

Studies from other groups utilizing the iron complexes of simple ligands (pyrazine-2-carboxylate, PCA) also catalyze the oxidation of cyclohexane to cyclohexanol (31% yield) with an A/K value of 2.4.[77] It was also shown that the (μ-oxo)diiron(III) complex of PCA catalyzed the oxidation of aliphatic (cyclohexane, cyclooctane, adamantane) and aromatic alkanes (toluene, ethylbenzene, and cumene) with a 20-50% yield. $[Fe^{II}(PCA)_2(solvent)_2]$ was proposed as the active species in solution in these reactions.[77] Studies involving iron(III) complex (**28** in Figure 1.3) of the trianionic ligand TAL (where, TAL = 3-(2-(2-(3-hydroxy-1,3-diphenyl-allylideneamino)-ethylamino)-ethylimino)-1,3-diphenyl-propen-1-ol) also showed to effect the oxidation of cyclohexane in a homogenous solution.[78]

Table 1.1: Catalytic oxidation of cyclohexane using non-heme iron complexes and H_2O_2

Catalyst	Ligand	Time (hr)	Efficiency (%)[a]	A/K[b]	KIE[c]	3°/2°[d]	RC *cis* (%)[e]	RC *trans* (%)[e]	Ref
1	BPMEN	0.5	63	8	3.2	15	100	100	52,57
2	TPA	0.5	32	5	4.3	17	100	100	52,79
3	3-Me_3-TPA	0.5	45	14	3.7	27	100	-	52
4	5-Me_3-TPA	0.5	40	9	3.8	21	96	-	52
5	5-(MeOOC)-TPA	0.5	40	5	-	-	100	-	52
6	5-$(MeOOC)_2$-TPA	0.5	23	19	3.7	15	100	-	52
7	6-Me-TPA	0.5	40	7	3.6	30	85	-	52
8	6-Me_2-TPA	0.5	29	2	4	33	64	-	52
9	6-Me_3-TPA	0.5	14	1	3.3	15	54	-	52
12	4-Cl-BPMEN	-	53	7.1	-	-	-	-	76
13	4-OMe-BPMEN	-	53	11	-	-	-	-	76
14	BPZMEN	-	38	2.3	-	-	-	-	76
17	iso-BPMEN	-	32	6.8	-	-	-	-	80
18	4-OMe-iso-BPMEN	-	28	4.7	-	-	-	-	76
19	4-Me-iso-BPMEN	-	34	6.6	-	-	-	-	76
20	4-Cl-iso-BPMEN	-	16	3.3	-	-	-	-	76
21	BPQA	0.5	58	10	3.4	30	89	-	52
22	BQPA	0.5	17	2	3.5	27	74	-	52
23	^{iPr,H}PyTACN	0.5	24	3.6	4.8	14	86	-	56
24	^{iPr,Me}PyTACN	0.5	8	2.7	-	21	78	-	56
25	^{Me,H}PyTACN	0.5	65	12.3	4.3	30	93	-	56
26	^{Me,Me}PyTACN	0.5	76	10.2	3.4	20	94	-	56
27	PCA	3	23	1.7		-	-	-	77
28	TAL	-	6	1.8	-	-	-	-	78
29	N4Py	0.5	31	1.4	1.5	3.3	27	16	81
30	TPA	0.5	43	5	-	-	-	-	52
Fe^{III}(Por)	Porphyrin	-	5 - 15	13	-	-	96	78	82-85
$Fe(OTf)_2$	-	-	3.8	1.6	-	-	-	-	76
HO•	-	-	-	~1	1 - 2	2	9	8	65,66,71,72

a Efficiency (%) = (cyclohexanol + cyclohexanone)/H_2O_2 × 100 in the oxidation of cyclohexane.
b A/K = Ratio of cyclohexanol to cyclohexanone in the oxidation of cyclohexane.
c KIE = Kinetic isotope effect in the oxidation of cyclohexane and cyclohexane-d_{12}.
d 3°/2°= 1-adamantanol/(2-adamantanol + 2-adamantaone) × 3in the oxidation of adamantine. The ratio is multiplied by 3 in order to normalize with respect to number of tertiary carbons.
e RC (%) = Retention of configuration in the oxidation of *tert*-C–H bonds of *cis*- or *trans*-1,2-dimethylcyclohexane, expressed as the ratio of alcohols: (*cis-trans)*/(*cis*+*trans*) for RC(*cis*) and (*trans-cis)*/(*cis*+*trans*) for RC(*trans*).
30 = $[Fe^{III}_2(O)(TPA)_2(H_2O)_2]^{4+}$.

1.3 Olefin Oxidation

Complexes **1** and **2** are among the first reported non-heme iron complexes to carry out olefin *cis*-dihydroxylation along with epoxidation using H_2O_2 as an oxidant.[53,58] In the case of oxidation of *cis*-cyclooctene, **1** was more selective towards epoxidation, while **2** formed almost equal amounts of epoxide and *cis*-diol. In both cases, about 70-80% of the oxidant used was converted to the products (Table 1.2). Despite differences in the ligand architecture in **1** and **2**, two features were common: both contained tetradentate N4 coordination and possessed two *cis* labile sites. The importance of the two available *cis* sites in both **1** and **2** was demonstrated by the lack of activity of the iron complex of the pentadentate N4Py ligand (possessing only one open co-ordination site) towards olefin oxidation (Table 1.2).[58]

The mentioned two different classes of iron catalysts – differentiated based on the spin states of the iron centers – also differed in their reactivity towards olefin oxidation.[53-55] A section of the low-spin complexes (Class A) were selective towards epoxidation, while the high-spin complexes (Class B) predominantly catalyzed the formation of *cis*-diol.[53,54] The different reactivity pattern of the Class B catalysts (**8**, **9**, and **11**) towards olefin oxidation – as pointed out by the observed *cis*-diol-to-epoxide ratio – was more prominent in the BPMEN series of complexes than the TPA series. Addition of two methyl groups at the 6-positions of the pyridine rings of the BPMEN ligand (**11**) led to

the 32-fold change in the selectivity of the oxidation from epoxidation to *cis*-dihydroxylation (Table 1.2).

Similar to the alkane oxidation studies, ^{18}O labeling experiments were again proved to be crucial in identifying the reaction mechanisms involved. The observations of incorporation of O atom from water into the epoxide and *cis*-diol products for the Class A-assisted oxidations suggested that both olefins and alkanes were oxidized in a similar mechanistic pathway (left side in Scheme 1.1).[53] The identification of a well-characterized $[Fe^{III}(TPA)(OOH)]^{2+}$ intermediate[79,86] and the indication of the involvement of a high-valent iron-oxo species (as evidenced by the O atom exchange with water) put the water-assisted mechanism on a firmer ground. Interestingly, the ^{18}O-labeling results (experiments performed with both $H_2{}^{18}O_2$ and $H_2{}^{18}O$) of the Class B catalysts (**8** and **9**) demonstrated near quantitative incorporation of the ^{18}O atom from $H_2{}^{18}O_2$ into the *cis*-diol, while no ^{18}O from $H_2{}^{18}O$ was incorporated into the epoxide. These results suggested that water was not involved in the reaction pathway of the high-spin iron catalysts and thus the left branch of mechanism in Scheme 1.1 was discarded. It was proposed that a high-spin Fe^{III}-OOH intermediate was generated in the case of Class B catalysts, which could directly attack or could undergo a rearrangement to yield a high-valent oxo-iron oxidant that carried out the olefin oxidation (right side in Scheme 1.1).[53]

Interestingly it was also shown that for Class A complexes (**1** and **2**) the addition of acetic acid could perturb the relative ratio of formed epoxide and *cis*-diol. In the case of oxidation of *cis*-cyclooctene, as much as 99% of the added oxidant was converted to the epoxide product using a 0.5 mol% **1** or **2** and H_2O_2 in a 1/2 acetonitrile/acetic acid solvent mixture at 0 °C.[59] It was proposed that in the presence of acetic acid the oxidant was converted to $Fe^{V}(O)(OAc)$ from $Fe^{V}(O)(OH)$. The formed $Fe^{V}(O)(OAc)$ could either epoxidize olefin or undergo self-decay towards the formation of Fe^{IV}=O and AcO•. This competitive nature of the decay pathways of the $Fe^{V}(O)(OAc)$ species was demonstrated by the use of varying concentrations of added *cis*-cyclooctene in the presence of phenylacetic acid. When the concentration of the olefin was decreased, the reaction predominantly followed the self-decomposition pathway leading to the formation of $PhCH_2CO_2$•, which upon decarboxylation followed by the oxidation in air produced benzaldehyde. However, an increase in the concentration of *cis*-cyclooctene resulted in the enhancement of epoxide yield with a concomitant decrease in benzaldehyde formation.[59]

Table 1.2: Catalytic oxidation of *cis*-cyclooctene using non-heme iron complexes and H_2O_2[53]

Catalyst	Ligand	*cis*-Diol	Epoxide	*cis*-Diol:Epoxide	Conversion (%)
1	BPMEN	0.9	7.5	1:8	84
2	TPA	4	3.4	1.2:1	74
10	5-Me_2-BPMEN	1.3	7.8	1:6	91
11	6-Me_2-BPMEN	6.2	1.5	4:1	79
4	5-Me_3-TPA	3.9	2.8	1.4:1	67
7	6-Me-TPA	2.8	2.1	1.3:1	49
8	6-Me_2-TPA	5.5	1.1	5:1	66
9	6-Me_3-TPA	4.9	0.7	7:1	56
29	N4Py	0	0.6		6
30	TPA	4.1	4	1:1	81

Further investigations with a pair-wise competitive oxidation of olefins suggested that Class A catalysts preferentially oxidized electron donating olefins (e.g. *cis*-cyclooctene), while Class B ones preferred electron withdrawing ones (e.g. dimethyl fumarate).[63] The different substrate preferences of Class A and Class B catalytic systems reflected the electrophilic and nucleophilic nature of the oxidants, respectively, and bolstered our proposed reaction mechanisms.

1.4 Aromatic Hydroxylation

Hydroxylation of aromatic rings was also effected by the non-heme iron complexes using H_2O_2 or perbenzoic acids as the oxidant.[60,61] In some cases, the hydroxylation was intramolecular – where an aromatic ring on the ligand backbone was hydroxylated.[61] There were also examples of intermolecular aromatic hydroxylation, where an external aromatic substrate was hydroxylated by an iron complex and the oxidant.[62] These reactions are the first functional mimics of the pterin-dependent hydroxylases[12] using non-heme iron complexes.

1.4.1 Intramolecular Aromatic Hydroxylation

The non-heme iron complex, $[Fe^{II}(6\text{-Ph-TPA})]^{2+}$, was shown to be hydroxylated at the pendant phenyl ring of the ligand with *tert*-butyl hydroperoxide as the oxidant (Scheme 1.2).[87,88] Upon lowering the reaction temperature to -40 °C, a transient intermediate (λ_{max} = 650 nm, ε = 1300 M^{-1} cm^{-1}) was detected that was confirmed to be the $[Fe^{III}(6\text{-Ph-TPA})(OO^tBu)]^{2+}$ species by comparing its resonance Raman spectra to the spectra of the reported iron(III)-alkylperoxo species in the literature.[89-92] The nature of the cleavage of the O–O bond of this intermediate was studied using 2-methyl-1-phenylprop-2-yl hydroperoxide (MPPH) as a probe-oxidant, which gives different products depending on whether the O–O bond undergoes homolysis or heterolysis (Scheme 1.3). The observation of the formation of benzyl alcohol, 1,2-diphenylethane (under N_2) and

benzaldehyde (in air) as byproducts further pointed to the homolytic nature of the cleavage of the O–O bond. These observations led authors to propose the generation of an iron(IV)-oxo species as the active oxidant that could attack the phenyl ring via an aromatic electrophilic substitution. Interestingly, when the *ortho*-position of the phenyl ring was selectively labeled with a deuterium no net isotope effect was observed, however, 46% of the deuterium was found at the adjacent position, indicating a significant 1,2-deuterium shift ('NIH' shift). Similar 'NIH' shifts were observed before in the enzymatic hydroxylations.[93,94]

Scheme 1.2: Intramolecular aromatic hydroxylation at the ligand phenyl ring of [Fe(6-Ph-TPA)]$^{2+}$ with *tert*-butyl hydroperoxide as the oxidant

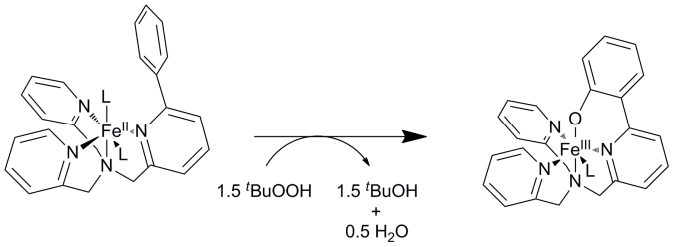

Scheme 1.3: Modes of O–O bond cleavage and possible outcome of products in the reaction of a non-heme iron center and MPPH

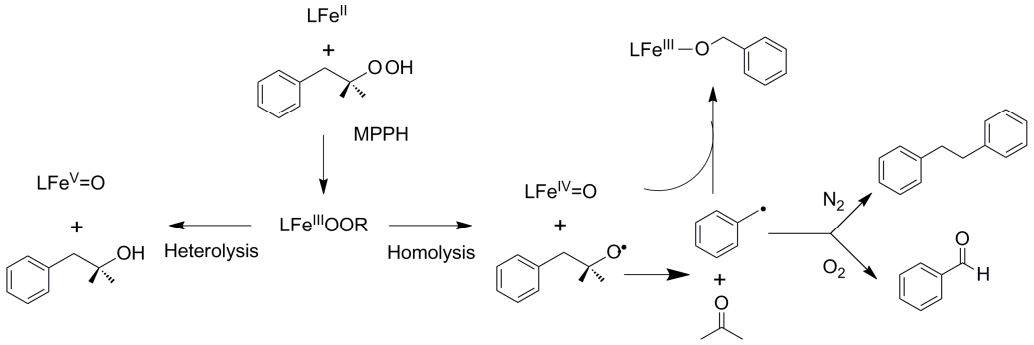

Ménage and co-workers also reported the hydroxylation at the aromatic ring of the ligand in the case of $Fe^{II}LCl_2$ (where, L = *N*,*N*′-bis(pyridin-2-ylmethyl)-*N*,*N*′-bis(3,4,5-trimethoxybenzyl)ethane-1,2-diamine) using H_2O_2 as an oxidant.[95] The addition of two equivalents of H_2O_2 to the acetonitrile solution of $Fe^{II}LCl_2$ led to the formation of a blue chromophore (λ_{max} = 740 nm), assigned as a phenolate-to-iron(III) charge-transfer transition. The extraction of the oxidized ligand and its analysis with ^{1}H-NMR suggested that one of the positions adjacent to the methoxy groups in one of the arene rings was hydroxylated. The ESI-MS results also suggested the incorporation of one O atom into the product. In fact, labeling studies with $H_2{}^{18}O_2$ demonstrated that the oxygen atom incorporated into the arene ring derived exclusively from the oxidant. Interestingly, control experiments with $H_2{}^{18}O_2$ in the presence of $H_2{}^{16}O$ did not perturb the yields of the ^{18}O-incorporated products.

Intramolecular ligand hydroxylation was also observed with iron(II) α-ketocarboxylate (pyruvate, benzoylformate) complexes of the sterically hindered face capping ligand Tp^{Ph2} (where, Tp^{Ph2} = hydrotris(3,5-diphenylpyrazol-1-yl)borate) upon activation of dixoxygen.[96] The hydroxylation of the aromatic ring was monitored by using UV-vis spectroscopy and the hydroxylated complex was characterized by X-ray crystallography. Analysis of the hydroxylated product of the reaction between $[Fe^{II}(Tp^{Ph2})(BF)]$ (where BF = benzoylformate) and $^{18}O_2$, by both ESI-MS and resonance Raman spectroscopy indicated ^{18}O-incorporation into the phenolate product. Further analysis of the benzoate generated from the decarboxylation of the bound benzoylformate showed approximately 80% incorporation of oxygen from $^{18}O_2$ (Scheme 1.4). The Hammett correlation on the rate of formation of iron(III)-phenolate species with substituents on the benzoylformate ligand showed a ρ value of +1.3 indicating a nucleophilic mechanism.[96] It was proposed that the binding of O_2 to the iron(II) center generated a putative iron(III)-superoxide species, which nucleophilically attacked the ketocarboxylate moiety. The subsequent decarboxylation of the formed adduct yielded the high-valent iron-oxo species that finally attacked the aromatic ring.

Scheme 1.4: Ligand self-hydroxylation of $[Fe^{II}(Tp^{Ph2})(BF)]$ with O_2

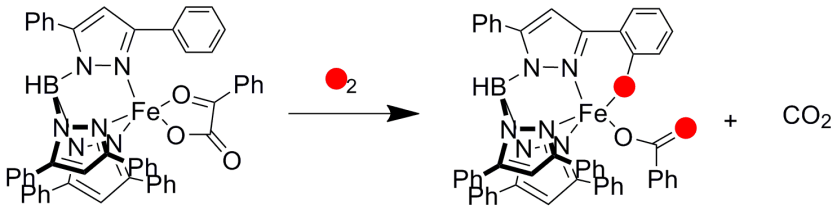

1.4.2 Intermolecular Aromatic Hydroxylation

Recently, it was reported that complex **1**, with H_2O_2 as the oxidant, could activate the aromatic rings of benzene as well as substituted benzenes producing phenols in the presence of large excess of substrate (300 equiv of benzene compared to **1**).[62] An intermediate, $[Fe^{III}(BPMEN)(OOH)]^{2+}$ was also observed in stopped flow kinetic studies. However, $[Fe^{III}(BPMEN)(OOH)]^{2+}$ was not the active oxidant, but rather decayed in a proposed rate limiting O–O bond cleavage step to generate a transient Fe^{V}=O species. The addition of acetic acid facilitated the formation of the Fe^{V}=O species, presumably by protonating the distal O atom of the hydroperoxo species. Acid-induced O–O bond heterolysis was further demonstrated by using MPPH and acetic acid. The identification of 2-methyl-1-phenyl-2-propanol, instead of benzaldehyde, supported a heterolytic O–O bond cleavage (Scheme 1.3).

Apart from the added substrates, the external oxidants containing the aromatic rings were also shown to be attacked by the non-heme iron-based oxidants to generate the hydroxylated aromatic products. Complex **2** was reported to effect the *ortho*-hydroxylation of added *m*CPBA (*meta*-chloroperbenzoic acid, used as an oxidant), leading to the formation of iron(III)-chloro-salicylates (Scheme 1.5).[61] Interestingly, the addition of *m*CPBA to **2** at -40 °C led to the formation of the $[Fe^{IV}(TPA)(O)]^{2+}$ (λ_{max} = 720 nm) that was subsequently converted to the $[Fe^{III}(TPA)(Cl\text{-salicylate})]^{+}$ product (λ_{max} = 560 nm). The observation of no aromatic hydroxylation upon addition of *meta*-chlorobenzoic acid to the $[Fe^{IV}(TPA)(O)]^{2+}$ species ruled out the involvement of the latter as the active oxidant. The authors, however, proposed the iron(V)-oxo species, generated from the reactions between the $[Fe^{IV}(TPA)(O)]^{2+}$ species and the peracids, as the active oxidant.[61]

Scheme 1.5: 2-catalyzed self-hydroxylation at the phenyl ring of *m*CPBA towards the formation of $[Fe^{III}(TPA)(Cl\text{-salicylate})]^{+}$ complex

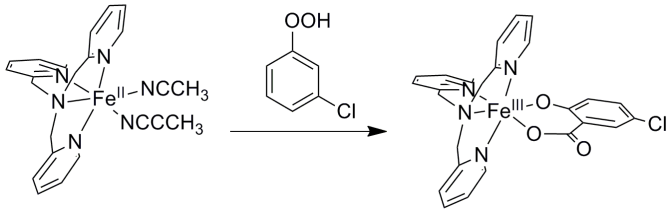

1.5 Scope and Aims of the Thesis

The principal goal of this thesis is to understand in detail the mechanistic landscapes of **1**- and **2**-catalyzed oxidative transformations using H_2O_2 as an oxidant through a combination of spectroscopic, kinetic and catalysis studies. The ultimately goal of this study is to design more effective catalysts by utilizing the knowledge garnered.

In the first part of the thesis we describe the observed new reactivity of **2** towards the oxidation of benzoic acids using H_2O_2 as an oxidant. Chapter 2 describes the regioselective *ortho*- and *ipso*-hydroxylation of benzoic acids, revealing that a metal-based oxo species is involved in these selective transformations. Chapter 3 presents the observation that *ipso*-hydroxylation with **2**/H_2O_2 can in fact be catalytic and competes with olefin oxidation. The detailed mechanistic study suggests the involvement of two separate channels of reaction, in equilibrium with each other, which are governed by the relative amounts of acid and water present in the medium.

The second part of the thesis involves detailed investigations on the kinetics of the observed oxidative transformations catalyzed by **2**/H_2O_2. Chapter 4 describes the kinetic studies of *ipso*-hydroxylation and olefin oxidation, which suggest that the O–O bond cleavage of the iron(III)-hydroperoxo species is a common rate limiting step in these oxidative transformations. The O–O bond is cleaved heterolytically by protonation, either by the added acid and/or water, at the distal O atom of the hydroperoxo intermediate.

Chapter 5 of this thesis describes a 'push-pull' effect in the cleavage of the O–O bond of the non-heme iron peroxo species, observed for the first time in a single model complex. This chapter describes synthetic modifications of the TPA and BPMEN ligands and the effects of introducing electron donating substituents on the pyridine rings in increasing the yields of alkane, olefin, and aromatic oxidations. This chapter also highlights the beneficial effects of acids in the enhancement of the 1-octene and cyclohexane oxidation yields.

Combined together this thesis is a dossier of the oxidative catalytic reactivity of the bio-inspired non-heme iron complexes and a detailed understanding of the reaction landscape underneath. This thesis also reflects our understanding of the mode of cleavage of the O–O bond in various oxidative transformations and provides the means of differentiating homo- and heterolytic O–O bond cleavage.

Chapter 2

Regioselective *ortho*- and *ipso*-Hydroxylation of Benzoates by Fe(TPA) and H_2O_2

This chapter is published in part as: Olga V. Makhlynets, Parthapratim Das, Sonia Taktak, Margaret Flook, Rubén Mas-Ballesté, Elena V. Rybak-Akimova, and Lawrence Que, Jr. "Iron-Promoted *ortho*- and/or *ipso*-Hydroxylation of Benzoic Acids with H_2O_2" *Chem.—Eur. J.* **2009**, *15*, 13171-13180

Portions reproduced from *Chem.—Eur. J.* **2009**, *15*, 13171-13180 with kind permission from Wiley-VCH

Copyright © 2009 WILEY-VCH Verlag GmbH & Co. KGaA, Weinheim

2.1 Introduction

In nature, aromatic hydroxylations are catalyzed by mononuclear non-heme iron centers in pterin-dependent aromatic amino acid hydroxylases,[1,3,97-99] and non-heme diiron centers in bacterial multicomponent monooxygenases (BMMs) such as methane and toluene monooxygenases.[100-103] In both families of the enzymes, highly regioselective hydroxylations are accomplished by properly orienting the aromatic rings with respect to the metal active sites in the enzyme pockets. Strong evidence has been obtained for the involvement of high-valent iron-oxo species[41,104,105] that carry out electrophilic attack of the target aromatic rings.[106-108] Despite significant recent progress in understanding the mechanisms of enzymatic aromatic hydroxylations, a detailed mechanistic picture has yet to be developed for these reactions.

Synthetically, aromatic hydroxylations involving cheap, environmentally friendly catalysts and oxidants (such as iron compounds and hydrogen peroxide) are very attractive for the late-stage oxidative derivatization and for metabolite preparation. Iron-catalyzed arene hydroxylations have been reported with Fenton's reagent (Fe salt/H_2O_2) and related systems.[109-111] Most of these reactions generate hydroxyl radicals,[112-114] but metal-based oxidants were also proposed in some cases.[115-120] While these reactions are undoubtedly useful, they are often non-selective, yielding isomers of aromatic hydroxylation compounds as well as products of side chain oxidation.

Recently, efficient and selective intramolecular aromatic hydroxylations were reported with mononuclear[88,96] or dinuclear[121-125] iron complexes where the aromatic ring is forced into close proximity of the iron center by a covalent linkage to the supporting polydentate ligand. The need to independently prepare the compounds containing both reactive iron center and the aromatic substrate, however, limits the applicability of these systems. Finding new selective intermolecular aromatic hydroxylation reactions remains an important challenge.

Orienting aromatic rings in close proximity to the metal center can be accomplished by coordinating aromatic substrates, via an anchoring group, to a vacant or labile site at the redox-active iron complex with a polydentate ligand. In one example of this strategy, phenols pre-bound to the iron center were hydroxylated selectively into the corresponding catecholato complexes.[126] We and others recently communicated additional examples of selective inner-sphere aromatic hydroxylation at non-heme iron centers: *ortho*-hydroxylation of benzoic acid with hydrogen peroxide promoted by $[Fe(BPMEN)]^{2+}$ [60] and self-hydroxylation of perbenzoic acids promoted by $[Fe(TPA)]^{2+}$ (**1**)[61] (see Figure 2.1). Both complexes contain aminopyridine ligands and are known to catalyze a number of oxidation reactions by activating H_2O_2,[12,48,127,128] including olefin epoxidation[53,59,129] or *cis*-dihydroxylation and alkane hydroxylation.[52,57] A recent detailed comparative study of FeBPMEN and FeTPA in olefin epoxidation with H_2O_2 in the presence of acetic acid[59] provided important mechanistic information on the role of various iron-oxygen intermediates, supporting carboxylic acid-assisted heterolytic O-O

bond cleavage as the key step in generating a proposed Fe(V) oxidant. Although FeBPMEN and FeTPA share common reaction pathways in olefin epoxidation, FeBPMEN is the more active catalyst. However, only limited characterization is available for the rather short-lived intermediates derived from FeBPMEN,[130,131] while the intermediates associated with **1** are longer lived and better characterized spectroscopically. These include $Fe^{III}(OOH)$,[79,86,132] $Fe^{III}(OOR)$,[88,89,133] and Fe^{IV}=O species.[134]

In this chapter, the reactivities of non-heme iron complex **1** are discussed in the carboxylate-directed regioselective hydroxylation of various substituted benzoic acids. Both complexes promote efficient *ortho*-hydroxylation of substituted benzoic acids with H_2O_2 to generate salicylate products. Furthermore, a new reaction pathway has been found wherein the benzoic acid is hydroxylated at the *ipso* position with concomitant decarboxylation. A mechanistic scheme is proposed that invokes a common oxidant despite the divergent outcomes.

2.2 Experimental section

2.2.1 Materials and Methods

All chemicals and solvents were purchased from Aldrich, Acros Organics or Fisher Scientific and were used without additional purification unless otherwise noted. CH_3CN solvent was dried over CaH_2 before use. $H_2{}^{18}O_2$ (90% ^{18}O-enriched, 2% solutions in

$H_2{}^{16}O$) was obtained from Cambridge Isotope Laboratories Inc. (Andover, MA). Complex $[Fe(TPA)(CH_3CN)_2(OTf)_2]$ (**1**) was prepared in an anaerobic glove box according to the published procedures.[134] UV-vis spectra were acquired on a Hewlett-Packard (Agilent) 8452 diode array spectrophotometer over a 190-1100 nm range. In some experiments, quartz cuvettes were cooled to the desired temperature in a liquid nitrogen cryostat by Unisoku Co. Ltd. (Osaka, Japan). ESI-MS spectra were obtained on a Bruker Biotof-II mass spectrometer under conditions of a spray chamber voltage of 4000 Volt and a dry gas temperature of 200 °C. GCMS experiments were carried out using an HP 6890 gas chromatograph (HP-5 column, 30m) with an Agilent 5973 mass detector. NMR spectra were recorded on a Varian Unity 500 spectrometer at ambient temperature. Chemical shifts (ppm) were reference to the residual protic solvent peaks. X-band EPR spectra were obtained at 2 K on a Bruker E-500 spectrometer equipped with an Oxford ESR-10 liquid-helium cryostat.

2.2.2 Reaction Conditions for Aromatic Hydroxylations

ortho and *ipso*-Hydroxylation of various aromatic acids in the presence of **1** were performed by mixing the iron complex (0.5 mM – 1 mM) with 2 equiv acid in acetonitrile in a glove box and then adding 3 equiv of hydrogen peroxide at room temperature. Spectroscopic experiments with $[Fe(TPA)(CH_3CN)_2(OTf)_2]$ were performed using a 1 mM solution in CH_3CN in a 1 cm quartz cuvette precooled at -40 °C. A total of 87 μL of 0.07 M H_2O_2 (3 equiv) was added to a solution containing the iron complex and excess amount (12 equiv) of acid. In other experiments meta stable $[Fe^{III}(TPA)(OOH)]^{2+}$ species

was generated by adding 3 equiv of H_2O_2 to 1 mM solution of **1** at -40 °C. $[Fe^{IV}(TPA)(O)]^{2+}$ species was generated at -40 °C in acetonitrile by adding 0.03 mL of 0.07 M (1 equiv) CH_3CO_3H to the 1 mM solution of **1** according to the published procedure.[134]

2.2.3 Product Identification for *ortho*-Hydroxylation

Isolation of *ortho*-hydroxylation products of the reaction between **1** (1 mM) with 3-methoxybenzoic acid (4 equiv) and hydrogen peroxide (3 equiv) at -40 ° C was performed by quenching the reaction mixture with concentrated acid (HCl). In the next step, adding a large volume of ether and putting the solution overnight in a freezer precipitated the iron complex out. After filtration and removal of water (dried over Na_2SO_4) the solution was evaporated to dryness. Organic products were dissolved in CD_3CN and analyzed by ^1H NMR spectroscopy.

2.2.4 Product Identification for *ipso*-Hydroxylation

A mixture of complex **1** (1 mM) and 2 equiv of aromatic acid in acetonitrile was prepared in air. H_2O_2 (3 equiv vs iron) was delivered into 1 mL of the mixture upon vigorous stirring. The reaction was quenched with 1-methylimidazole (0.1 mL) after 30 minutes followed by the addition of 1 mL acetic anhydride to esterify the products. Naphthalene was added as an internal standard. Organic products were extracted with chloroform (1-2 mL) and subjected to the GC and GC-MS analysis. All experiments were run at least in duplicate, the reported data is the average of these reactions.

2.2.5 Crystallographic Studies

Each crystal was placed onto the tip of a 0.1 mm diameter glass capillary and mounted on a CCD area detector diffractometer for a data collection at 173(2) K.[135] A preliminary set of cell constants was calculated from reflections harvested from three sets of 20 frames. These initial sets of frames were oriented such that orthogonal wedges of reciprocal space were surveyed. This produced initial orientation matrices determined from 67 reflections for $[Fe^{III}(TPA)(5\text{-MeO-salicylate})]^+$ and 44 reflections for $[Fe^{III}(TPA)(salicylate)]^+$. The data collection was carried out using MoKα radiation (graphite monochromator) with a frame time of 60 seconds and a detector distance of 4.9 cm. A randomly oriented region of reciprocal space was surveyed to the extent of one sphere and to a resolution of 0.84 Å. Four major sections of frames were collected with 0.30º steps in ω at four different ϕ settings and a detector position of -28º in 2θ. The intensity data were corrected for absorption and decay (SADABS).[136] Final cell constants were calculated from 2717 (for $[Fe^{III}(TPA)(5\text{-MeO-salicylate})]^+$) and 2950 (for $[Fe^{III}(TPA)(salicylate)]^+$) strong reflections from the actual data collection after integration (SAINT).[137] Please refer to Tables 2.2 and 2.3 for additional crystal and refinement information. The structure was solved and refined using Bruker SHELXTL.[138] The space groups for $[Fe^{III}(TPA)(5\text{-MeO-salicylate})]^+$ and $[Fe^{III}(TPA)(salicylate)]^+$ were Fdd2 and P2(1)/n, respectively and were determined based on systematic absences and intensity statistics. A direct-methods solution was calculated which provided most non-hydrogen atoms from the E-map. Full-

matrix least squares / difference Fourier cycles were performed which located the remaining non-hydrogen atoms. All non-hydrogen atoms were refined with anisotropic displacement parameters. All hydrogen atoms were placed in ideal positions and refined as riding atoms with relative isotropic displacement parameters. The final full matrix least squares refinement converged to $R1 = 0.0368$ and $wR2 = 0.0850$ for $[Fe^{III}(TPA)(5\text{-MeO-salicylate})]^+$ and $R1 = 0.0566$ and $wR2 = 0.1616$ for $[Fe^{III}(TPA)(salicylate)]^+$. CCDC-732099 & 732100 contain the supplementary crystallographic data for this paper. These data can be obtained free of charge from the Cambridge Crystallographic Data Centre via www.ccdc.cam.ac.uk/data_request/cif.

2.3 Results and Discussion

2.3.1 *ortho*-Hydroxylation

It was recently reported that addition of hydrogen peroxide to $[Fe^{II}(BPMEN)(CH_3CN)_2](ClO_4)_2$ in the presence of benzoic acid resulted in rapid (ca. 5 min) formation of $[Fe^{III}(BPMEN)(salicylate)]^+$ at room temperature.[60,139] The reaction was accompanied by the appearance of a deep blue color ($\lambda_{max} = 590$ nm). The final UV-vis spectrum was identical to that of the independently prepared salicylate complex $[Fe^{III}(BPMEN)(salicylate)](ClO_4)$, which was crystallographically characterized.[60] A similar *ortho*-hydroxylation reaction was reported with a related iron(II) aminopyridine complex, $[Fe^{II}(TPA)(CH_3CN)_2](OTf)_2$ (**1**), but with *m*-chloroperbenzoic acid as oxidant.[61]

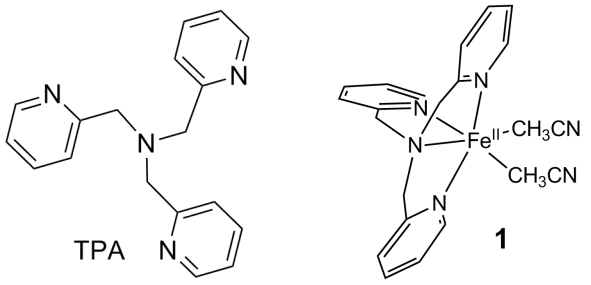

Figure 2.1 Representation of the ligand and the complex studied in this work: TPA and $[Fe^{II}(TPA)(CH_3CN)_2](OTf)_2$ (**1**).

Upon further studies, complex **1** was found to effect the *ortho*-hydroxylation of various benzoic acids with H_2O_2 as the oxidant, but the amounts of salicylate formed depended upon the nature of ring substituents and the iron complex. The outcomes of the hydroxylation reactions were conveniently monitored in solution by UV-vis spectroscopy, following the appearance of the intense visible absorption bands of the iron(III)-salicylate products (Table 2.1). The maxima of these absorption bands depended on the electronic nature of the substituent, consistent with the assignment of this absorbance as a phenolate-to-iron(III) charge transfer transition. As expected, electron-donating groups caused the λ_{max} of the salicylate complex to red-shift, whereas electron withdrawing groups had the opposite effect. For example, the λ_{max} of 560 nm for $[Fe^{III}(TPA)(salicylate)]^+$ was red-shifted to 650 nm in the corresponding 3- or 5-MeO-salicylate derivative (Figure 2.2 and Table 2.1). The extinction coefficients were determined for representative salicylate complexes ($[Fe^{III}(TPA)(5\text{-Cl-salicylate})]^+$, ε_{560} =

2100 L*mol^{-1}*cm^{-1}; [Fe^{III}(TPA)(5-MeO-salicylate)]$^{+}$, ε_{650} = 2100 L*mol^{-1}*cm^{-1}) and were assumed to be similar for all *ortho*-hydroxylation products. Crystal structures of [Fe^{III}(TPA)(5-MeO-salicylate)]$^{+}$ (Figure 2.3) and [Fe^{III}(TPA)(salicylate)]$^{+}$ (Figure 2.4) were obtained from single crystals grown in the presence of air from a 1:1:1 reaction mixture of **1**, triethylamine and the appropriate salicylic acid. Details of the crystal data and structural refinement are provided in Table 2.2 and Table 2.3, and their structural parameters are compared with that of [Fe^{III}(TPA)(5-Cl-salicylate)]$^{+}$ [61] in Table 2.4.

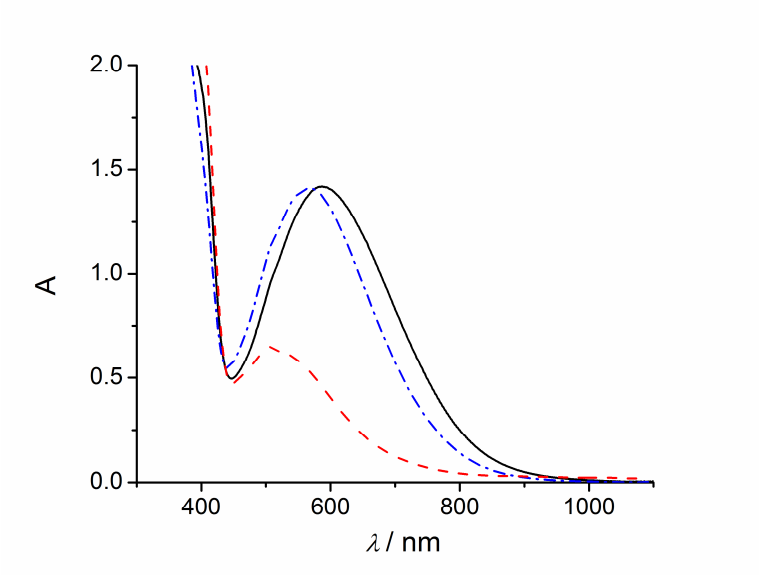

Figure 2.2. Visible spectra of **1**/H_2O_2-catalyzed oxidation products derived from 2-chlorobenzoic (black solid line), 3-chlorobenzoic (blue dashed-dot line), perfluorobenzoic (red dashed line). Reactions were carried out in CH_3CN at 20 °C by adding H_2O_2 (3 equiv vs **1**) to a mixture of **1** (1 mM) and the appropriate acid (2 equiv vs **1**).

Table 2.1: The amounts of *ortho*- and *ipso*-hydroxylation products relative to iron complex observed from the reactions of **1**, with a **1**/benzoic acid/H_2O_2 ratio of 1/2/3 at room temperature based on UV-vis (*ortho*) and GC (*ipso*) data

Substituent	Position	% yield of the hydroxylated products		λ_{max} (nm) of the chromophore	
		ortho	*ipso*	*ortho*	*ipso*
OMe	*ortho*	-	14	-	broad
	meta	48	-	650	-
	para	-	-	-	broad
Me	*ortho*	-	26	-	566
	meta	58	-	595	-
	para	-	30	-	584
H		51	21	560	
Cl	*ortho*	-	90	-	586
	meta	61	-	568	-
	para	-	54	-	580
NO_2	*ortho*	-	12	-	550
	meta	-	-	-	-
	para	-	-	-	530

'-' indicates no reaction

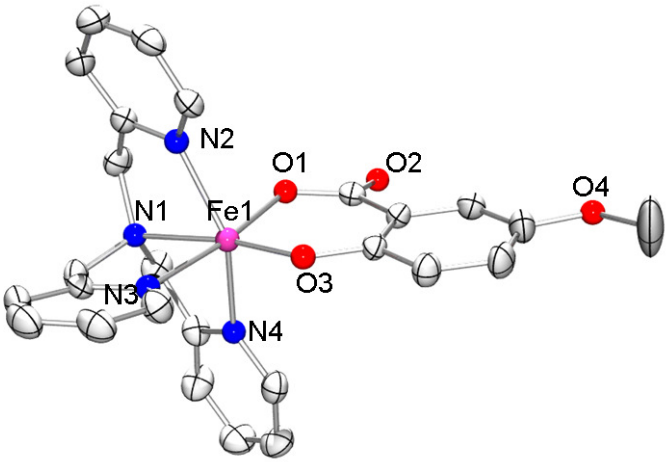

Figure 2.3: X-ray crystal structure of $[Fe^{III}(TPA)(5\text{-MeO-salicylate})]^{+}$. Oak Ridge thermal ellipsoid plot (ORTEP) drawing with atoms at 50% probability, hydrogen atoms have been omitted for clarity.

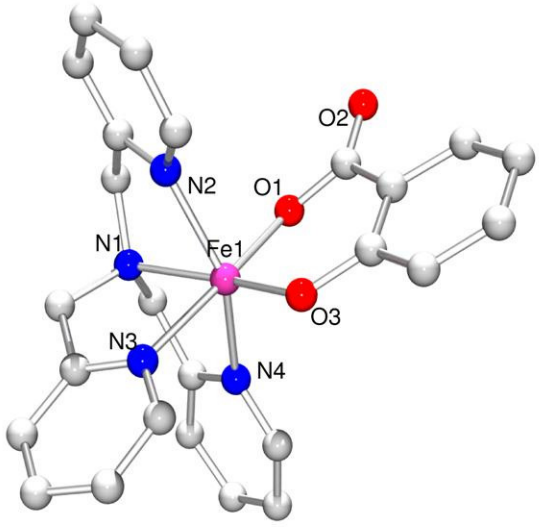

Figure 2.4: X-ray crystal structure of $[Fe^{III}(TPA)(salicylate)]^{+}$. ORTEP drawing with atoms at 50% probability, hydrogen atoms have been omitted for clarity.

Table 2.2. Crystal data and structure refinement for $[Fe^{III}(TPA)(5\text{-}CH_3O\text{-}O_2CC_6H_3O)]^+$

Empirical formula	$C_{27}\ H_{24}\ F_3\ Fe\ N_4\ O_7\ S$	
Formula weight	661.41	
Temperature	173(2) K	
Wavelength	0.71073 Å	
Crystal system	Orthorhombic	
Space group	Fdd2	
Unit cell dimensions	a = 26.279(2) Å	$\alpha = 90°$
	b = 52.814(5) Å	$\beta = 90°$
	c = 8.3068(8) Å	$\gamma = 90°$
Volume	11529.0(18) $Å^3$	
Z	16	
Density (calculated)	1.524 Mg/m^3	
Absorption coefficient	0.667 mm^{-1}	
F(000)	5424	
Crystal color, morphology	Blue, Needle	
Crystal size	0.50 x 0.07 x 0.06 mm^3	
Theta range for data collection	1.54 to 25.04°	
Index ranges	$0 \le h \le 31$, $0 \le k \le 62$, $-9 \le l \le 9$	
Reflections collected	22656	
Independent reflections	5092 [R(int) = 0.0496]	
Observed reflections	4182	
Completeness to theta = 25.04°	100.0%	
Absorption correction	Multi-scan	
Max. and min. transmission	0.9611 and 0.7314	
Refinement method	Full-matrix least-squares on F^2	
Data / restraints / parameters	5092 / 9 / 399	
Goodness-of-fit on F^2	1.055	
Final R indices [I>2sigma(I)]	$R1$ = 0.0368, $wR2$ = 0.0790	
R indices (all data)	$R1$ = 0.0516, $wR2$ = 0.0850	
Absolute structure parameter	0.024(16)	
Largest diff. peak and hole	0.279 and -0.265 e.$Å^{-3}$	

Table 2.3. Crystal data and structure refinement for $[Fe^{III}(TPA)(O_2CC_6H_4O)]^+$

Empirical formula	C26 H22 F3 Fe N4 O6 S	
Formula weight	631.39	
Temperature	173(2) K	
Wavelength	0.71073 Å	
Crystal system	Monoclinic	
Space group	P2(1)/n	
Unit cell dimensions	a = 8.014(2) Å	α = 90°
	b = 13.079(3) Å	β = 94.309(4)°
	c = 25.250(7) Å	γ = 90°
Volume	2639.1(12) $Å^3$	
Z	4	
Density (calculated)	1.589 Mg/m^3	
Absorption coefficient	0.722 mm^{-1}	
F(000)	1292	
Crystal color, morphology	purple, needles	
Crystal size	0.38 x 0.20 x 0.03 mm^3	
Theta range for data collection	1.62 to 25.14°	
Index ranges	$-9 \le \eta \le 9$, $-15 \le \kappa \le 15$, $-29 \le \lambda \le 29$	
Reflections collected	17334	
Independent reflections	4696 [R(int) = 0.0608]	
Observed reflections	3241	
Completeness to theta = 25.14°	99.4%	
Absorption correction	Multi-scan	
Max. and min. transmission	0.9787 and 0.7710	
Refinement method	Full-matrix least-squares on F^2	
Data / restraints / parameters	4696 / 48 / 395	
Goodness-of-fit on F^2	1.058	
Final R indices [I>2sigma(I)]	$R1$ = 0.0566, $wR2$ = 0.1404	
R indices (all data)	$R1$ = 0.0905, $wR2$ = 0.1616	
Largest diff. peak and hole	0.640 and -0.824 $e.Å^{-3}$	

Table 2.4: Comparison of the crystallographic data of $[Fe^{III}(TPA)(5\text{-MeO-salicylate})]^+$ with $[Fe^{III}(TPA)(5\text{-Cl-salicylate})]^+$ and $[Fe^{III}(TPA)(salicylate)]^+$.[a]

Bonds/Bond Angles	$[Fe(TPA)(5\text{-OMe-sal})]^+$	$[Fe(TPA)(5\text{-Cl-sal})]^+$	$[Fe(TPA)(sal)]^+$
Fe1-O3	1.851(2)	1.845(7)	1.859(3)
Fe1-O1	1.928(2)	1.914(7)	1.919(3)
Fe1-N2	2.142(3)	2.156(10)	2.140(4)
Fe1-N4	2.125(3)	2.137(8)	2.142(4)
Fe1-N3	2.137(3)	2.216(9)	2.131(3)
Fe1-N1	2.201(3)	2.129(9)	2.191(3)
C20-O3	1.344(4)	1.342(11)	1.352(5)
C25-O1	1.299(4)	1.316(11)	1.323(5)
C25-O2	1.215(4)	1.200(12)	1.219(5)
O3-Fe1-N2	106.62(10)	106.3(3)	99.97(13)
O3-Fe1-N4	99.55(10)	100.8(4)	106.23(13)
O3-Fe1-N3	92.69(10)	88.5(3)	91.82(12)
O3-Fe1-N1	171.21(11)	168.4(3)	170.80(13)
O3-Fe1-O1	93.83(10)	93.8(3)	93.88(12)

[a] Atoms have been numbered as per the $[Fe^{III}(TPA)(5\text{-MeO-salicylate})]^+$ structure published in this report. The bonds and bond angels in the same row represent the $[Fe^{III}(TPA)(5\text{-MeO-salicylate})]^+$ counterparts in the other two structures.

Salicylic acid was the major product in the reactions of benzoic acid and **1**/H_2O_2. Complex **1**, however, was very selective: only 3-substituted benzoic acids were hydroxylated at the *ortho*-position. 50-60% yields of salicylate products were found for benzoic acid, 3-methylbenzoic acid and 3-chlorobenzoic acid with respect to the iron complex (Table 2.1). No salicylic acid product was observed for nitro-substituted substrates, presumably because of the lower reactivity of electron-poor nitrobenzoic acids. On the contrary, electron donating benzoic acids suffered the risk of over oxidation of the formed salicylates. In support, adding a smaller amount of H_2O_2 (2 equivalents relative to iron complex) increased the yield of the corresponding salicylate of 3–methylbenzoic acid to 62% from 58%. The source of the O atom in the formed salicylate complex was found to be H_2O_2 as the $H_2{}^{18}O_2$ experiment suggested a 2-unit increase in mass in the ESI-MS spectrum (Figure 2.5).

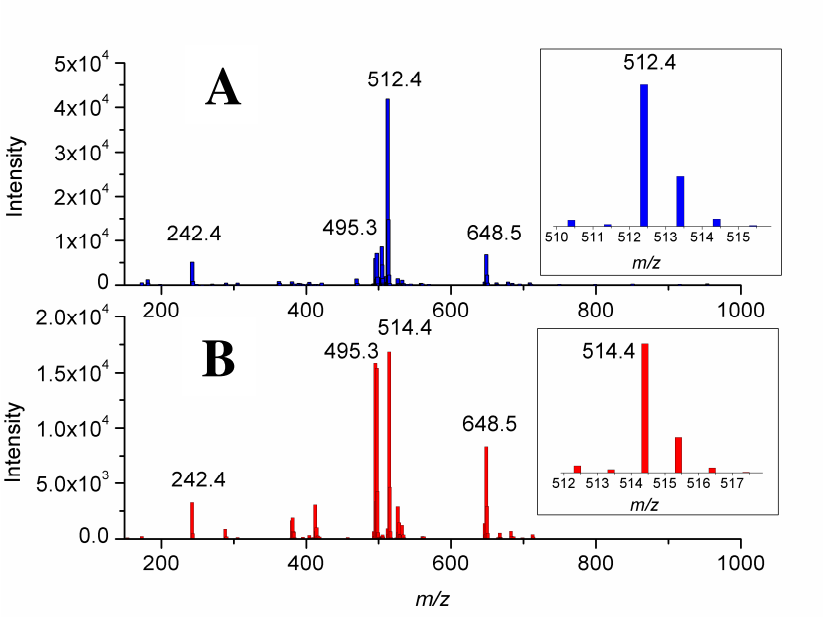

Figure 2.5: ESI-MS analysis of the end product of the aromatic hydroxylation reaction performed by **1** (1 mM), 3-methoxybenzoic acid and natural isotopically abundant (A) or ^{18}O-labeled H_2O_2 (B). Inset is the zoom-in of the target peak (*m/z* = 512.4, assigned as $[Fe^{III}(TPA)(5\text{-MeO-salicylate})]^+$) showing the isotope distribution pattern.

For 3-substituted benzoic acids, there were two available positions for *ortho*-hydroxylation, which would generate 3- and/or 5-substituted salicylic acids (Scheme 2.1). ^1H NMR analysis of the products of the reaction with **1** showed that the 5-substituted salicylic acid was the major product (formed in a 3:1 ratio) over 3-substituted isomer (Figure 2.6). The preference for the 5-substituted isomer was not surprising on the basis of steric effects; the hydroxylation of the *para*-position with respect to the substituent

should be sterically less demanding than the incorporation of a hydroxyl group between two existing substituents.

Scheme 2.1: Possible sites of *ortho*-hydroxylation in 3-methoxybenzoic acid

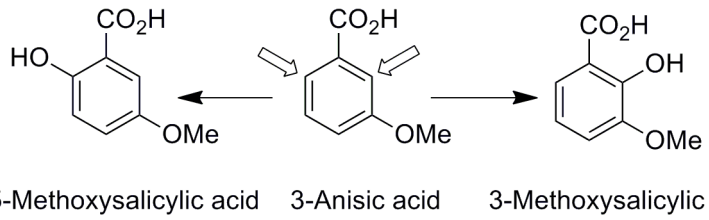

5-Methoxysalicylic acid 3-Anisic acid 3-Methoxysalicylic acid

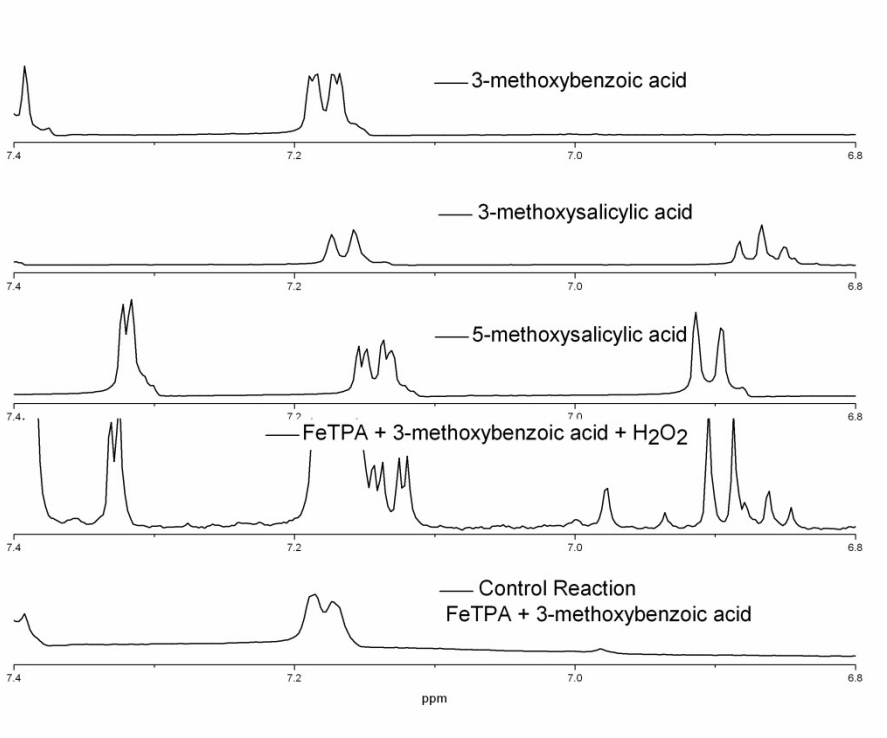

Figure 2.6: ^{1}H-NMR analysis of salicylate products from **1**/H_2O_2-catalyzed oxidation of 3-methoxybenzoic acid.

2.3.2 Oxidative Decarboxylation Leading to *ipso*-Hydroxylation

The remarkable ability of mononuclear iron(II) complex **1** to efficiently and selectively hydroxylate benzoic acids to their corresponding salicylic acids using H_2O_2 has some limitations. Surprisingly, some benzoic acids with electron donating substituents did not afford salicylate products. For example, the reaction of **1**, H_2O_2, and the 2-chlorobenzoic acid instead generated a transient green species (Figure 2.2). Moreover, a similar chromophore could also be observed after the addition of H_2O_2 to a mixture of perfluorobenzoic acid and **1**. Since both *ortho* positions of perfluorobenzoic acid were occupied, the purple species could not result from an *ortho*-hydroxylation reaction. Quenching the reactions with 1-methylimidazole followed by acetylation and GC-MS analysis allowed us to identify the organic products as 2-chlorophenol and perfluorophenol, which were respectively obtained in 90% and 15% yields from the reaction mixtures of **1**/benzoic acid/H_2O_2 in a 1/2/3 ratio. These phenol products resulted from oxidative decarboxylation of 2-chloro- and perfluorobenzoic acids followed by *ipso*-hydroxylation (Scheme 2.3). Coordination of the phenolate products to Fe^{III}(TPA) then generated the observed chromophores.

Scheme 2.2: Conversion of benzoic acids to salicylates and phenolates by **1** and H_2O_2

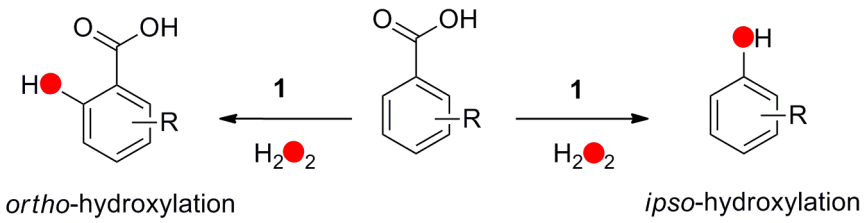

Further experiments established that *ipso*-hydroxylation extended beyond the two examples described above. This transformation depended on the electronic properties of substituents on the benzoic acid, and their positions with respect to -COOH group (Table 2.1). *Ipso*-hydroxylation could be observed for benzoic acids with either electron donating or electron withdrawing substituents in the 2- or 4-position, but not for 3-substituted benzoic acids where only *ortho*-hydroxylation was found. For the unsubstituted benzoic acid, however, both *ortho*- and *ipso*-hydroxylation were observed (Table 2.1).

Electron-donating substituents that increase electron density at the *ipso* position with respect to the carboxylate group promoted decarboxylation leading to *ipso*-hydroxylation. Blocking *ortho*-hydroxylation by placing substituents in 2- or and/or 6-positions with respect to carboxylate also favored *ipso*-hydroxylation. *Meta*-substituted benzoic acids studied in this work did not afford *ipso*-hydroxylation products. Electron-withdrawing (NO_2, Cl) *meta* substituents drastically decreased electron density in the *ipso*-position and prevented the electrophilic attack by the metal-based oxidant, hampering the *ipso*-

hydroxylation process. On the other hand, strong electron donating substituents (MeO) *meta* with respect to carboxylate preferentially underwent a competing electrophilic attack at the most electron-rich site of the aromatic ring, yielding *ortho*-hydroxylated products (salicylates).

Labeling experiments were also carried out in the *ipso*-hydroxylation of perfluorobenzoic acid. The formed product, after quenching the reaction with 1-methylimidazole, was acetylated with acetic anhydride and was analyzed in a GC-MS instrument. The reactions with hydrogen peroxide having natural isotopic abundance showed a peak at m/z = 227, which could be ascribed as the ammonium cation of the perfluorophenyl acetate (NH_3 was used as a carrier gas in the GC-MS). Under identical reaction conditions but changing the oxidant to $H_2{}^{18}O_2$ generated a peak at m/z = 229 that demonstrated that an O atom from hydrogen peroxide was incorporated into the phenol product (Scheme 2.2).

2.4 Mechanistic Insights

The regioselectivity of these reactions, which results in the incorporation of an –OH group either next to or in place of the carboxylate substituent, indicates the involvement of a metal-based oxidant, rather than hydroxyl radical that would derive from metal promoted O-O bond homolysis of H_2O_2. Reactivity trends suggest that the oxidant is electrophilic. Coordination of aromatic carboxylic acids to **1** positions the aromatic ring in the immediate vicinity of the redox-active metal center. Isotope substitution studies provide additional insight into possible hydroxylation mechanisms. Experiments with the deuterated substrate, d_5-PhCOOH and a related complex FeBPMEN, exhibited no significant H/D kinetic isotope effect on the rates of *ortho*-hydroxylation with H_2O_2 in the presence of complex FeBPMEN.[132,140] Competition experiments also showed no preference of FeBPMEN in reacting with either protio or deuterio isotopomers, so C-H bond breaking on the phenyl ring cannot be a rate limiting step in this transformation.[60] Similarly small H/D KIE values (≤ 1) were also reported for other aromatic oxidations promoted by biological and synthetic iron centers,[131] and interpreted in terms of either a rate-limiting formation of an iron-oxo intermediate or a rate-limiting electrophilic attack of the aromatic ring by a metal-based oxidant (a process that is typically characterized by only a small but inverse isotope effect).[120,141-144]

^{18}O-labeling experiments with $H_2{}^{18}O_2$ unambiguously showed the incorporation of one oxygen atom into the phenolate or salicylate product derived from the oxidations of benzoic acids (Figure 2.5), underscoring the fact that hydrogen peroxide is the sole

source of the oxygen atom incorporated into the products. This conclusion applies to both *ortho*-hydroxylation and decarboxylation/*ipso*-hydroxylation, as determined by mass spectrometry (Figure 2.5). Thus the metal-based oxidant must derive from the combination of the iron catalyst and H_2O_2.

An obvious starting point with respect to the identity of the metal-based oxidant is an Fe^{III}-OOH intermediate. Such species have been observed for both FeBPMEN[62,130,131] and FeTPA.[79,86,132] The intermediate $[Fe^{III}(TPA)(OOH)]^{2+}$, however, can be obtained in much higher yield and is thus better characterized. This intermediate is thus one of the most important species in our mechanistic discussion.

As previously reported, the reaction of **1** and excess H_2O_2 in CH_3CN at -40 °C gave the corresponding Fe^{III}-OOH intermediate (**1a**) with a λ_{max} at 540 nm (Figure 2.7, dashed-line spectra). Subsequent addition of 3-methoxybenzoic acid to this intermediate elicited a new band at 650 nm that is associated with the formation of the corresponding salicylate complex (Figure 2.7, solid-line spectra). Reversing the order of addition of the oxidant and the substrate also generated the same chromophore at 650 nm, but the 540-nm absorption feature of the Fe^{III}-OOH species was much less pronounced (Figure 2.8). Similar spectral changes were observed in parallel experiments for 2-methoxybenzoic acid (Figure 2.9 and Figure 2.10). The Fe^{III}-OOH intermediate would thus appear to be involved in the aromatic hydroxylation.

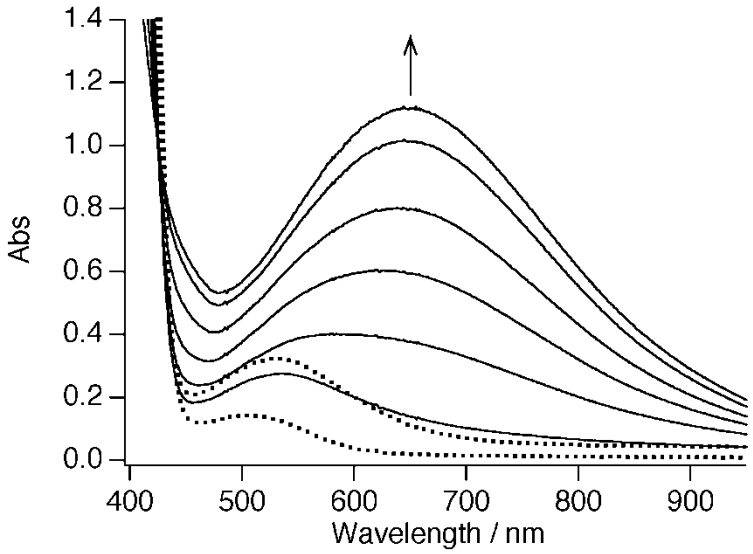

Figure 2.7: Spectral changes observed in the reaction of **1** (1 mM) with 3 equiv H_2O_2 and 12 equiv 3-methoxybenzoic acid at -40 °C. Dashed lines represent spectra obtained immediately after mixing **1** and H_2O_2 and after 9 min. Solid lines correspond to spectra obtained subsequent to the addition of 3-methoxybenzoic acid (taken at 10, 20, 50, 90, 150 and 210 min after addition of the acid).

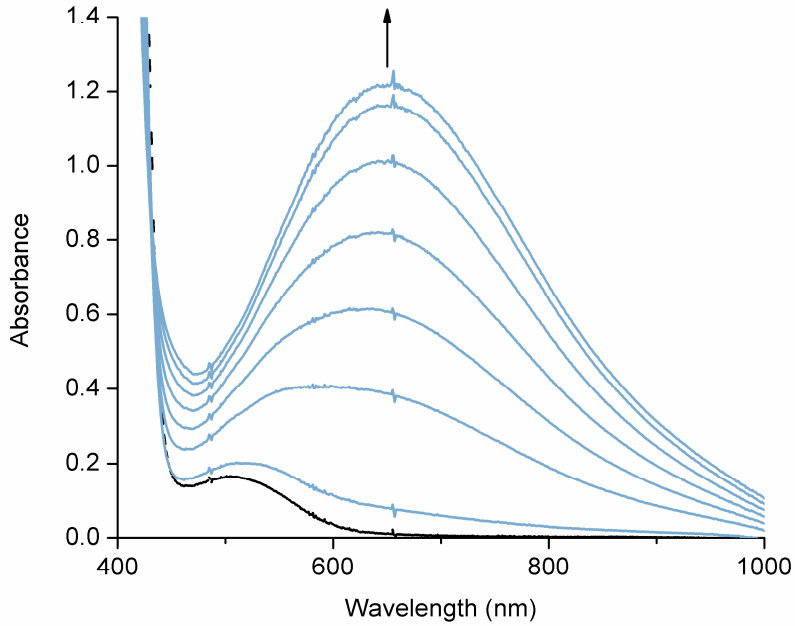

Figure 2.8: Spectral changes upon addition of H_2O_2 (3 equiv) to the mixture of **1** (1 mM) and 3-methoxybenzoic acid (12 equiv) at -40 °C. The first spectrum was taken immediately after mixing. Subsequent spectra (shown in turquoise; absorbance increases over time) were taken at 5, 24, 36, 47, 59 and 73 minutes.

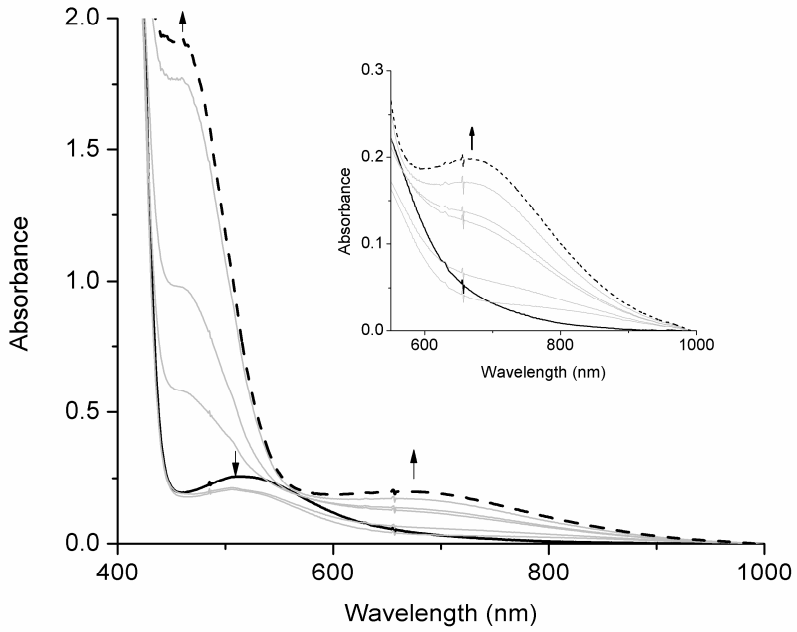

Figure 2.9: UV-vis spectral change upon addition of 2-methoxybenzoic acid (12 equiv) to a solution of preformed Fe^{III}-OOH (prepared by reacting 3 equiv H_2O_2 with 1 mM solution of **1**) at -40 °C. Addition of 2-methoxybenzoic acid led to the formation of a band around 460 nm and 650 nm. Inset is the blow up of 650 nm region of the spectra. The black spectrum was collected immediately after mixing. The gray spectra, in ascending order, were taken at 8, 9, 19, 25, and 33 minutes. The final dashed black spectrum was taken at 45 minutes.

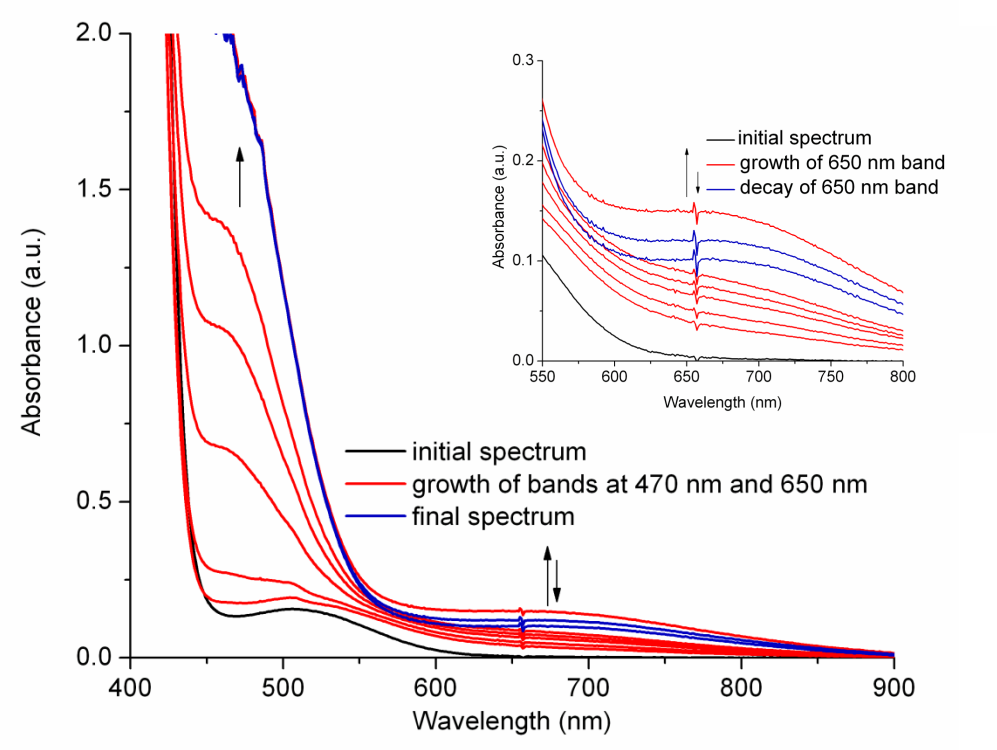

Figure 2.10 : UV-Vis spectral change upon addition of H_2O_2 (3 equiv) to the mixture of **1** and 2-methoxybenzoic acid (1 mM in **1**, 12 equiv of 2-methoxybenzoic acid vs. **1**) at -40 °C. Addition of hydrogen peroxide led to the formation of a band around 470 nm and 650 nm. Inset is the blow up of 650 nm region of the spectra. The black spectrum was recorded immediately after mixing. The red spectra in ascending order were taken at 6, 11, 18, 24, 29, 54 minutes. The final two blue spectra were taken at 65 and 72 minutes.

Scheme 2.3 illustrates the various possible roles of the Fe^{III}-OOH intermediate (**1b**) in the aromatic hydroxylation reaction, where it could either be the oxidant itself or the precursor thereof. A similar mechanistic landscape was discussed previously for olefin epoxidation and *cis*-dihydroxylation with **1**/H_2O_2.[53,59] Three pathways were considered for the evolution of the Fe^{III}-OOH intermediate. The hydroperoxo ligand could attack the carboxylate of the bound benzoic acid to generate an acylperoxoiron(III) species (**1c** in Scheme 2.3). Formation of such an acetylperoxoiron(III) species has been detected[131] in a mixture of FeBPMEN, acetic acid, and H_2O_2, but the yield was very low. In addition, Nam and co-workers reported the self-hydroxylation of peroxybenzoic acids in the presence of **1** to form salicylate products.[61] This pathway however requires the formation of a doubly labeled salicylate product from labeled H_2O_2 (Scheme 2.3). Since only singly labeled salicylate is observed in the ^{18}O-labeling experiments, this pathway can be excluded as a mechanistic option for the aromatic hydroxylations under our experimental conditions.

Scheme 2.3: Mechanisms of *ortho*-hydroxylation and *ipso*-hydroxylation by **1**.

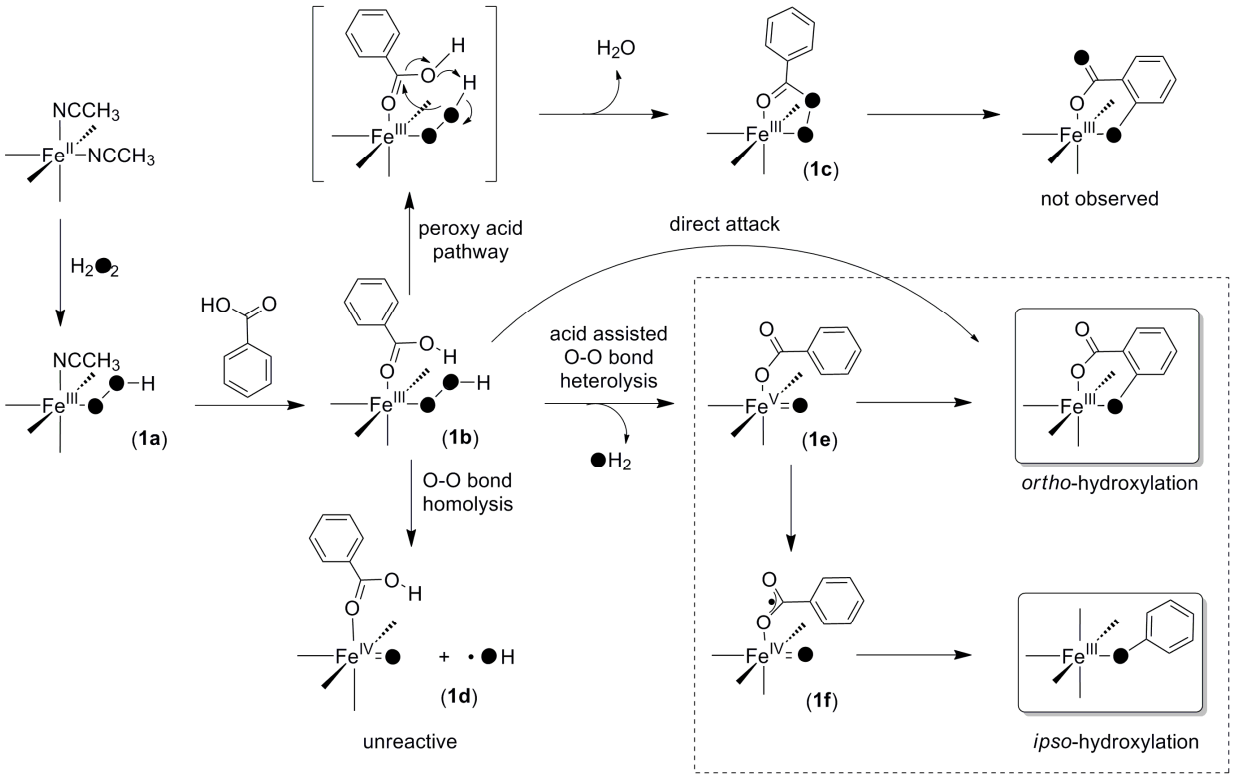

A second option for the evolution of the Fe^{III}-OOH intermediate is O-O bond homolysis, which would afford $[(TPA)Fe^{IV}(O)]^{2+}$ and hydroxyl radical (**1d** in Scheme 2.3). The oxidative power of the Fe^{IV}=O species has been demonstrated in several iron-promoted oxidation reactions,[69,70,120,134,145,146] including aromatic hydroxylation of anthracene.[120] In fact, Fe^{IV}=O complexes were also detected in the reactions of **1** with hydrogen peroxide

and acetic acid.[59] However, a detailed study on **1**-catalyzed olefin epoxidation clearly excluded $[(TPA)Fe^{IV}=O]^{2+}$ as the oxidant in this transformation.[59] Similarly, even though we found that *meta*-chlorobenzoic acid was *ortho*-hydroxylated by **1** and H_2O_2 (Table 1), $[(TPA)Fe^{IV}=O]^{2+}$ did not effect the *ortho*-hydroxylation of *meta*-chlorobenzoic acid.[61] Even the more reactive electron-rich substrates (3-methoxybenzoic acid for *ortho*-hydroxylation and 2-methoxybenzoic acid for *ipso*-hydroxylation) were not oxidized by independently generated $[(TPA)Fe^{IV}=O]^{2+}$ (Figures 2.11 and 2.12). These observations conclusively eliminate $Fe^{IV}=O$ as a probable oxidant in these aromatic hydroxylation reactions. Furthermore, since hydroxyl radicals are known to attack benzoic acid, affording a statistical mixture of *o*-, *m*, and *p*-hydroxylated products,[147] the observed regioselectivity of aromatic hydroxylation with **1**/H_2O_2 excludes the participation of HO• radicals.

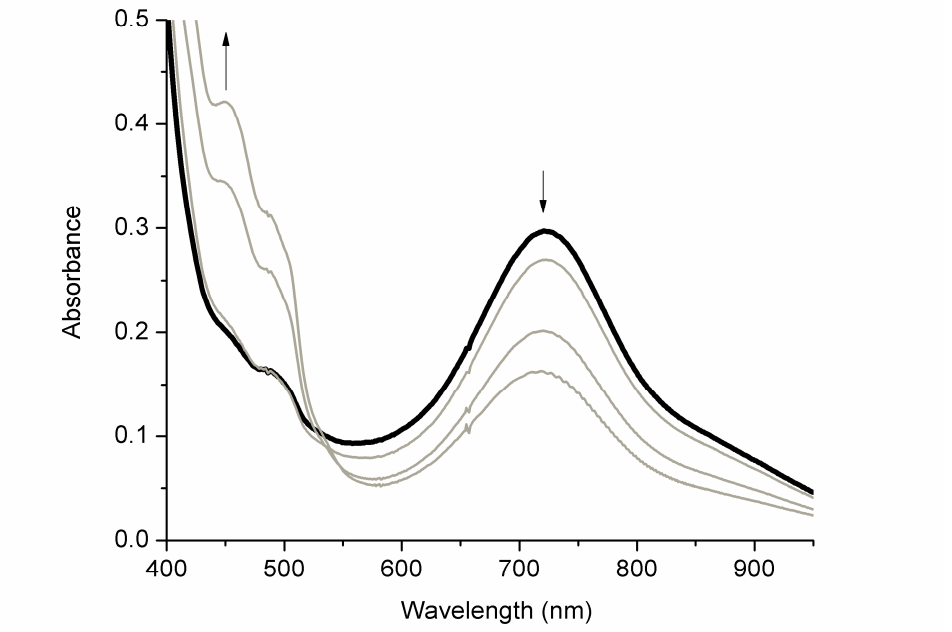

Figure 2.11: UV-vis spectral changes indicating the decay of Fe^{IV}=O (bold solid line) upon addition of 3-methoxybenzoic acid to pre-formed (TPA)Fe^{IV}=O (1 mM solution in CH_3CN), which was generated at 0 °C after addition of CH_3CO_3H (1 equiv) to **1** (**1**:CH_3CO_3H:3-methoxybenzoic acid = 1:1:12). The other three spectra (from top to bottom) were taken after 2, 40 and 99 minutes of reaction, respectively.

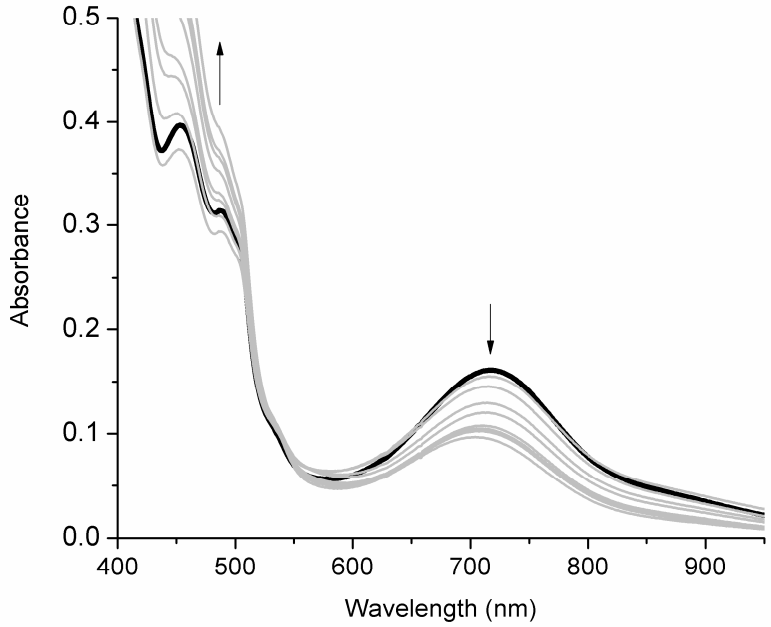

Figure 2.12: UV-vis spectral changes indicating the decay of Fe^{IV}=O (bold solid line) upon addition of 2-methoxybenzoic acid to pre-formed (TPA)Fe^{IV}=O (1 mM solution in CH_3CN), which was generated at 0 °C after addition of CH_3CO_3H (1 equiv) to **1** (**1**:CH_3CO_3H:2-methoxybenzoic acid = 1:1:12). (TPA)Fe^{IV}=O (black spectrum) is almost instantly recorded after addition of CH_3CO_3H to the solution of **1**. The other spectra (from top to bottom) are taken at 1.2, 1.3, 1.5, 1.7, 3.1, 4.7, 6, and 13 minutes, respectively.

With the arguments presented above, only two possible pathways remain for the Fe^{III}-OOH intermediate en route to the observed aromatic hydroxylation products (Scheme 2.3): either direct electrophilic attack of the organic substrate, or heterolytic cleavage of the O–O bond to generate a formally Fe^{V}=O species[53,59,148] that attacks the iron-bound benzoic acid. The limited existing data on the reactivity of Fe^{III}-OOH species[128] indicate that these appear to be sluggish oxidants.[149] In particular, the decay of $[(TPA)Fe^{III}(OOH)]^{2+}$ at -45 ºC was shown not to depend on thioanisole or cyclohexene concentration,[149] although such substrates were oxidized by the combination of **1** and H_2O_2 at higher temperatures. We thus favor the carboxylic acid-assisted O–O bond heterolysis pathway leading to an unobserved Fe^{V}=O oxidant, which was postulated by Mas-Ballesté and Que in the efficient **1**-catalyzed epoxidation of olefins by H_2O_2 in the presence of acetic acid.[59] Although it may be argued that a direct electrophilic attack of the aromatic ring by **1b** is plausible, particularly for benzoic acids with electron donating substituents, the broad scope of both *ortho*- and *ipso*-hydroxylation reactions promoted by **1** suggests that a highly electrophilic intermediate is likely to be involved, which we propose is **1e**. A similar oxidant has been proposed for the **1**-catalyzed self-hydroxylation of aryl peroxyacids,[61] for the intramolecular hydroxylation of the aromatic ring covalently appended to the analog of FeBPMEN,[124] and for the *ortho*-hydroxylation of benzyl alcohol by another aminopyridine iron complex.[150] Although only one non-heme iron(V)-oxo complexes has been directly observed at low temperature as a transient species and characterized by a variety of spectroscopic methods,[151] indirect evidence supporting participation of non-heme Fe^{V}-oxo intermediates in oxidations of alcohols,[152]

olefins,[53,59,153] and arenes[124,150,154] continues to accumulate. The coordination of the carboxylate *cis* to the oxo moiety in the putative oxoiron(V) oxidant **1e**[153] positions the aromatic ring well for the attack of the oxo group at the carbon atom *ortho* to the carboxylate function. Such an attack would form a six-membered ring in the transition state, facilitating formation of the product complex with a bidentate salicylate. Such directed reactivity was reported for an iron catalyst closely related to FeBPMEN by Chen and White.[155] The substrates that are consistently *ortho*-hydroxylated are those with substituents *meta* to the carboxylate functionality; in no case is *ipso*-hydroxylation observed.

In contrast, *ipso*-hydroxylation products are formed for benzoic acids with *ortho* or *para* substituents. The observation of *ipso*-hydroxylation products can most easily be rationalized by postulating formation of a coordinated arylcarboxyl radical (**1f**) that undergoes spontaneous loss of CO_2,[59,156] affording an aryl radical that immediately rebounds with the oxoiron(IV) center to form the phenolate product. The radical may derive from O-O bond homolysis of the precursor $Fe^{III}(OOH)(O_2CAr)$ intermediate (**1b**) or intramolecular electron transfer from the coordinated carboxylate to the oxoiron(V) center in **1e**, in both cases generating the carboxyl radical and an oxoiron(IV) center. Oxidative decarboxylation is precedented in the reaction of phenylacetic acid with **1** and H_2O_2, where benzyl radical is formed and then trapped by O_2 to yield benzaldehyde as the observed product.[59] Unlike the resonance-stabilized benzyl radical, the phenyl radical would be expected to be short-lived and undergo rapid oxygen rebound. The fact that

ortho-substituted benzoic acids are converted mainly to *ipso*-hydroxylation products suggests that steric factors may promote this reactivity mode, but the observation of low yields of phenols derived from electron-poor substrates (such as nitro-benzoic acids) indicate that electronic factors also contribute to the efficiency of *ipso*-hydroxylation. Since benzoic acid can yield both *ortho*- and *ipso*-hydroxylation products, these reactions must proceed via competing pathways. The factors governing the outcome of this competition include relative electron density in the *ortho*- and *ipso*-positions, and steric accessibility of the *ortho* sites.

In summary, highly regioselective hydroxylation of a broad range of substituted aromatic acids with hydrogen peroxide in the presence of **1** proceeds readily at room temperature. The hydroxylation occurs exclusively in the vicinity of the anchoring carboxylate functional group: *ortho*-hydroxylation affords salicylates, and *ipso*-attack results in decarboxylation and *ipso*-hydroxylation, yielding phenolates. A similar proximity effect can be postulated for the highly selective hydroxylation of tertiary C-H bonds on carbons gamma to the carboxylate functionality in what Chen and White call the carboxylate-directed method to form 5-membered lactone rings.[155] An electrophilic, metal-based oxidant must be involved in carboxylic-acid directed aromatic hydroxylation. Fe^{IV}=O species are unreactive in aromatic hydroxylations described herein. Fe^{III}-OOH is definitely involved in the hydroxylation pathways, most likely via intramolecular acid-assisted O-O bond heterolysis, yielding transient, highly reactive Fe^{V}=O species that have yet to be directly observed.

Acknowledgements. This work was supported by the US Department of Energy (Grants DE-FG02-06ER15799 to ERA and DE-FG02-03ER15455 to LQ). We thank Dr. Victor G. Young, Jr. of the University of Minnesota X-ray Crystallographic Laboratory and Andrew J. Fielding for determining the crystal structures.

Chapter 3

Iron Catalyzed Competitive Olefin Oxidation and *ipso*-Hydroxylation of Benzoic Acids: Further Evidence for an Fe^{V}=O oxidant

This chapter was published in its entirety as: Parthapratim Das and Lawrence Que, Jr. "Iron Catalyzed Competitive Olefin Oxidation and ipso-Hydroxylation of Benzoic Acids: Further Evidence for an Fe^{V}=O Oxidant" *Inorg. Chem.* **2010**, *49*, 9479-9486.

Portions reproduced from *Inorg. Chem.* **2010**, *49*, 9479-9486 with kind permission from the American Chemical Society

Copyright © 2010 American Chemical Society

3.1 Introduction

Non-heme iron oxygenases have emerged as a very important group of enzymes that perform a variety of interesting oxidative transformations.[1,3,12] Of particular interest is the family of Rieske dioxygenases[15,157] that catalyze the *cis*-dihydroxylation of arene double bonds in the bio-degradation of aromatic molecules by soil bacteria.[12,16,158] Such a transformation was unique to a biological iron center, until quite recently. We initiated an effort more than ten years ago to develop bio-inspired non-heme iron complexes that can carry out the *cis*-dihydroxylation of C=C double bonds and found a family of complexes exemplified by $[Fe^{II}(TPA)(MeCN)_2]^{2+}$(**1**) that represented the first examples of catalysts for olefin *cis*-dihydroxylation by a non-biological iron center. These catalysts used H_2O_2 as oxidant in place of the combination of O_2, electrons, and protons required in the enzyme reactions. Complex **1** and other non-heme iron complexes have also been shown to use H_2O_2 as oxidant for a variety of other reactions[54] including the hydroxylation of alkanes,[52,56,57,159-162] the epoxidation of olefins,[53,56,58,163-165] and the hydroxylation of arenes.[60,61,140,154,166] Very recently the **1**/H_2O_2 combination was shown to carry out the *cis*-dihydroxylation of naphthalene to *cis*-1,2-dihydro-1,2-naphthalenediol, making it the first functional model of the enzyme naphthalene 1,2-dioxygenase.[154]

In this chapter we focus on the *ipso*-hydroxylation of benzoic acids catalyzed by **1**, its relationship with olefin epoxidation and *cis*-dihydroxylation, and mechanistic insights derived therefrom. Complex **1** has been shown to hydroxylate benzoic acids

regioselectively with H_2O_2 as an oxidant. Depending on the position of the substituent in the arene ring, the benzoic acid can undergo either *ortho*-hydroxylation (forming salicylates) or oxidative decarboxylation followed by hydroxylation at the *ipso*-carbon (making phenols).[140] The salicylates obtained from *ortho*-hydroxylation are excellent bidentate ligands and form stable iron(III) complexes that exclude the possibility of catalytic turnover. However, as reported in this chapter, the phenolates obtained from *ipso*-hydroxylation are more susceptible to displacement by substrate, and multiple turnovers of phenol formation are observed for benzoic acids with electron withdrawing substituents. Furthermore, experiments in the presence of 1-octene or *tert*-butyl acrylate show that *ipso*-hydroxylation and olefin oxidation are competitive reactions and provide further support for the Fe^{V}=O oxidant proposed for **1**-catalyzed oxidations.

3.2 Experimental Section

3.2.1 Materials and Methods

All chemicals and solvents were purchased from Aldrich and were used without additional purification unless otherwise noted. CH_3CN solvent was dried over CaH_2 before use. $H_2{}^{18}O$ (97% ^{18}O-enriched) was obtained from Cambridge Isotope Laboratories Inc. (Andover, MA). $H_2{}^{18}O_2$ (90% ^{18}O-enriched) was obtained from Isotec (Sigma-Aldrich) Inc. The complex $[Fe^{II}(TPA)(CH_3CN)_2](OTf)_2$ (**1**) was prepared in an anaerobic glove box according to the published procedures.[134] Product analyses were

performed on a Perkin-Elmer Sigma 3 gas chromatograph (AT-1701 column, 30 m) with a flame ionization detector. GC-MS experiments were carried using an HP 6890 gas chromatograph (HP-5 column, 30 m) with an Agilent 5973 mass detector.

3.2.2 Catalytic studies

Catalytic studies were performed by using 0.2 mL of a 10-mM solution of **1** along with 0.287 mL of a 70-mM solution of H_2O_2 (10 equiv) at room temperature in acetonitrile where the final concentration of **1** in the solution was 1 mM. H_2O_2 was added using a syringe pump over 25 minutes with an additional 5 min of stirring. 10, 25, or 50 equivalents (relative to **1**) of perfluorobenzoic, 2-nitrobenzoic, or 2-chlorobenzoic acid were added in various experiments. For competition experiments with olefins, various amounts of olefin were added prior to the introduction of H_2O_2. Each catalytic result reported represented the average of at least three experiments.

3.3 Results and Discussion

[$Fe^{II}(TPA)(CH_3CN)_2](OTf)_2$ (**1**) has been shown to be an effective olefin oxidation catalyst to produce *cis*-diol and epoxide with H_2O_2 as the oxidant.[53] The **1**/H_2O_2 combination has also been shown to attack a variety of benzoic acids and effect either *ortho*-hydroxylation (producing salicylates) or *ipso*-hydroxylation (producing phenolates),[140] depending on the position of the substituent in the aromatic ring. 3-

substituted benzoic acids are converted to salicylates, while 2- and 4-substituted ones produce phenolates as a result of oxidative decarboxylation and *ipso*-hydroxylation. Further explorations of this chemistry, presented in this paper with benzoic acids having electron-withdrawing substituents, reveal that *ipso*-hydroxylation can be catalytic.

Figure 3.1 shows the results of experiments with **1** as catalyst, 10 equiv of H_2O_2, and varying amounts of benzoic acid. We chose to study the oxidations of perfluoro-, 2-nitro-, and 2-chlorobenzoic acids, which have respective pK_a's of 1.88, 2.19, and 2.92. The yields of the corresponding *ipso*-hydroxylated products increased with a larger excess of the benzoic acid. As much as 75% of the H_2O_2 was converted to phenol product. The phenol products were readily identified by their characteristic GC retention times and their mass spectral patterns from GC-MS analysis. This is the first example of the catalytic production of phenol from benzoic acids using an iron catalyst and H_2O_2 at ambient temperature and pressure. However, much lower phenol yields were observed for benzoic acids with electron donating substituents due to over-oxidation of the resulting phenols (Figure 3.2). For example, in the **1**-catalyzed oxidation of 2,6-dimethylbenzoic acid, the products found were 0.5 equiv of 2,6-dimethylphenol and 1 equiv 2,6-dimethylbenzoquinone. As a consequence, our subsequent experiments focused only on the benzoic acids with electron withdrawing substituents. The observed increased yield of phenol products in Figure 3.1 with higher concentrations of benzoic acid reflects pre-equilibrium binding of the benzoic acid to iron(III)-hydroperoxo species **A** prior to O-O bond cleavage that leads to the formation of **C**, as proposed in Scheme 3.1.

Scheme 3.1: Proposed pre-equilibrium binding of the benzoic acid to the Fe^{III}-OOH intermediate.

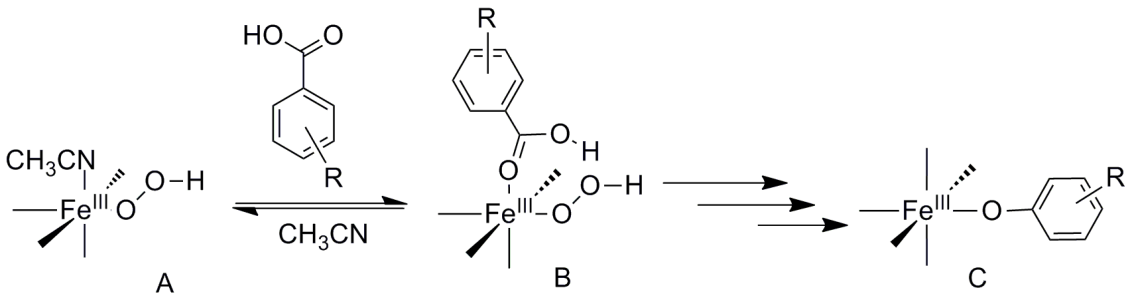

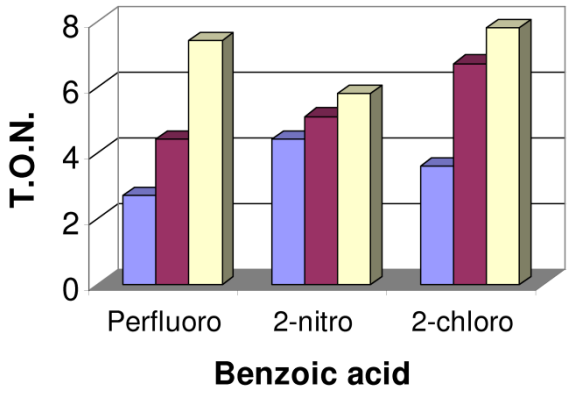

Figure 3.4: Phenol formation catalyzed 1 (1 mM) with 10 equivalents of H_2O_2 as oxidant in the presence of 10 (lavender-blue), 25 (maroon) or 50 (yellow) equivalents of benzoic acids at room temperature. T.O.N. (Turn over number) was calculated as moles of product / mole of the catalyst.

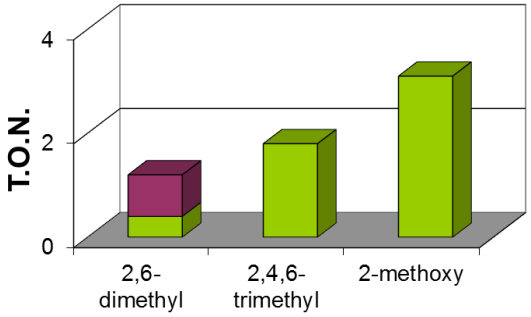

Figure 3.2 *Ipso*-hydroxylation performed by **1**/H_2O_2 in the presence of benzoic acids (**1**/H_2O_2/benzoic acid = 1/10/50) possessing electron donating substituents using the conditions as described in Figure 3.1. Phenol and quinone products observed are indicated by green and maroon blocks, respectively.

To gain further insight into the relative reactivities of the electron withdrawing benzoic acids with respect to **1**/H_2O_2, reactions were performed involving pairwise combinations of perfluoro-, 2-nitro- and 2-chlorobenzoic acids. These competition experiments (Figure 3.3, Table 3.1) showed that 2-chlorobenzoic acid was the easiest to oxidize and perfluorobenzoic acid was the hardest, consistent with the cumulative electron-withdrawing abilities of the substituents, as reflected by the pK_a's of the three acids. This trend may be rationalized by a) the lower affinity of the stronger acid for Fe^{III}-OOH (Scheme 3.1) and/or b) a greater difficulty in oxidizing the benzoate with more electron withdrawing substituents.

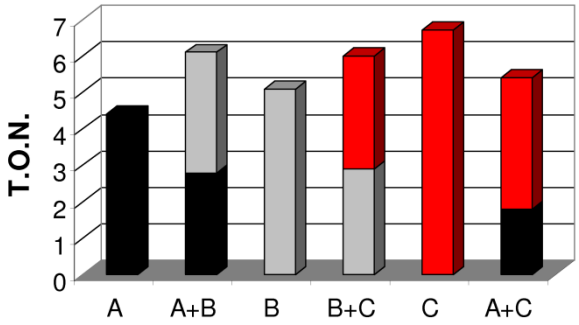

Figure 3.3: Competition reactions between any two of perfluoro- (A), 2-nitro- (B), and 2-chlorobenzoic acid (C) (25 equiv each with respect to **1**) and **1**/H_2O_2 (1/10) at room temperature. Data for the reactions of **1**/H_2O_2 and the individual benzoic acids (25 equiv with respect to **1**) are also shown for comparison. Black, gray, and red blocks depict amounts of perfluorophenol, 2-nitrophenol, and 2-chlorophenol, respectively.

Table 3.1: 1-catalyzed competitive *ipso*-hydroxylation of benzoic acids[a]

Benzoic acid	perfluorophenol	2-nitrophenol	2-chlorophenol
A	4.4 (1)		
A+B	2.8 (2)	3.3 (2)	
B		5.1 (1)	
B+C		2.9 (1)	3.1 (3)
C			6.7 (4)
A+C	1.8 (1)		3.6 (3)

[a] Reaction conditions: **1** (1 mM), 10 equiv H_2O_2, 25 equiv of each benzoic acid designated in acetonitrile at room temperature. A, B and C represent perfluoro-, 2-nitro-, and 2-chlorobenzoic acid, respectively.

3.3.1 Competition Between Olefin Oxidation and *ipso*-Hydroxylation

Complex **1** has been previously shown to be an effective catalyst for olefin epoxidation and *cis*-dihydroxylation using H_2O_2 as an oxidant.[53,63,167] Furthermore, the addition of acetic acid to the aforementioned catalytic system led to significantly increased formation of epoxide at the expense of *cis*-diol.[59,167] It was proposed that the presence of acetic acid changed the nature of the active oxidant in the catalytic reaction from $Fe^{V}(O)(OH)$, where one or both oxygen atoms could be transferred to the olefin substrate, to $Fe^{V}(O)(OAc)$, where only oxo-atom transfer could occur.[59] However, the effect of aromatic acids (e.g. benzoic acids) on olefin oxidation catalysis has not been investigated. It would be interesting to know how the addition of benzoic acids might affect the epoxide/*cis*-diol ratio and whether the oxidation of the arene ring was competitive with olefin oxidation.

Figure 3.4 presents the results of catalytic olefin oxidation experiments by **1**/H_2O_2 carried out with different amounts of added benzoic acid in the presence of a 100-fold excess of 1-octene or *tert*-butyl acrylate (relative to **1**); these results are also tabulated in Table 3.2. Olefin oxidation products (*cis*-diol and epoxide for 1-octene and *cis*-diol for *tert*-butyl acrylate) were observed in the reactions along with multiple turnovers of phenol, clearly suggesting that *ipso*-hydroxylation of the benzoic acids competes with olefin oxidation. Adding more benzoic acid increased the yield of phenol at the expense of the olefin oxidation products. The results of the competition experiments are similar for both 1-octene and *tert*-butyl acrylate (Figure 3.4), despite the fact that two olefins are quite different in terms of their electronic properties. Indeed in a previously reported competitive oxidation of 1-octene and *tert*-butyl acrylate in the absence of added benzoic acid, 1-octene oxidation products were favored by 4:1 over those of *tert*-butyl acrylate, indicating that 1-octene is the olefin more preferably oxidized by the **1**/H_2O_2 combination.[63] However, in all experiments presented in Figure 3.4, phenols were the dominant products. These results demonstrate that *ipso*-hydroxylation of the benzoic acids is favored over olefin oxidation, despite the lower concentration of the benzoic acid. This advantage may derive from the likely intramolecular nature of the *ipso*-hydroxylation versus the intermolecular nature of the olefin oxidation.

Table 3.2: Competitive olefin oxidation and *ipso*-hydroxylation experiments catalyzed by **1**[a]

Benzoic Acid	1-octene	10 equiv acid			25 equiv acid			50 equiv acid		
		Phenol	Epox	Diol	Phenol	Epox	Diol	Phenol	Epox	Diol
perfluoro	0	2.7 (2)			4.4 (1)			7.4 (3)		
	100	4.0 (2)	0.5 (1)	1.4 (1)	4.2 (3)	0.4 (1)	0.9 (1)	4.3 (3)	0.4 (1)	1.0 (4)
	250				3.4 (3)	1.2 (1)	2.1 (2)			
	500				2.6 (2)	1.8 (4)	1.7 (2)			
	1000				1.8 (2)	2.0 (3)	1.5 (5)			
2-nitro	0	4.4 (2)			5.1 (1)			5.8 (1)		
	100	3.6 (2)	0.3 (2)	1.1 (4)	4.2 (3)	0.2 (1)	1.1 (2)	4.6 (2)	0	0.4 (2)
	250				3.8 (4)	0.6 (2)	1.0 (3)			
	500				3.3 (3)	1.2 (3)	1.0 (3)			
	1000				2.9 (4)	1.5 (5)	0.9 (3)			
2-chloro	0	3.6 (2)			6.7 (4)			7.8 (1)		
	100	4.8 (2)	0	3.2 (4)	6.8 (2)	0	1.0 (2)	8.0 (3)	0	0.5 (1)
	250				7.1 (5)	0	1.0 (1)			
	500				7.2 (3)	0	1.3 (2)			
	1000				6.8 (4)	0	1.5 (3)			

	tert-butyl acrylate	10 equiv acid			25 equiv acid			50 equiv acid		
		Phenol	Epox	Diol	Phenol	Epox	Diol	Phenol	Epox	Diol
perfluoro	0	2.7 (2)			4.4 (1)			7.4 (3)		
	100	4.1 (1)	0	3.1 (4)	5.4 (3)	0	2.1 (1)	6.2 (2)	0	1.5 (1)
2-nitro	0	4.4 (2)			5.1 (1)			5.8 (1)		
	100	3.3 (1)	0	1.9 (4)	4.1 (2)	0	1.2 (5)	4.8 (1)	0	0.5 (2)
2-chloro	0	3.6 (2)			6.7 (4)			7.8 (1)		
	100	3.7 (4)	0	2.3 (5)	6.4 (4)	0	1.0 (5)	7.8 (2)	0	0.6 (3)

[a] Competitive oxidations carried out in acetonitrile at room temperature with 1 mM **1**, 10 equiv H_2O_2, and 100 equiv olefin in the presence of various amounts of the listed benzoic acid. H_2O_2 was delivered by a syringe pump over 25 min with an additional 5 min of stirring before the reaction was worked up. Values listed reflect the average of at least three experiments. A TON value of 0 is listed for experiments where the actual TON is < 0.1.

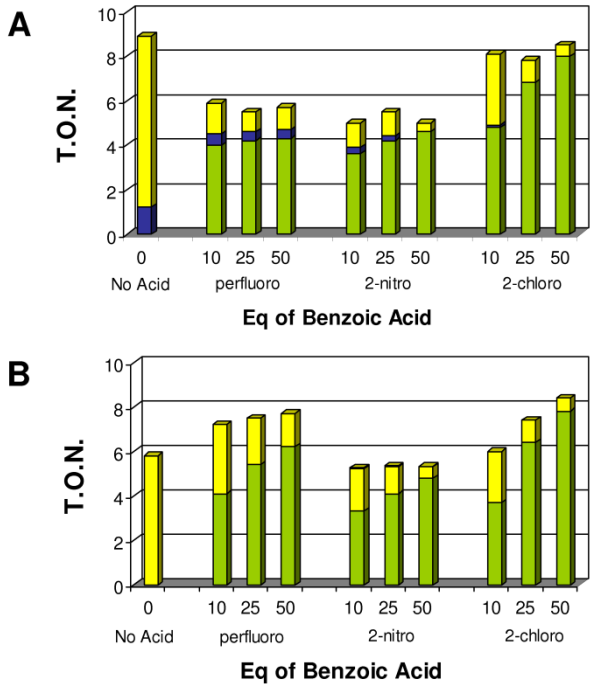

Figure 3.4: 1-octene (A) and *tert*-butyl acrylate (B) oxidation by H_2O_2 with 1 mM **1** as catalyst at room temperature (**1**/H_2O_2/1-octene = 1/10/100) in the presence of different amounts of substituted benzoic acids. Green, blue and yellow blocks represent phenol, epoxide, and *cis*-diol products, respectively.

Figure 3.5 and Table 3.2 present results of experiments where the amount of olefin added was varied from 100 to 1000 equivalents in the presence of 25 equiv benzoic acid, resulting in an increase in the yields of olefin oxidation products. For 2-chlorobenzoic acid (Figure 3.5C), the amount of 2-chlorophenol formed remained constant at about 6.9 TON, while the amount of *cis*-diol product increased from 1 to 1.5 TON; however, less

than 0.1 TON epoxide was observed. For 2-nitrobenzoic acid (Figure 3.5B), the amount of *cis*-diol product remained approximately constant at 1 TON, but the yield of epoxide increased at the expense of phenol, with the combined amount of phenol and epoxide holding constant at about 4.4 TON. In this series of experiments, the diol-to-epoxide ratio of 7 observed in the absence of added acid decreased to 0.6 upon addition of 1000 equiv 1-octene (Table 3.2). A similar behavior was observed for perfluorobenzoic acid (Figure 3.5A), with epoxide yield increasing at the expense of phenol and the combined amount of phenol and epoxide remaining at about 4 TON. Interestingly for this acid, the amount of *cis*-diol formed increased from 0.9 TON at 100 equiv 1-octene to 2.1 TON at 250 equiv, which then decreased with more added olefin. Similar to that observed for 2-nitrobenzoic acid, the diol-to-epoxide ratio in the presence of 1000 equiv of 1-octene decreased from 7 in the absence of acid to 0.8 in its presence. These results demonstrate the likely participation of multiple equilibria and oxidation pathways that determine the outcome of the catalysis experiments.

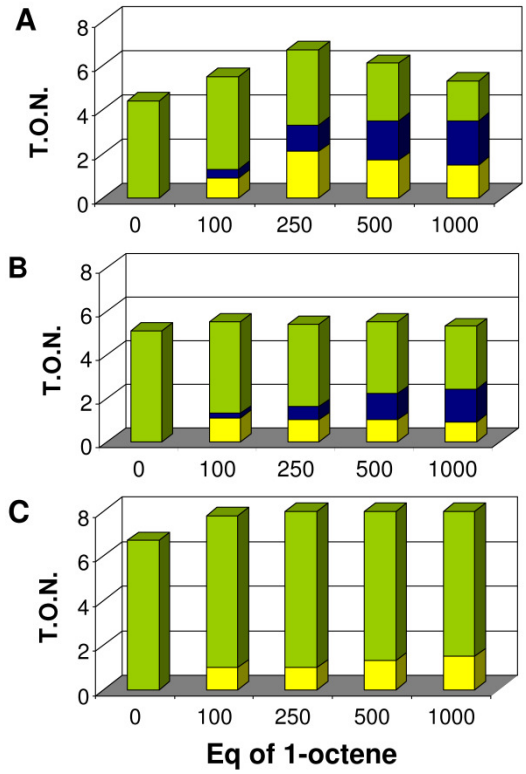

Figure 3.5: Oxidation of perfluorobenzoic acid (A), 2-nitrobenzoic acid (B) and 2-chlorobenzoic acid (C) catalyzed by **1** (1 mM) with H_2O_2 as oxidant in the presence of variable amounts of 1-octene at room temperature (**1**/H_2O_2/substituted benzoic acid = 1/10/25). Yellow, blue, and green blocks represent *cis*-diol, epoxide, and phenol, respectively.

The preference of **1**-catalyzed oxidation for *ipso*-hydroxylation could be counteracted by the addition of water. Experiments carried out by introducing varying amounts of water at a fixed concentration of acid and olefin (Figure 3.6) showed that water competes with the

benzoic acid in determining the nature of the products. The results indicated that higher amounts of water in the medium increased the yield of *cis*-diol at the expense of phenol formation, while epoxide yield remained relatively low in all experiments, unlike the results presented in Figure 3.5. There would appear to be multiple equilibria that affect the outcome of these catalytic oxidation experiments.

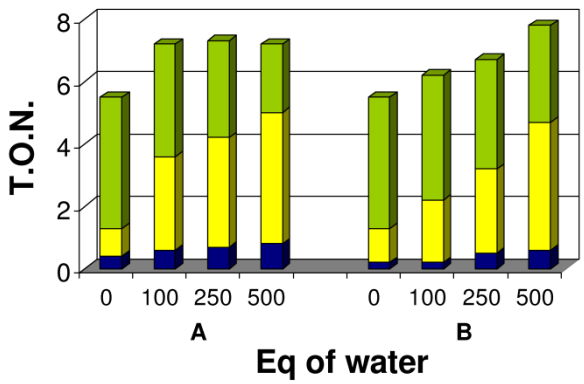

Figure 3.6: 1-octene oxidation catalyzed by **1** (1 mM) with H_2O_2 as oxidant at room temperature (**1**/1-octene/substituted benzoic acid/H_2O_2 = 1/100/25/10) in the presence of variable amounts of water. The left side (A) represents the results for perfluorobenzoic acid, while the right side (B) depicts the study with 2-nitrobenzoic acid. Blue, yellow and green blocks represent epoxide, *cis*-diol and phenol, respectively.

3.3.2 Labeling studies

^{18}O labeling experiments have previously provided important insights into the mechanism of olefin oxidation by the Fe^{II}TPA catalyst family[53] and are also useful in the present case for discerning the reaction pathways available. We showed previously that **1**-catalyzed olefin oxidations afforded epoxide products where about 10% of the incorporated oxygen atom derived from H_2O and the other 90% from H_2O_2, and *cis*-diol products where one O atom derived from H_2O and the other from H_2O_2.[53] The incorporation of label from H_2O implicated a water-assisted mechanism for O–O bond cleavage. By comparing the ^{18}O labeling results in the presence or absence of perfluorobenzoic acid, it should be possible to discern what effect the added benzoic acid has on the mechanism of **1**-catalyzed oxidation.

The ^{18}O labeling results are listed in Table 3.3. As previously reported, the addition of increasing amounts of $H_2{}^{18}O$ resulted in a greater incorporation of ^{18}O into the *cis*-diol and epoxide products in the absence of added benzoic acid. In the presence of 25 equiv $C_6F_5CO_2H$, the labeling outcome for the *cis*-diol was similar; however much less ^{18}O from $H_2{}^{18}O$ was incorporated into the epoxide product, as previously reported for **1**-catalyzed epoxidations in the presence of acetic acid.[59] Interestingly, in the complementary labeling experiment performed with 10 equiv of $H_2{}^{18}O_2$ in the presence of 1000 equiv from $H_2{}^{16}O$, there was almost no change in the extent of label incorporation for *cis*-diol in the presence and absence of added perfluorobenzoic acid, but the fraction of ^{18}O-labeled epoxide increased from 82% in the absence of added acid to

92% in the presence of 25 equiv of $C_6F_5CO_2H$. The same extent of ^{18}O label incorporation was also observed for perfluorophenol. Given that the H_2O_2 used was 90% ^{18}O labeled, the labeling of epoxide and phenol by $H_2{}^{18}O_2$ was essentially quantitative, implicating a common oxidant that effects these two oxidative transformations but is different from the oxidant that carries out the *cis*-dihydroxylation.

Table 3.3: The effect of added $C_6F_5CO_2H$ on the ^{18}O-label distributions in the products of **1**-catalyzed oxidation of 1-octene by H_2O_2[a]

Equiv added	No Acid					25 equiv $C_6F_5CO_2H$						
	1,2-epoxyoctane		1,2-octanediol			1,2-epoxyoctane		1,2-octanediol			Phenol	
	^{16}O	^{18}O	$^{16}O^{16}O$	$^{16}O^{18}O$	$^{18}O^{18}O$	^{16}O	^{18}O	$^{16}O^{16}O$	$^{16}O^{18}O$	$^{18}O^{18}O$	^{16}O	^{18}O
200 $H_2{}^{18}O$	96	4	43	57	-	100	-	46	54	-	100	-
500 $H_2{}^{18}O$	93	7	32	68	-	98	2	38	62	-	100	-
1000 $H_2{}^{18}O$	91	9	23	77	-	98	2	31	69	-	100	-
10 $H_2{}^{18}O_2$[b]	18	82	5	92	3	8	92	5	93	2	9	91

[a] Reaction conditions: **1**(1 mM)/H_2O_2/1-octene = 1/10/1000 in acetonitrile at room temperature.

[b] The commercially available 2% aqueous solution of $H_2{}^{18}O_2$ contains a 1:100 molar ratio of $H_2{}^{18}O_2$ and $H_2{}^{16}O$.

3.4 Mechanistic Insights

Scheme 3.2 depicts our current understanding of the mechanistic landscape for **1**-catalyzed olefin oxidation and *ipso*-hydroxylation, which takes into account the results from this paper and from our previous work on olefin oxidation[53,29] and arene ring oxidation.[140] The iron(III)-hydroperoxo species (**P1**), generated from the reaction of **1** and H_2O_2, has been trapped and characterized in detail by various spectroscopic techniques, namely UV-vis,[79] ESI-MS,[79] EPR[79,132] and resonance Raman spectroscopy.[86,132] We propose that intermediate **P1** is the branching point in the reaction of **1** and H_2O_2 leading to the formation of various high-valent iron oxidants. The eventual fate of **P1** is dependent on what is bound at the labile sixth site and can be tracked by monitoring the percent ^{18}O incorporation into the products. The addition of a large excess of H_2O results in the displacement of the CH_3CN ligand on **P1** to form the aquated intermediate **P2**. Decay of **P2** via a water-assisted heterolytic O-O bond cleavage step affords the $Fe^{V}(O)(OH)$ (**O2**) oxidant where the oxo atom derives from H_2O_2 and the hydroxo O atom derives from H_2O. These notions are corroborated by ^{18}O-labeling experiments (Table 3.3). Olefin oxidation in the presence of 1000 equiv $H_2{}^{18}O$ results in the incorporation of ^{18}O label into the oxidation products with 9% into the epoxide and 77% into one oxygen atom of the *cis*-diol. The complementary labeling experiment carried out with a 2% solution of $H_2{}^{18}O_2$ (containing 100 equiv $H_2{}^{16}O$ per equiv $H_2{}^{18}O_2$ added) confirms the $H_2{}^{18}O$ result, where the epoxide product is 82% labeled and 92% of the *cis*-diol is singly labeled.

As the amount of excess H_2O is decreased, the extent of water incorporation into the olefin oxidation products diminishes, as expected. For example, with 20 equiv added $H_2{}^{18}O$ (per H_2O_2 used), there is a significant fraction (~45%) of the *cis*-diol that is unlabeled (Table 3.3), implying that both oxygen atoms of H_2O_2 must be incorporated into the *cis*-diol for this subpopulation. Thus **P1** itself must be involved in *cis*-dihydroxylation via a non-water-assisted mechanism that cleaves the O–O bond of the iron(III)-hydroperoxo intermediate and delivers both the O atoms to the *cis*-diol product. In fact, such a non-water-assisted O–O bond cleavage to form a $Fe^V(O)(OH)$ species (**O1**) has been proposed on the basis of DFT calculations for the related FeBPMEN [BPMEN = *N,N′*-dimethyl-*N,N′*-bis(2-pyridylmethyl)ethane-1,2-diamine] complex and found to be energetically viable.[168] Thus, both **P1** and **P2** participate in this mechanistic landscape, with their respective involvement being determined by the extent of solvent exchange between MeCN and H_2O.

The addition of carboxylic acids complicates this mechanistic landscape by introducing yet another potential ligand that can displace the CH_3CN solvate from **P1**. In the case of added acetic acid, olefin oxidation yields predominantly epoxide, with the epoxide O-atom derived exclusively from H_2O_2.[59] These results can be rationalized by the formation of an $Fe^V(O)(O_2CR)$ (**O3**) oxidant from **P3** in a carboxylic-acid-assisted pathway. This oxidant acts mainly as an oxo transfer agent, converting the olefin substrate into epoxide. Lacking a bound hydroxo group, **O3** cannot effect olefin *cis*-dihydroxylation**,** although a small amount of a novel byproduct has been identified that derives from the transfer of

both the oxo and acetato groups to the substrate, resulting in the *cis*-hydroxyacetoxylation of the olefin.[169]

This same carboxylic-acid-assisted pathway can also be invoked to rationalize the results presented in this paper on the effect of adding benzoic acids with electron withdrawing substituents. With benzoate replacing acetate in **O3**, an additional wrinkle to the mechanism is introduced, as the benzoate can undergo oxidative decarboxylation and *ipso*-hydroxylation to afford phenol as a product. In fact, electron withdrawing benzoic acids are catalytically converted to phenols. The catalytic results presented in this paper demonstrate the existence of an equilibrium among **P1**, **P2**, and **P3**, as indicated by an increase in the yields of phenol products as more benzoic acid is added to the catalytic oxidation system (Figure 3.1) and a corresponding decrease when water is added (Figure 3.6). When olefin is present in the reaction mixture, there is a competition between *ipso*-hydroxylation and olefin epoxidation that is affected by the relative amounts of benzoic acid and olefin (Figures 3.4 and 3.5) and the phenol and epoxide products exhibit the same extent of label incorporation from $H_2{}^{18}O_2$ (Table 3.3), suggesting that they share a common oxidant.

The observed oxidative decarboxylation and *ipso*-hydroxylation of electron withdrawing benzoic acids is postulated to occur via intermediate **O3**. Internal electron transfer from the bound benzoate to the Fe^{V}=O center generates a carboxyl radical and an Fe^{IV}=O species, which then re-combine after loss of CO_2 to form the *ipso*-hydroxylated product.

However, it is also plausible for the decay of **P3** to bypass **O3** entirely and proceed directly by O–O bond homolysis to generate the carboxyl radical and the Fe^{IV}=O species. Figure 3.5 shows data that strongly disfavor the homolysis alternative. With the amount of perfluorobenzoic acid held constant at 25 equiv, the introduction of 1-octene resulted in the formation of the corresponding epoxide and diol products. Interestingly, as the 1-octene concentration increased, the yield of *cis*-diol changed by a factor of 2, but the amount of epoxide formed grew five- to seven-fold. Thus, the diol-to-epoxide ratio decreased from 7:1 in the absence of the acid to 0.8:1 in its presence. Furthermore the epoxide appeared to form at the expense of the phenol product. In our interpretation of the data, the amount of diol formed reflects the extent to which the water-assisted pathway is operating, consistent with the amount of label incorporation into the diol from $H_2{}^{18}O$ (Table 3.3). However, in the presence of perfluorobenzoic acid, label incorporation into the epoxide decreased from $H_2{}^{18}O$ and increased from $H_2{}^{18}O_2$. Both observations are consistent with a switch in the oxidant that forms epoxide from **O2** in the absence of added perfluorobenzoic acid to **O3** in its presence (Table 3.3). Thus there is a competition between *ipso*-hydroxylation of the bound perfluorobenzoate and the epoxidation of added 1-octene, an outcome that can only be rationalized by the involvement of **O3**, which is derived from the carboxylic-acid-assisted heterolysis of the O–O bond of **P3**. A similar reactivity pattern was observed for 2-nitrobenzoic acid (Figure 3.5B). In the case of 2-chlorobenzoic acid (Figure 3.5C), less than 0.1 equiv epoxide could be detected under all conditions studied; the very low yield of epoxide may be attributed to the greater ease of oxidizing 2-chlorobenzoate versus perfluoro- or 2-nitrobenzoate. A similar competition

between olefin epoxidation and oxidative decarboxylation has been noted previously for the catalysis of olefin epoxidation by **1**/H_2O_2 in the presence of phenylacetic acid, where the yield of epoxide was correlated inversely with the yield of benzaldehyde, which derived from oxidative decarboxylation of the acid.[59] In the case of acetic acid, **O3** appears directed only towards the olefin epoxidation.

Lastly, the absence of any label incorporation from $H_2{}^{18}O$ into C_6F_5OH (Table 3.3) excludes the participation of the Fe^V=O oxidant **O2** in *ipso*-hydroxylation. Were the water-assisted pathway also involved in *ipso*-hydroxylation, the phenol would have been partially ^{18}O labeled, resulting from the formation of **O3'** from **O2** by ligand exchange after the oxo/hydroxo tautomerization of **O2** had occurred (Scheme 3.2). That the water-assisted pathway is not involved is supported by the essentially quantitative incorporation of label from $H_2{}^{18}O_2$ in the C_6F_5OH product (91% from 90% labeled peroxide). Also, the almost identical ^{18}O label distribution in *cis*-diol with $H_2{}^{18}O_2$ in the presence or absence of added perfluorobenzoic acid further emphasizes that *cis*-dihydroxylation derives purely from the water-assisted pathway (via **P2** and **O2**). The clear difference in labeling outcomes for the diol and the phenol products demonstrates that olefin *cis*-dihydroxylation and *ipso*-hydroxylation must result from two related but distinct reaction pathways that involve two different Fe^V=O oxidants.

These mechanistic speculations are supported by recent EPR evidence reported by Talsi and co-workers that suggest the trapping of an Fe^V=O oxidant in the reaction of **1** and

peracids at -70 °C.[153] This transient S = ½ species was shown to decay at a rate dependent on the concentration of the added olefin and found to yield epoxide, demonstrating its involvement in olefin epoxidation. However, direct proof of the iron oxidation state of the epoxidizing species was not obtained; such proof will be essential to place the mechanistic landscape of Scheme 3.2 on even firmer ground.

Scheme 3.2: Mechanistic landscape for oxidations by the non-heme iron catalyst **1** with H_2O_2 as oxidant. **P** and **O** represent the various proposed iron-hydroperoxo and iron-oxo intermediates, respectively.

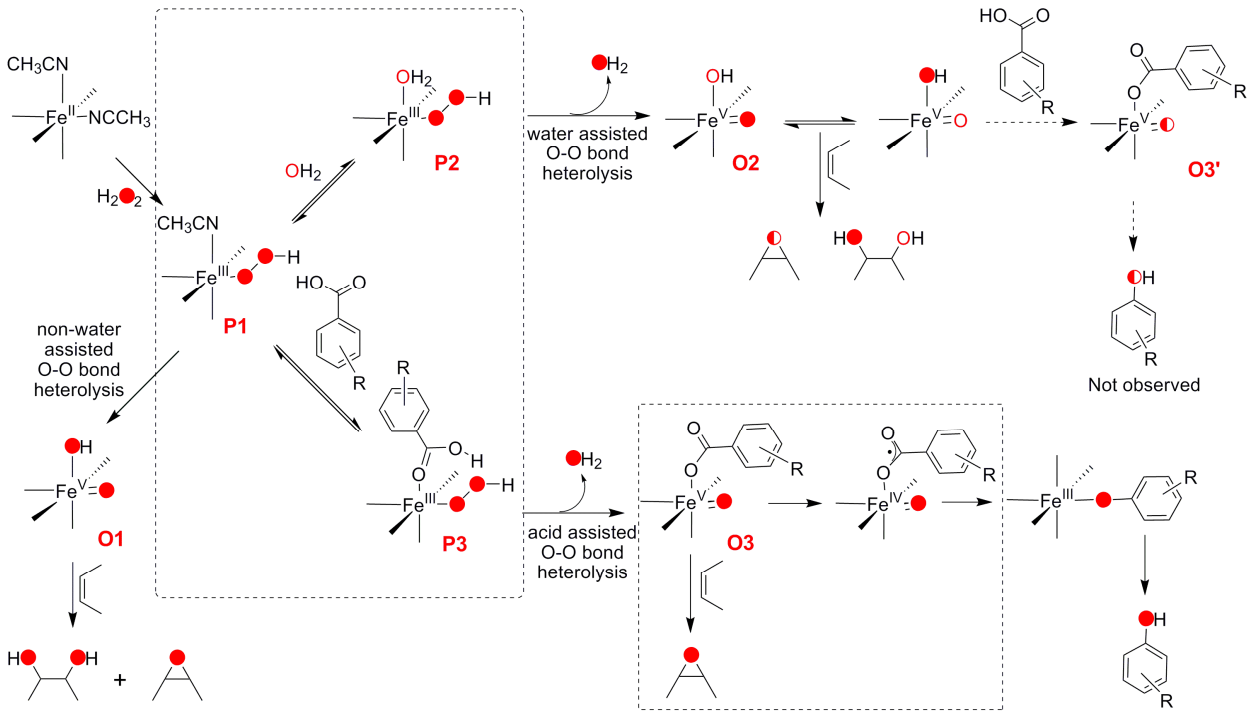

Acknowledgment. This work was supported by a grant from the U.S. Department of Energy (FFG02-03ER15455 to L.Q.).

Chapter 4

Kinetics of the O–O Bond Cleavage Step in Fe(TPA)/H_2O_2-Catalyzed Oxidative Transformations

4.1 Introduction

O–O bond cleavage is one of the most fundamental processes in the oxidation chemistry. In Nature, O_2 activation towards oxidative transformations involves the cleavage of the O–O bond in both heme[170,171] and non-heme[1,12] iron enzymes. The functioning of Cytochrome P450,[2,172,173] chloroperoxidase,[174] horseradish peroxidase,[174,175] some of the most studied heme enzymes, involve the rate limiting cleavage of the O–O bond leading to the generation of the oxidant compound I.[145,170,171,176,177] Similarly, in the iron-porphyrin chemistry, it is shown that the iron(IV)-oxo porphyrin π-cation radical, generated from the O–O bond cleavage is the active oxidant.[145,178-181] O–O bond cleavage is also proposed to be a very important step in the reaction cycle of non-heme iron enzyme α-ketoglutarate-dependent dioxygenases.[12,31,182] O–O bond cleavage of the iron(III)-peroxo species, which occurs at the iron containing active site of both of the heme and non-heme enzymes, leads to the generation of various high-valent iron-oxo species responsible for C-H bond hydroxylation, olefin oxidation, and aromatic hydroxylation. It is therefore important to understand the nature of the O–O bond cleavage in the iron/dioxygen chemistry. While the O–O bond cleavage is well documented in heme[183] and porphyrin[184,185] systems, there is a need to enhance our understanding on the non-heme side. In our non-heme model systems, the availability of the intermediates, such as iron(III)-hydroperoxo,[79,132,186,187] makes it easier to study the process of O–O bond cleavage in detail.

The iron(III)-hydroperoxo intermediates are good starting points to monitor the cleavage of the O–O bond that ultimately generates high-valent species: Fe^{IV}=O (via homolysis) and Fe^{V}=O (via heterolysis). Although homo- and heterolytic cleavage of the O–O bond in the same system has been documented in heme[188] and porphyrin[189] chemistry, no such direct comparison exists to date for non-heme iron complexes. It is therefore important to study these cleavage patterns in detail to enhance our understanding.

Complex **1** (Figure 4.1), as a prototypical example of the pyridylamine-based non-heme iron system, was shown over the past decade to effect various oxidative transformations like alkane oxidation,[52,57,79] olefin epoxidation[53,59] and *cis*-dihydroxylation[53,58] and regioselective aromatic hydroxylation[140,190] with the help of H_2O_2 as the oxidant in the acetonitrile solvent. The detailed characterization of the iron(III)-hydroperoxo intermediate $[Fe^{III}(TPA)(OOH)]^{2+}$ (**1a**)[79,86,132] made it more useful in studying the reaction mechanisms. The observation of incorporation of the O-atom from H_2O into cyclohexanol and into *cis*-cyclooctene oxide and *cis*-1,2-octanediol products suggested that $Fe^{V}(O)(OH)$ is the active oxidant in the case of hydrocarbon oxidation.[52,53] The addition of acetic acid to the reaction medium changed the nature of the oxidant to $Fe^{V}(O)(OAc)$ from $Fe^{V}(O)(OH)$ and made the catalyst epoxide selective (quantitative conversion in the case of *cis*-cyclooctene).[59] Similarly, the addition of benzoic acid in the **1**/H_2O_2-catalyzed reaction led to the formation of the $Fe^{V}(O)(O_2CAr)$ oxidant that led to both *ortho*- and *ipso*-hydroxylation of arenes.[140] While *ortho*-hydroxylation led to the stoichiometric formation of the stable six-membered iron(III)-salicylate chelate, *ipso*-

hydroxylation was shown to be catalytic.[190] Interestingly, the important step for all of these transformations is the conversion of the iron(III)-peroxo species to the iron(V)-oxo species, essentially the heterolytic cleavage O–O bond leading to the 2 e^- oxidation of the iron center. Interestingly, the observation and detailed characterization of a different iron(III)-peroxo intermediate, $[Fe^{III}(TPA)(\kappa^2\text{-}OOC(CH_3)_2OH)]^{2+}$ (**1c**), was also reported in acetone.[132] The intermediate **1c** decayed to the Fe^{IV}=O species with an isosbestic point, suggesting an O–O bond homolysis. However, **1**/H_2O_2 in acetone showed a lower conversion efficiency in both cyclohexane and *cis*-cyclooctene oxidation than in acetonitrile. We discuss below the detailed kinetic studies involving these oxidative processes.

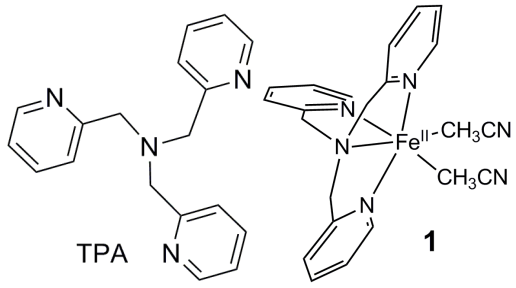

Figure 4.1: Structures of the TPA ligand and the corresponding iron(II) complex **1**.

4.2 Experimental Section

4.2.1 Materials and Methods

All chemicals and solvents were purchased from Aldrich and were used without additional purification unless otherwise noted. CH_3CN and $(CH_3)_2CO$ were dried over CaH_2 before use. $H_2{}^{18}O_2$ (90% ^{18}O-enriched) and D_2O_2 were purchased from Isotec (Sigma-Aldrich) Inc. The complex $[Fe^{II}(TPA)(CH_3CN)_2](OTf)_2$ (**1**) was prepared in an anaerobic glovebox according to the published procedures.[134] Product analyses were performed on a Perkin-Elmer Sigma 3 gas chromatograph (AT-1701 column, 30 m) with a flame ionization detector. GC-MS experiments were carried using an HP 6890 gas chromatograph (HP-5 column, 30 m) with an Agilent 5973 mass detector.

4.2.2 Kinetic Studies

Spectroscopic studies with $[Fe^{II}(TPA)(CH_3CN)_2](OTf)_2$ (**1**) were performed on a 1 mM CH_3CN solution in a 1-cm quartz cuvette precooled to the desired range of temperature (-40 °C to 25 °C). $[Fe^{III}(TPA)(OOH)(CH_3CN)]^{2+}$ (**1a**) species was generated by adding a 29 μL of a 0.7 M H_2O_2 (10 equiv) to **1** at -40 °C. To this solution 0.12 mL of a 0.33 M (20 equiv) 2-chlorobenzoic acid solution was added to generate the $[Fe^{III}(TPA)(OOH)(O_2C_7H_5\text{-}2\text{-}Cl)]^{2+}$ (**1b**). In the other cases of *ipso*-hydroxylation, a 0.4 mL of a 1.0 M (20 equiv) solution of $C_6F_5CO_2H$ and 2-chloro-6-nitrobenzoic acid, a 0.8 mL of a 0.5 M (20 equiv) solution of 2-nitrobenzoic and 2,6-dichlorobenzoic acid was added to the pre-generated **1a**. In the self-decay study of the $[Fe^{III}(TPA)(\kappa^2\text{-}$

$OOC(CH_3)_2OH)]^{2+}$ (**1c**) at -50 °C a 29 μL of a 0.7 M H_2O_2 (10 equiv) was added to **1** (1 mM). In the case of pyridine *N*-oxide-induced decay of **1c** at -90 °C, a 0.024 mL of a 1.0 M (12 equiv) solution of pyridine *N*-oxide was added. Reported kinetic results were carried out in triplicate unless mentioned otherwise.

4.2.3 Catalytic Studies

Catalysis studies were done in a mixed solvent of a 1/1 acetonitrile and aceic acid at -15 °C in a low-temperature reaction setup maintained by a cold bath. A 0.219 mL (200 equiv) or 1.098 mL (1000 equiv) of 6.37 M 1-octene solution was added to 1 mM **1**. For *cis*-cyclooctene reactions 0.192 mL of 7.29 M (200 equiv) substrate was added. Alternately 0.205 mL (200 equiv) of 6.82 M of *tert*-butyl acrylate and 0.7 mL (50 equiv), 1.4 mL (100 equiv) and 2.8 mL (200 equiv) of dimethyl fumarate was added. To this solution, added was 0.21 mL 10 M (300 equiv) H_2O_2 solution. The reaction was monitored and at the specified times, an aliquot of 0.25 mL was taken and added to a vial, containing 0.1 mL 1-methylimidazole, for quenching. After that, all the vials containing the reaction mixture quenched at different times were treated with acetic anhydride and external standard naphthalene was added to it. The reaction solution was extracted through a series of acid, base and water workup and analyzed for quantification with a GC. For experiments with **1** (1 mM) in acetone a 0.313 mL of 6.37 M 1-octene (1000 equiv) and 0.287 mL 70 mM H_2O_2 (10 equiv) were added at room temperature. Products were analyzed as mentioned above.

4.3 Results and Discussion

Complex **1** is a versatile non-heme iron catalyst, which with its simple ligand framework (Figure 4.1) and using H_2O_2 as an oxidant continues to catalyze various oxidative transformations: alkane[52] and olefin[53] oxidation and aromatic *ortho*- and *ipso*-hydroxylation.[140] Mechanistic studies on **1**/H_2O_2 system reported to date supported the idea of a common reaction landscape. Here in this chapter, we report detailed kinetic understanding of these oxidative catalytic processes.

4.3.1 Kinetics of *ipso*-Hydroxylation

Complex **1** was found to effect *ipso*-hydroxylation of benzoic acids[140] and the reaction was demonstrated to be catalytic with the electron withdrawing substituents at the *ortho-/para*-position of the ring.[190] It was also shown that the benzoic acids with more electron withdrawing substituents were harder to oxidize by **1**/H_2O_2 compared to the ones with fewer electron withdrawing groups, which was consistent with their electron-withdrawing abilities, as reflected by their corresponding pKa values.[190] Compared to the *ipso*-hydroxylation reaction reported at room temperature,[140,190] reactions were monitored at low temperatures using a cryostat and a diode array spectrophotometer to observe the involvement of any reactive intermediate.

The availability of the spectroscopically well characterized intermediate **1a** makes it a good starting point in monitoring the reaction by UV-vis spectroscopy (Figure 4.2). Interestingly, the *ipso*-hydroxylation of 2-chlorobenzoic acid led to the observation of an

intermediate with a λ_{max} at 550 nm, which decayed and ultimately led to the formation of a band centered at 576 nm (Figure 4.3A). The spin states of the two observed species were identified by EPR spectroscopy and revealed that the 550-nm and 576-nm species contain a low-spin iron(III) and a high-spin iron(III) center, respectively (Figure 4.3B and 4.3C). The 576-nm species was confirmed as an iron(III)-phenolate species upon comparing with the UV-vis spectrum of the independently generated $[Fe^{III}(TPA)(OC_6H_4\text{-}2\text{-}Cl)]^{2+}$ species from the reaction of $[Fe^{III}_2O(TPA)_2(H_2O)(ClO_4)](ClO_4)_3$ and 2-chlorophenol (Figure 4.4). The associated high-spin iron(III) signal in the EPR spectrum – in comparison of the spin states of the reported iron-phenolates[95,191,192] – also supported this assignment. The 550 nm chromophore, on the other hand, was proposed to be another low-spin iron(III)-hydroperoxo species the $([(TPA)Fe^{III}(OOH)(C_6H_4\text{-}2\text{-}Cl\text{-}CO_2H)]^{2+}$ (**1b**), where 2-chlorobenzoic acid displaced the solvate acetonitrile of **1a** by comparing it to our previous results with acetic acid, where acetic acid was proposed to bind at the iron center.[59] The notion of the binding of the benzoic acid ($ArCO_2H$) and not the benzoate anion ($ArCO_2^-$) was supported by the reaction of **1a** with $C_6F_5CO_2^-$ anion, where the addition of the anion led to the formation of the diiron species $[Fe^{III}_2(TPA)_2(\mu\text{-}O)(\mu\text{-}O_2CC_6F_5)]^{3+}$ (Figure 4.4). The formulation of the diiron species was confirmed by independent synthesis of the $[Fe^{III}_2(TPA)_2(\mu\text{-}O)(\mu\text{-}O_2CC_6F_5)]^{3+}$ complex[193] (Figure 4.6). Interestingly, the addition of perfluorobenzoic acid to the preformed **1a** at -40 °C did not yield any intermediate, but rather led to the formation of a visible band at λ_{max} = 520 nm (Figure 4.7). The addition of H_2O_2 to a pre-mixed solution of **1** and perfluorobenzoic acid

(reverse addition) also led to formation of the same chromophore. Similar to the 2-chlorobenzoic acid study, the identity of the 520 nm species as iron(III)-phenolate was affirmed by the identical UV-vis spectrum obtained with the independently generated $[Fe^{III}(TPA)(OC_6F_5)]^{2+}$ from the reaction of $[Fe^{III}_2O(TPA)_2(H_2O)(ClO_4)](ClO_4)_3$ and perfluorophenol (Figure 4.8) and corroborated by the high-spin iron(III) species observed by EPR spectroscopy (Figure 4.9). The $[Fe^{III}(TPA)(OC_6F_5)]^{2+}$ species could also be generated by reacting **1** with 1 equiv of $[Ce(NH_4)_2](NO_3)_6$ and 10 equiv of C_6F_5OH at -40 °C (Figure 4.10).

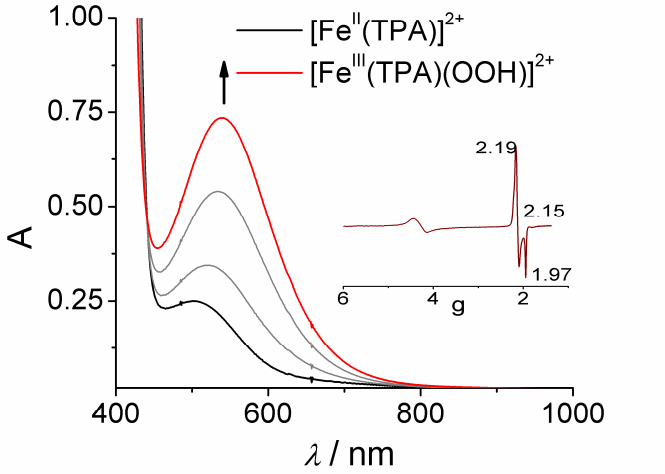

Figure 4.25: UV-vis spectral generation of **1a** starting from **1** (1 mM) and H_2O_2 (10 mM) at -40 °C. The inset shows the X-band EPR spectra of **1a** species recorded at 2.3 K.

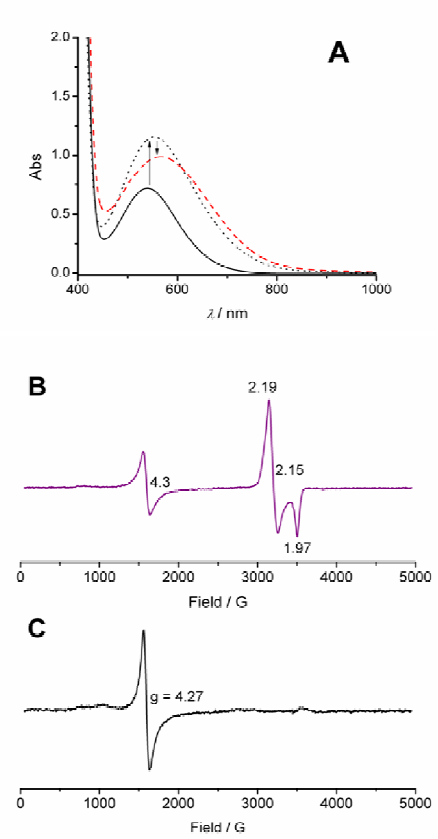

Figure 4.3: (A) The UV-vis spectrum of the reaction of **1**/H_2O_2 and 2-chlorobenzoic acid in acetonitrile at -40 °C. The low-spin hydroperoxo species **1a** (black solid spectrum) was converted to a new intermediate **1b** (black dashed spectrum) en route iron(III)-phenolate species (red dashed spectrum). (B) The X-band EPR spectrum of **1b**. (C) The X-band EPR spectrum of the $[Fe^{III}(TPA)(OC_6H_4Cl)]^{2+}$ species.

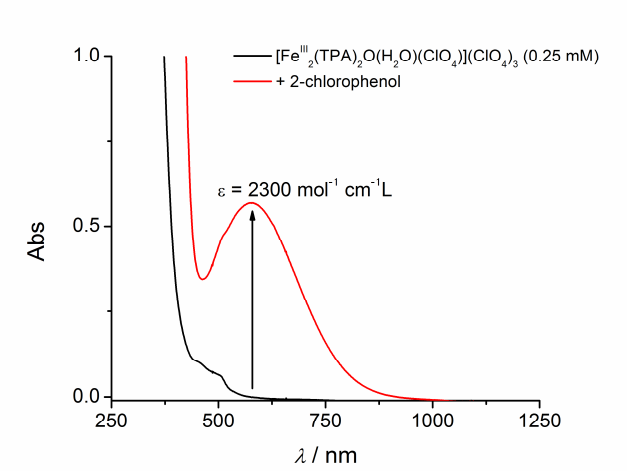

Figure 4.4: The formation of $[Fe^{III}(TPA)(OC_6H_4\text{-}2\text{-}Cl)]^{2+}$ from the reaction of $[Fe^{III}{}_2O(TPA)_2(H_2O)(ClO_4)](ClO_4)_3$ (0.25 mM) and 2-chlorophenol (15 mM) in acetonitrile at -40 °C.

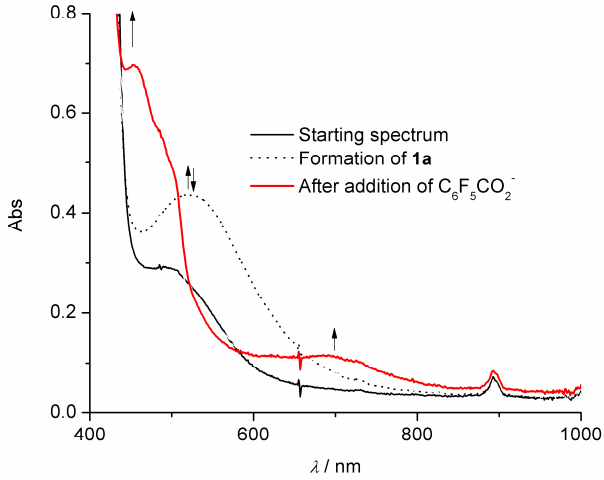

Figure 4.4: The addition of one equivalent of $C_6F_5CO_2^-$ to the preformed low-spin species **1a** at -40 °C. The spectra shown above contain a 1 mM iron solution.

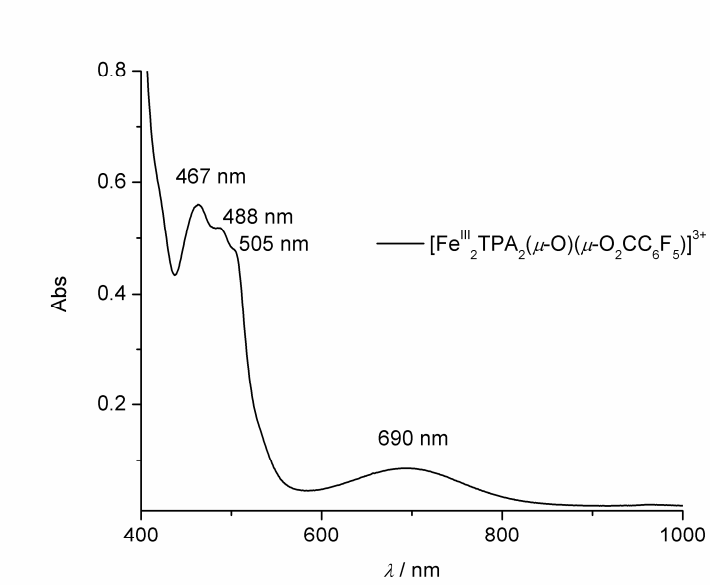

Figure 4.6: UV-vis spectrum of the independently synthesized $[Fe^{III}_2(TPA)_2(\mu\text{-}O)(\mu\text{-}O_2CC_6F_5)]^{3+}$ complex at room temperature. The spectrum contains a 1 mM solution of iron.

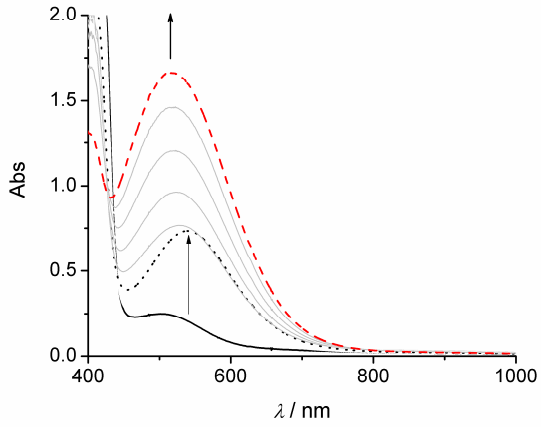

Figure 4.7: UV-vis spectra of the sample generated at -40 °C from **1** (1 mM, black solid line) upon addition of H_2O_2 (10 mM, black dotted line) and followed by the addition of $C_6F_5CO_2H$ (20 mM, red dashed line) using a 1-cm cuvette.

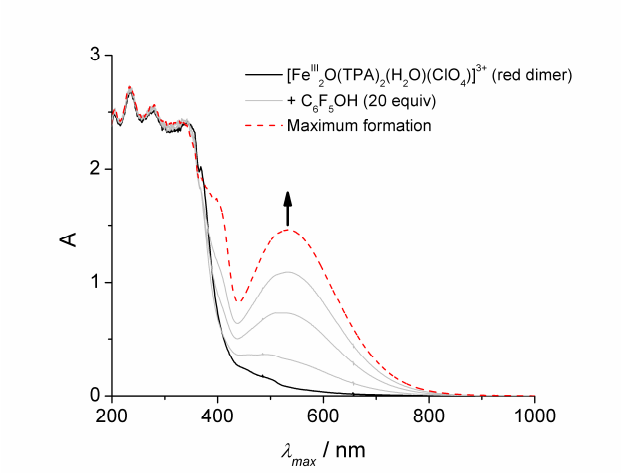

Figure 4.8: The formation of $[Fe^{III}(TPA)(OC_6F_5)]^{2+}$ from the reaction of $[Fe^{III}_2O(TPA)_2(H_2O)(ClO_4)](ClO_4)_3$ (1 mM) and perfluorophenol (20 mM) in acetonitrile at -40 °C.

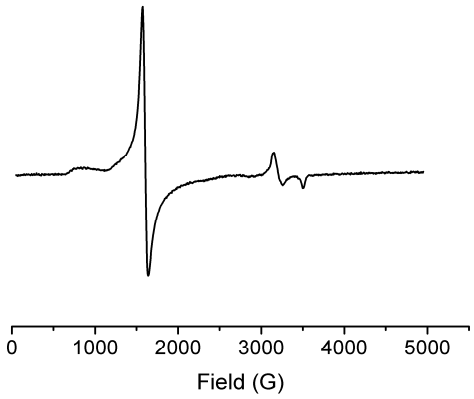

Figure 4.9: X-band EPR spectrum of the species generated from the reaction between **1a** with 20 eq $C_6F_5CO_2H$ in acetonirile at -40 °C.

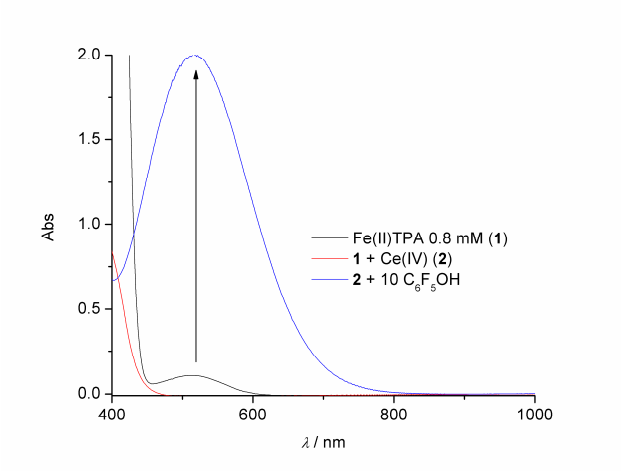

Figure 4.10: The UV-vis spectrum of the reaction of 1 mM **1** and 1 equiv of $[Ce(NH_4)_2](NO_3)_6$ at -40 °C in acetonitrile to generate iron(III) species. Upon addition of 10 equiv of C_6F_5OH to this solution led to the formation of $[Fe^{III}(TPA)(OC_6F_5)]^{2+}$ species.

To understand the kinetics of the *ipso*-hydroxylation reaction, we have monitored the formation of the iron(III)-phenolate species (520 nm band in the case of perfluorobenzoic acid) starting from **1a** at -40 °C. The kinetic data showed good fits to a first-order rate equation in the presence of a large excess (20 equiv) of perfluorobenzoic acid (Figure 4.11A). Similar fittings of the kinetic data to a first order rate equation were also observed in the *ipso*-hydroxylation of 2-nitro-, 2-chloro-6-nitro-, and 2,6-dichlorobenzoic acids (Figures 4.12, 4.13, and 4.14). The second order rate constants (k_2) were also determined by plotting the observed rates at different concentrations of substrates (Figure 4.15). The k_2 for 2-nitrobenzoic acid was 4 times higher than those of perfluoro- or 2-

chloro-6-nitrobenzoic acid (Table 4.1), suggesting that the lower number of electron withdrawing groups increased the rate of the reaction. Interestingly, this could be explained invoking the better binding in the case of 2-nitrobenzoic acid to the iron(III) center (A to B in Scheme 4.1) since its conjugate base is the strongest among the three used in the study.

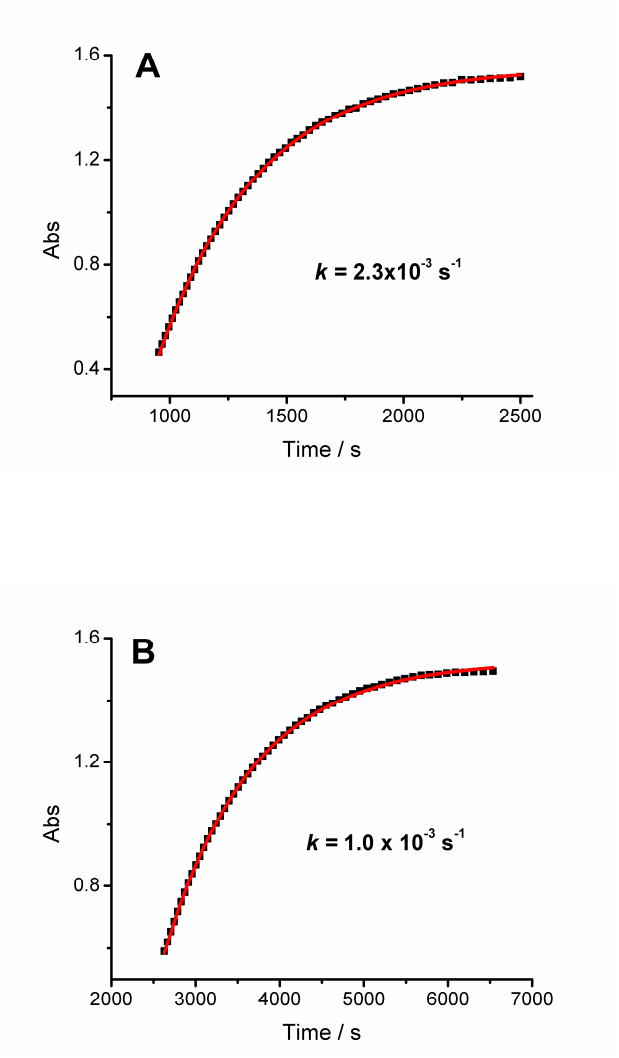

Figure 4.11: The kinetics of *ipso*-hydroxylation of perfluorobenzoic acid. 20 mM perfluorobenzoic acid was added to the pregenerated **1a** (by the reaction of 1 mM **1** and 10 equiv of H_2O_2 (A) and D_2O_2 (B)) at -40 °C.

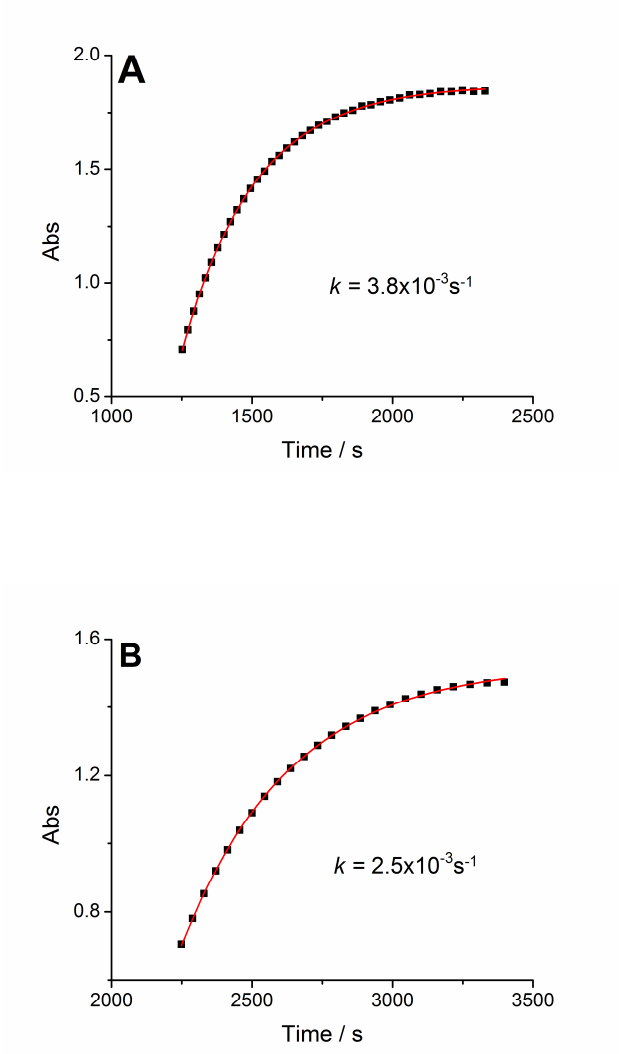

Figure 4.12: Kinetics of **1** (1 mM)/H_2O_2-catalyzed *ipso*-hydroxylation of 2-nitrobenzoic acid (20 mM) with (A) H_2O_2 and (B) D_2O_2 in acetonitrile at -40 °C.

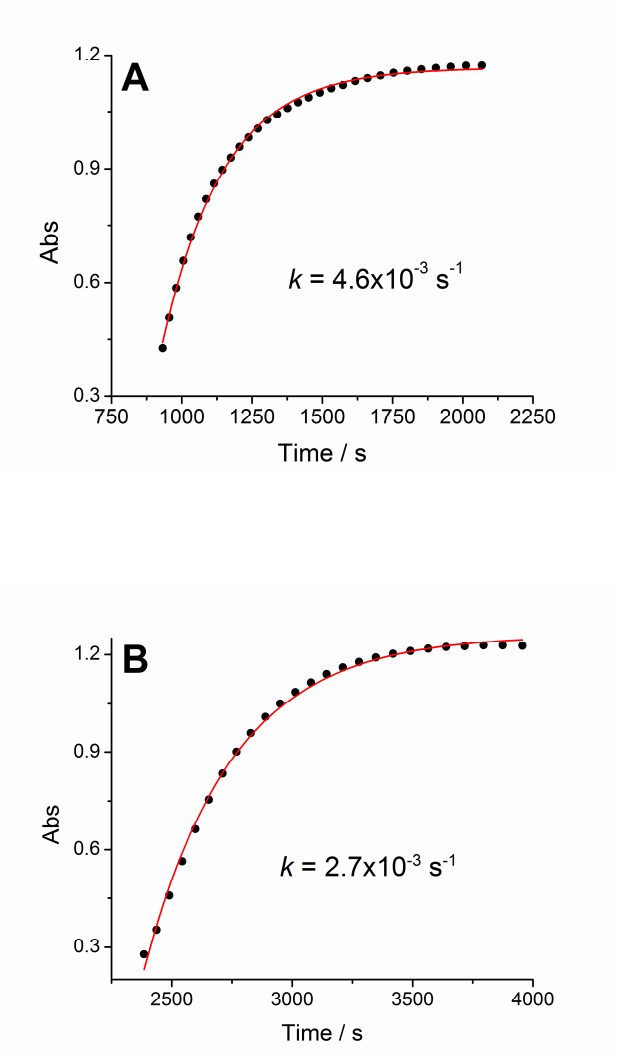

Figure 4.13: Kinetics of **1** (1 mM)/H_2O_2-catalyzed *ipso*-hydroxylation of 2-chloro-6-nitrobenzoic acid (20 mM) with (A) H_2O_2 and (B) D_2O_2 in acetonitrile at -40 °C.

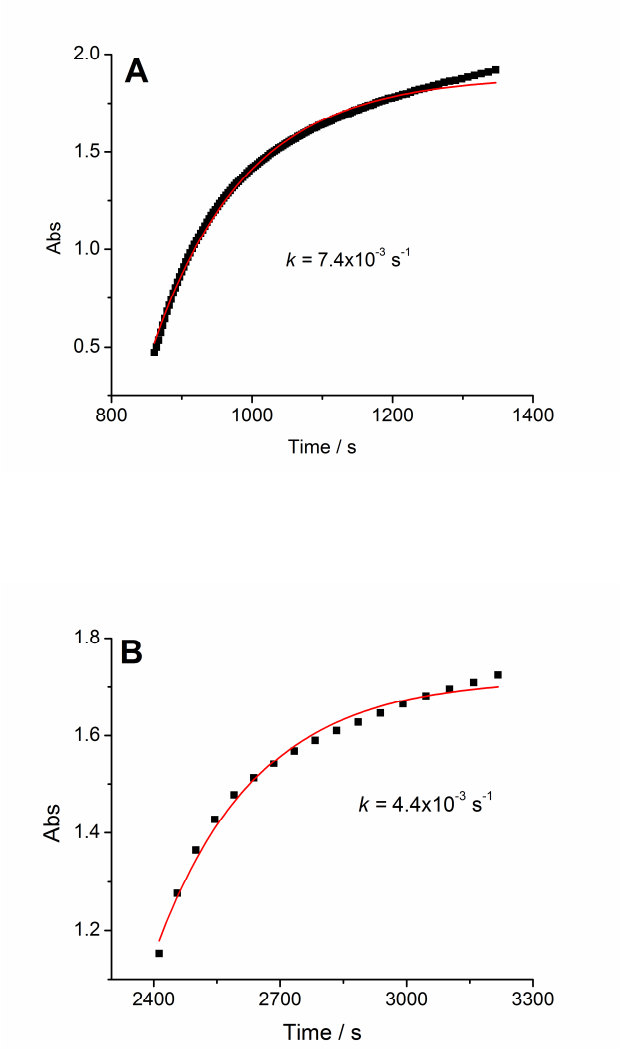

Figure 4.14: Kinetics of **1** (1 mM)/H_2O_2-catalyzed *ipso*-hydroxylation of 2,6-dichlorobenzoic acid (20 mM) with (A) H_2O_2 and (B) D_2O_2 in acetonitrile at -40 °C.

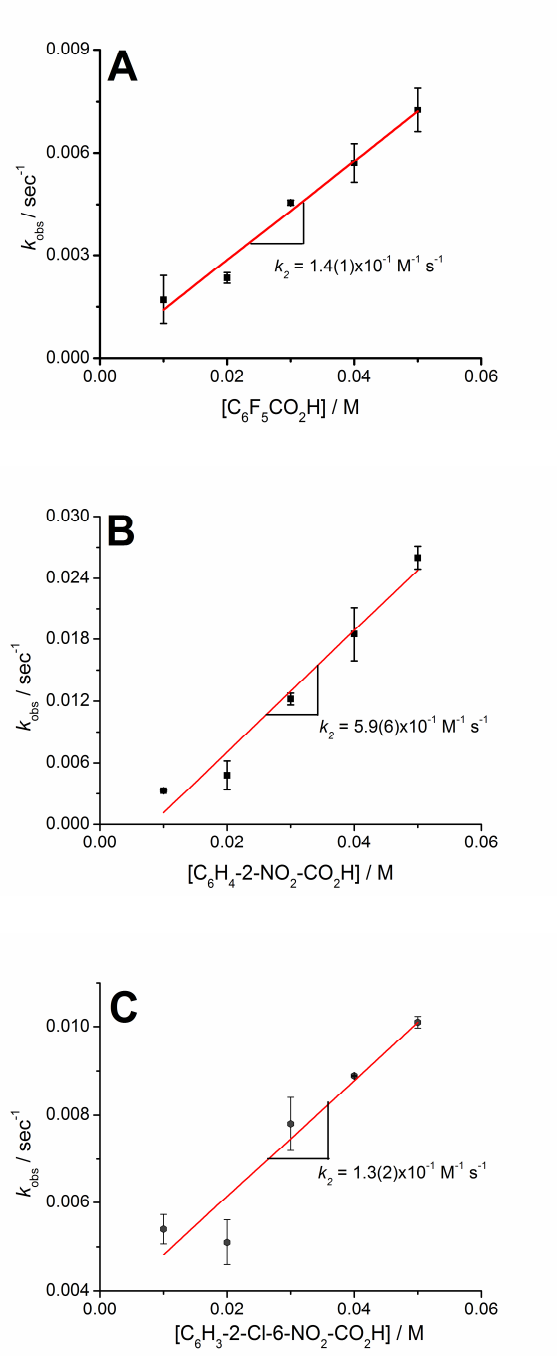

Figure 4.15: Perfluoro- (A), 2-nitro- (B), and 2-chloro-6-nitrobenzoic acid (C) concentration dependence on the rate of formation of the corresponding phenols from **1a** (generated via **1**/H_2O_2 in a 1/10 ratio) at -40 °C.

Table 4.1: Comparison of the second order rate constants for the formation of the $[Fe^{III}(TPA)(OAr)]^{2+}$ species from the $[Fe^{III}(TPA)(OOH)]^{2+}$ species with various benzoic acids

Benzoic acid	*pK_a*	*k_2 at -40 °C (M^{-1} s^{-1})*
2-Chloro-6-nitro	1.32	$1.3(2)x10^{-1}$
Perfluoro	1.88	$1.4(1)x10^{-1}$
2-Nitro	2.19	$5.9(6)x10^{-1}$

Scheme 4.1 depicts our proposed reaction mechanism for **1**-catalyzed *ipso*-hydroxylation of benzoates. It is also important to mention that in the investigation of the reaction mechanism of **1**/H_2O_2-catalyzed oxidations we took the spectroscopically well characterized $[Fe^{III}(TPA)(OOH)]^{2+}$ species[52,53,132] (**A** in Scheme 4.1) as the starting point in our mechanistic discussions. Upon addition of $ArCO_2H$ to **A**, the solvate acetonitrile is replaced with the benzoic acid (**B**) as observed in the case of 2-chlorobenzoic acid (Figures 4.3A and 4.3B). The pre-equlibrium binding of the benzoic acid to **A** is also reflected by the concentration dependence of benzoic acid on the rate of formation of the iron-phenolate (Figure 4.15). The addition of the acid leads to the protonation of the distal O atom of the hydroperoxo moiety in the rate limiting step to generate a putative high-valent Fe^{V}=O species (**C**). The 1-e^- oxidation of the bound benzoate by **C** leads to the formation of an Fe^{IV}=O species (**D**). Species **D** then undergoes decarboxylation and rebound at the *ipso* carbon to form the iron(III)-phenolate species (**E**). The quantitative retention of ^{18}O from $H_2{}^{18}O_2$ in the phenol product suggests a fast rate of rebound of the aryl radical to Fe^{IV}=O upon decarboxylation of **D**.[140]

Scheme 4.1: The proposed mechanism of *ipso*-hydroxylation of benzoates by **1**/H_2O_2.

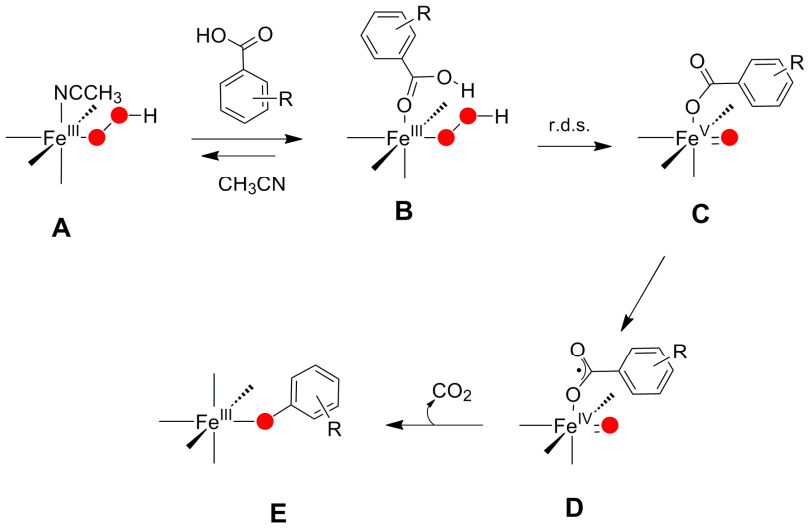

As the O–O bond cleavage was proposed as the rate determining step (r.d.s.) in *ipso*-hydroxylation (Scheme 4.1),[140,190] the rate of phenol formation would indicate the conversion of Fe^{III}-OOH to Fe^{V}=O species. This is essentially a two-electron oxidation of the iron center corresponding to the heterolysis of the O–O bond. Activation parameters for this process were measured from the Eyring plots (Figure 4.16). $\Delta H^{\neq}$ and $\Delta S^{\neq}$ values of 65 (2) $kJmol^{-1}$ and -14 (8) $Jmol^{-1}K^{-1}$ were obtained for $C_6F_5CO_2H$-assisted O-O bond cleavage. Activation parameters for the O–O bond cleavage of the **1**/H_2O_2-catalyzed *ipso*-hydroxylation of other acids (namely 2-nitro-, and 2-chloro-6-nitrobenzoic acids) were also determined over the same range of 50 °C and are listed in Table 4.2. The obtained data suggested that the $\Delta H^{\neq}$ values for this transformation were in the range of 50-60 $kJmol^{-1}$, while the $\Delta S^{\neq}$ values varied greatly.

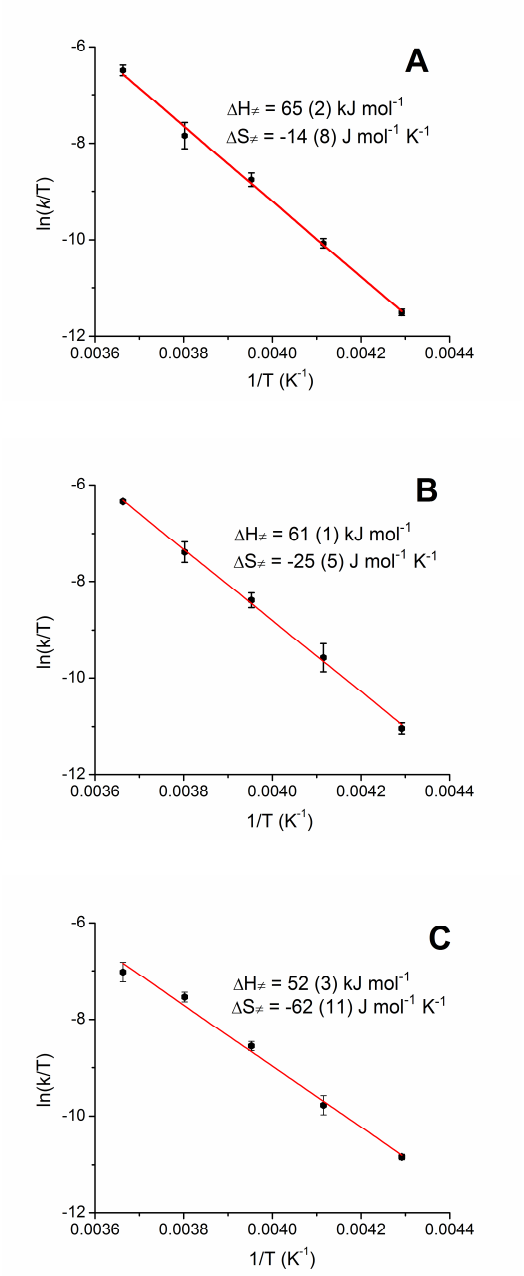

Figure 4.16: Eyring plots for the (A) perfluoro-, (B) 2-nitro-, and (C) 2-chloro-6-nitrobenzoic acid-catalyzed conversion of $[(TPA)Fe^{III}\text{-}OOH]^{2+}$ to $[(TPA)Fe^{III}(OAr)]^{2+}$ in acetonitrile in the temperature range of 0 to -40 °C upon addition of 20 mM substituted benzoic acid to 1 mM **1a**.

Table 4.2: List of activation parameters for homo- and heterolytic O–O bond cleavage of both heme and non-heme iron-peroxo species

Species/Reaction	*Homo- or heterolysis*	*k at -40 °C (s^{-1})*	*$\Delta H^{\neq}$ ($kJ\ mol^{-1}$)*	*$\Delta S^{\neq}$ ($J\ mol^{-1}\ K^{-1}$)*	*Ref*
$[Fe^{III}(TPA)(OOH)]^{2+}$ + $C_6F_5CO_2H$	Hetero	2.3 (2)×10^{-3}	65 (2)	-14 (8)	[a]
$[Fe^{III}(TPA)(OOH)]^{2+}$ + 2-Cl-6-NO_2-$C_6H_3CO_2H$	Hetero	4.6 (3)x10^{-3}	52 (3)	-62 (11)	[a]
$[Fe^{III}(TPA)(OOH)]^{2+}$ + 2-NO_2-$C_6H_4CO_2H$	Hetero	3.8 (4)×10^{-3}	61 (1)	-25 (5)	[a]
$[Fe^{III}(TPA)(OOH)]^{2+}$ + AcOH	Hetero	7.1 (4) ×10^{-3}	41 (2)	-110 (10)	[a]
$[Fe^{II}L_3]^{2+}$ + H_2O_2 (pH = 3 to 6)	Hetero	-	34 (2)	-150 (6)	194
$[Fe^{II}(TMC)]^{2+}$ + H_2O_2 + 2,6-lutidine	Hetero	-	29 (2)	-144 (10)	195
$[Fe^{III}(TMC)(OOH)]^{2+}$ + $HClO_4$	Hetero	3.0 (5) ×10^{-2}	44 (2)	-90 (10)	196
$[Fe^{III}(TPA)(OOR)]^{2+}$	Homo	1.25×10^{-3}	52 (1)	-74 (3)	197
$[Fe^{III}(TPA)(OOR)]^{2+}$ + PyO	Homo	1.8×10^{-1}	50 (2)	-42 (10)	197
$[(TPA)Fe^{III}(\kappa^2$-$O_2C(CH_3)_2OH)]$	Homo	3.3×10^{-2}	54 (3)	-35 (13)	132
$[Fe^{III}(TMP)(O_3CR_1)]$	Hetero	3.94×10^{-3}	23	-191	188
$[Fe^{III}(TMP)(O_3CR_1)]$ + 1-PhIm	Hetero	1.12×10^{-2}	15	-178	188
$[Fe^{III}(TMP)(O_3CR_2)]$	Homo	2.0×10^{-3}	31	-161	188
$[Fe^{III}(TMP)(O_3CR_2)]$ + 1-PhIm	Homo	3.3×10^{-3}	26	-180	188
$[(TMP)Fe^{III}$-O-O-$Fe^{III}(TMP)]$	Homo	-	61	-60	198

[a] This work

Abbreviations used: L_3 = bispidine, TMC = 1,4,8,11-tetramethyl-1,4,8,11-tetraazacyclotetradecane, TMP = dianionic form of Tetramesitylporphyrin, 1-PhIm = 1 – phenylimidazole, R = ^{t}Bu, R_1 = C_6H_4Cl, R_2 = CH_2Ph.

To check the involvement of a proton in the r.d.s. the kinetic isotopic effect (KIE = k_H/k_D) values for the conversion of **1a** to the iron(III)-phenolate species have also been determined for several of the benzoic acids (Table 4.3). To obtain a value of k_H/k_D, reactions were performed with H_2O_2 and D_2O_2 under identical experimental conditions. In the case of perfluorobenzoic acid, a KIE value of 2.3 was obtained (Figure 4.11). Similar KIE values of 1.7 were obtained with both 2-chloro-6-nitro-, 2,6-dichlorobenzoic acid (Figures 4.13 and 4.14), while 2-nitrobenzoic acid yielded a KIE value of 1.5 (Figure 4.12). The observed KIE values suggested the involvement of a proton in the rate limiting conversion of Fe^{III}–OOH to Fe^{V}=O via acid-assisted heterolysis of the O–O bond. The KIE values for all benzoic acids tried along with the KIE values are listed in Table 4.3. The determination of k_H/k_D at a higher temperature (-20 °C) for *ipso*-hydroxylation of perfluorobenzoic acid yielded a value of 2.0, lower than that observed at -40 °C (Figure 4.17).

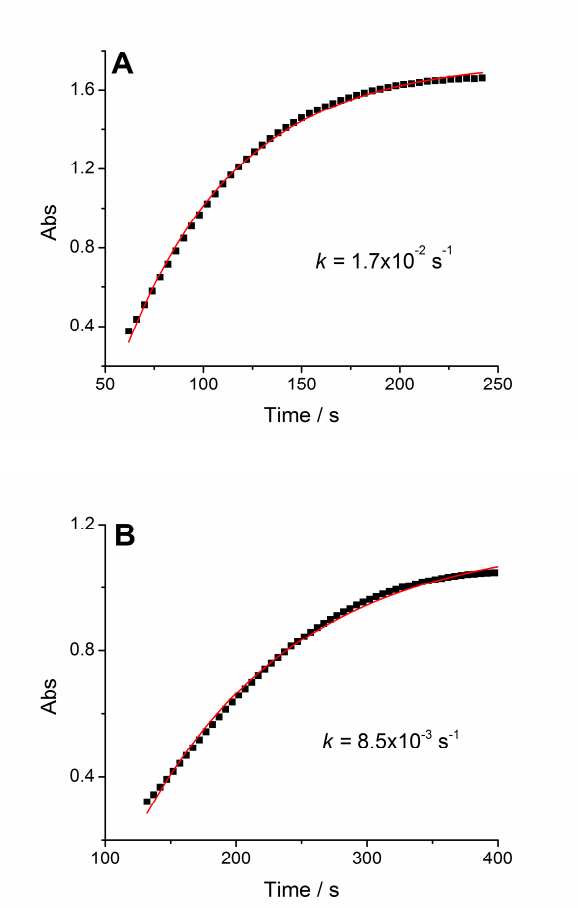

Figure 4.17: Kinetics of **1** (1 mM)/H_2O_2-catalyzed *ipso*-hydroxylation of perfluorobenzoic acid (20 mM) with (A) H_2O_2 and (B) D_2O_2 in acetonitrile at -20 °C.

Table 4.3: List of KIE values for the O–O bond cleavage by heme and non-heme iron complexes (in acetonitrile, unless specified)

O–O Bond Cleavage Reactions	*KIE*	*Ref*
Iron(III)porphyrin + peracids	~2.0	[199]
Cpd I formation of Horseradish peroxidase	1.6	[175]
$[Fe^{II}TMC]^{2+}$ + H_2O_2 + 2,6-lutidine	3.7	[195]
1a + AcOH at -30 °C	2	[59]
1a + perfluorobenzoic acid at -40 °C	2.3	[a]
1a + 2-chloro-6-nitrobenzoic acid at -40 °C	1.7	[a]
1a + 2,6-dichlorobenzoic acid at -40 °C	1.7	[a]
1a + 2-nitrobenzoic acid at -40 °C	1.5	[a]
1a + perfluorobenzoic acid at -20 °C	2.0	[a]
Epoxidation reactions at -15 °C		
1 + AcOH + H_2O_2 + *cis*-cyclooctene	2.4	[a]
1 + AcOH + H_2O_2 + 1-octene	1.9	[a]
Epoxidation reaction in acetone at -15 °C		
1 + AcOH + H_2O_2 + 1-octene	1.3	[a]
cis-Dihydroxylation reactions at -15 °C		
1 + AcOH + H_2O_2 + *cis*-cyclooctene	2.1	[a]
1 + AcOH + H_2O_2 + 1-octene	1.7	[a]
1 + AcOH + H_2O_2 + dimethyl fumarate	1.5	[a]
cis-Dihydroxylation reaction in acetone at -15 °C		
1 + AcOH + H_2O_2 + 1-octene	1.5	[a]
Decay of **1c** at -50 °C	0.8	[a]
1c + Pyridine *N*-Oxide at -90 °C	0.8	[a]

[a] This work

4.3.2 Olefin Oxidation Kinetics

Complex **1** was also among the first iron catalysts that could *cis*-dihydroxylate olefin C=C bonds using H_2O_2 as an oxidant.[53,55,58] However, the need for syringe-pump to avoid disproportionation of H_2O_2 in the **1**/H_2O_2-catalyzed olefin oxidation barred us from performing a kinetic analysis of this reaction.[53,55,58] It was also reported in the literature that the addition of acetic acid to **1** quantitatively converted *cis*-cyclooctene to its epoxide in one minute at 0 °C and did not require the syringe pumping of H_2O_2.[59] This observation would give us for the first time an opportunity to monitor the kinetics of the olefin oxidation by following the amounts of the oxidation products formed with time to obtain a direct measure of the rate of olefin oxidation. To be able to collect more data points for a more accurate determination of the reaction rate, the temperature of the reaction solution was lowered to -15 °C. The kinetic data for **1**/H_2O_2-catalyzed 1-octene oxidation at -15 °C in a 1/1 solvent mixture of acetonitrile and acetic acid are shown in Figure 4.18 and similar rates of formation of *cis*-diol and epoxide were noted. This observation further suggested a similar rate limiting step for these two transformations. While either $Fe^{V}(O)(OH)$ or $Fe^{V}(O)(O_2CR)$ (Scheme 4.2) could be the oxidant responsible for olefin epoxidation,[53] $Fe^{V}(O)(OH)$, and not $Fe^{V}(O)(O_2CR)$, is the only oxidant capable of *cis*-dihydroxylation.[59,190] The similar rates of epoxidation and *cis*-dihydroxylation further suggested that acetic acid effected rate limiting O–O bond cleavage in a similar way as water in the generation of these high-valent oxidants.

This hypothesis of rate limiting cleavage of the O–O bond was further tested by studying the kinetics at different concentrations of 1-octene (Scheme 4.2). The similar observed rates of reaction for both 200 and 1000 equiv of 1-octene bolstered the hypothesis that O–O bond cleavage was the rate determining step (Figure 4.18).

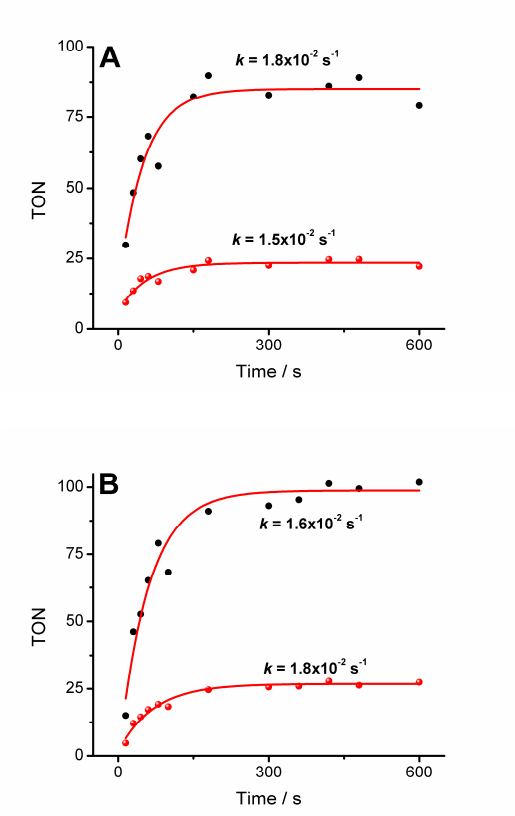

Figure 4.18: 1-catalyzed oxidation of 1-octene with H_2O_2 (300 equiv) in a 1/1 acetonitrile/acetic acid solvent at -15 °C in the presence of 200 equiv (A) or 1000 equiv (B) of substrate. Black and red filled circles stand for epoxide and *cis*-diol, respectively.

Scheme 4.2: The mechanistic scheme showing the rate determining water- or acid-assisted O-O bond cleavage towards olefin oxidation.

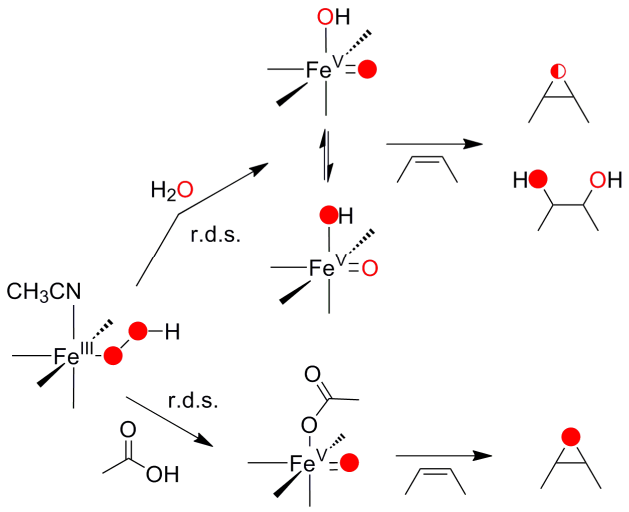

The use of AcOH opened the possibility to study the kinetic isotope effect in the olefin oxidation by comparing the reaction rates in the presence of AcOH and AcOD. The k_H/k_D data for both epoxidation and *cis*-dihydroxylation of 1-octene are shown in Figure 4.19. The KIE values of 1.8 and 1.5 were observed at -15 °C for epoxidation and *cis*-dihydroxylation, respectively. These results further suggested that the proton was involved in the rate limiting heterolysis of the O–O bond. To compare the energetics of the AcOH-assisted cleavage of the O–O bond with other O–O bond cleaving reactions, activation parameters were determined from the decay of **1a** in the presence of acetic acid (Figure 4.20). The obtained $\Delta H^{\ddagger}$ value was closer to the values obtained in the case of *ipso*-hydroxylation suggesting a similar nature of the bond cleavage at the r.d.s. (Table

4.2).The more negative $\Delta S^{\ddagger}$ value might suggest a more ordered transition state in the case of AcOH than for the substituted benzoic acids.

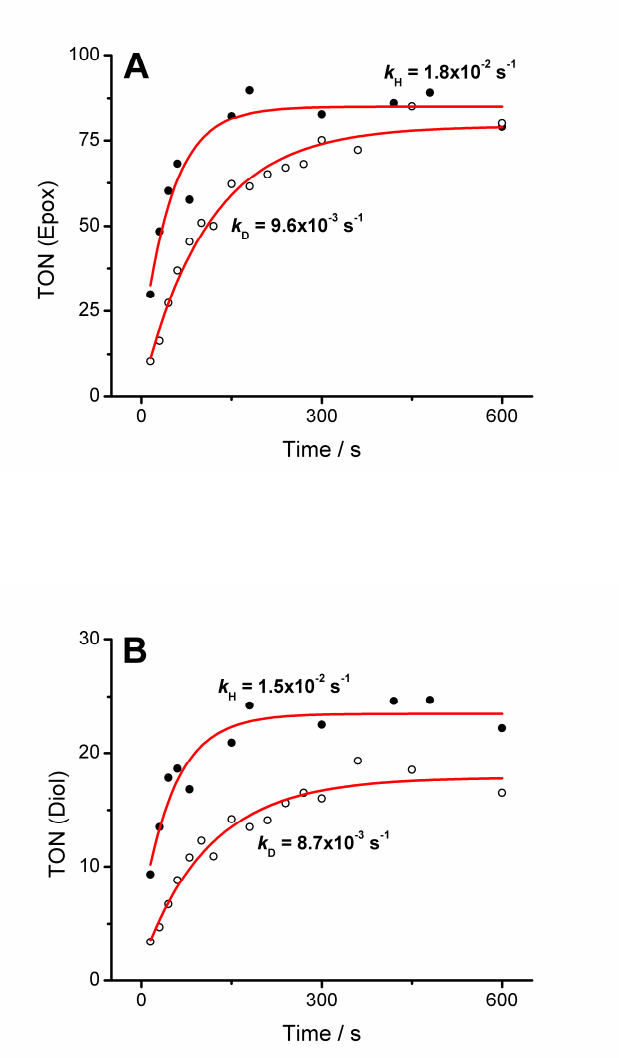

Figure 4.19: The kinetics of **1**/H_2O_2-catalyzed oxidation of 1-octene. Epoxidation (A) and *cis*-dihydroxylation (B) kinetics were carried out in the presence of 0.5 mol% **1** and H_2O_2 (300 equiv) in either a 1/1 solvent mixture of acetonitrile/acetic acid (●) or acetonitrile/acetic acid-d_1 (○) at -15 °C.

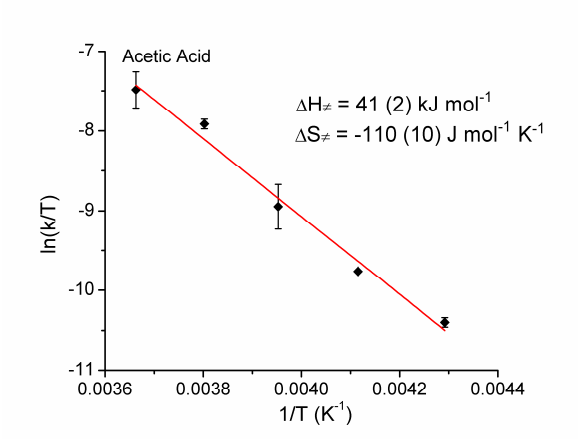

Figure 4.20: Eyring plot for the decay of **1a**, generated from **1** (1 mM) and 10 equiv H_2O_2 in the presence of acetic acid (20 mM), over a temperature range of 0 to -40 °C.

To check whether the rate of **1**/H_2O_2-catalyzed olefin oxidation depended on the nature of the substrates, further kinetic investigations were carried out with *cis*-cyclooctene. The kinetic data revealed similar obtained rate constants for both olefin epoxidation and *cis*-dihydroxylation (Figure 4.21) with both *cis*-cyclooctene and 1-octene (Table 4.4). This result further pointed out the fact that the r.d.s. was prior to the substrate oxidation step. The measured KIE values of 2.4 and 2.1 for *cis*-cyclooctene epoxidation and *cis*-dihydroxylation, respectively, corroborated the idea of proton-assisted cleavage of the O–O bond as rate limiting.

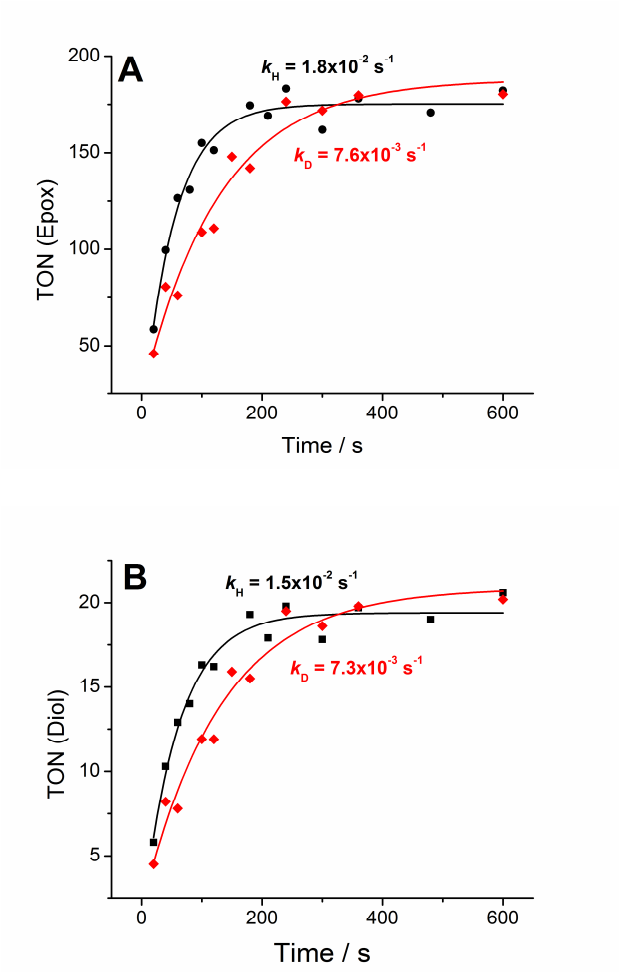

Figure 4.21: Epoxidation (A) and *cis*-dihydroxylation (B) kinetics of *cis*-cyclooctene by **1**/H_2O_2 under the conditions used in Figure 4.19 in either a 1/1 acetonitrile/acetic acid (●) or a 1/1 acetonitrile/acetic acid-d_1 (◆) solvent at -15 °C.

Table 4.4: Comparison of the rates of olefin oxidations catalyzed by **1**/H_2O_2 at -15 °C in a 1/1 acetonitrile/acetic acid solvent mixture[a]

Olefin	*Added Equivalents*[b]	*Rate of Epoxidation* (s^{-1})	*Rate of Dihydroxylation* (s^{-1})
cis-Cyclooctene	200	$1.8(2)\times10^{-2}$	$1.5(1)\times10^{-2}$
1-Octene	200	$1.8(2)\times10^{-2}$	$1.5(5)\times10^{-2}$
	1000	$1.6(1)\times10^{-2}$	$1.8(3)\times10^{-2}$
tert-Butyl acrylate	200	$8(1)\times10^{-3}$	$7(1)\times10^{-3}$
Dimethyl fumarate	50	-	$3.7(2)\times10^{-3}$
	100	-	$4.7(2)\times10^{-3}$
	200	-	$4.3(3)\times10^{-3}$
1-Octene in acetone[c]	200	$1.6(1)\times10^{-3}$	$1.5(1)\times10^{-3}$

[a]300 equivalents of H_2O_2 was added to 1mM **1**. [b]Compared to **1**. [c]Values listed reflect the average of at least two experiments.

The effect of electron withdrawing olefins on the rate of **1**/H_2O_2-catalyzed olefin oxidation was tested by using *tert*-butyl acrylate (containing one ester group) as a substrate. By comparing the similar rates of oxidation of 1-octene and *cis*-cyclooctene, one might think that substrate was not involved in the r.d.s. and the rate would be unchanged even with the electron-deficient olefins. The data, however, suggested the rate of *tert*-butyl acrylate oxidation was two times slower than 1-octene or *cis*-cyclooctene. Interestingly, we could also detect a small amount of epoxide product under our kinetic conditions and the rate constants for both epoxidation and *cis*-dihydroxylation were almost same (Figure 4.22). The very low yield (0.5% based on the added oxidant) of the epoxide product could be the reason for a larger error bar in the observed rate constant.

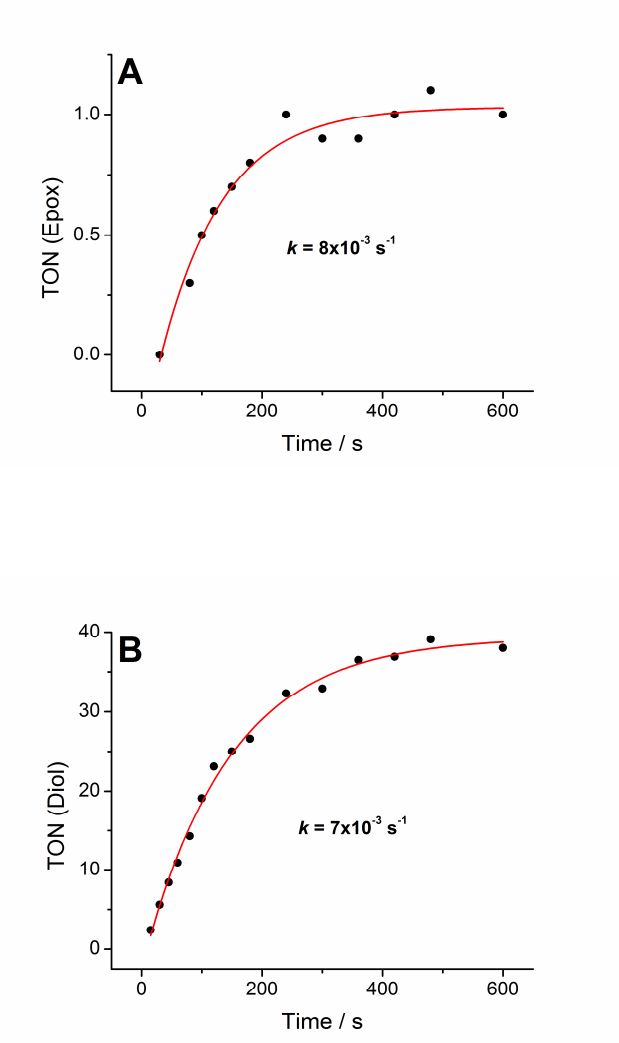

Figure 4.22: The kinetics of **1**/H_2O_2-catalyzed oxidation of *tert*-butyl acrylate. Epoxidation (A) and *cis*-dihydroxylation (B) kinetics were carried out under the conditions described in Figure 4.19.

To better understand the kinetic behaviors of the electron deficient olefins we tried dimethyl fumarate (containing two ester groups) as a substrate (Figure 4.23A). It turned out that the rate constants were even two times slower (Figure 4.23 and Table 4.4) than for *tert*-butyl acrylate (containing one ester group). Although the difference in the reaction rates between *cis*-cyclooctene or 1-octene and dimethyl fumarate by a factor of four was not huge in the kinetics terms, still we investigated whether the subsequent step of the O–O bond cleavage, the attack of the olefin by the Fe^{V}=O species (step 2 in Scheme 4.3), could become partially rate limiting. If this is an option, one should see a change in the rate of olefin oxidation with different concentrations of the substrate. However, the kinetic reactions performed with different amounts of dimethyl fumarate under identical reaction conditions did not show any appreciable change in the rate (Figure 4.23 and Table 4.4) that suggested that step 2 in **Error! Reference source not found.**3 was not involved in the rate limiting step. Interestingly, we note that a previous study on **1**/H_2O_2-catalyzed competitive oxidation of olefins showed that *cis*-cyclooctene was preferentially oxidized over dimethyl fumarate by a factor of four,[63] which indicated that the product determining step was faster in the case of *cis*-cyclooctene.

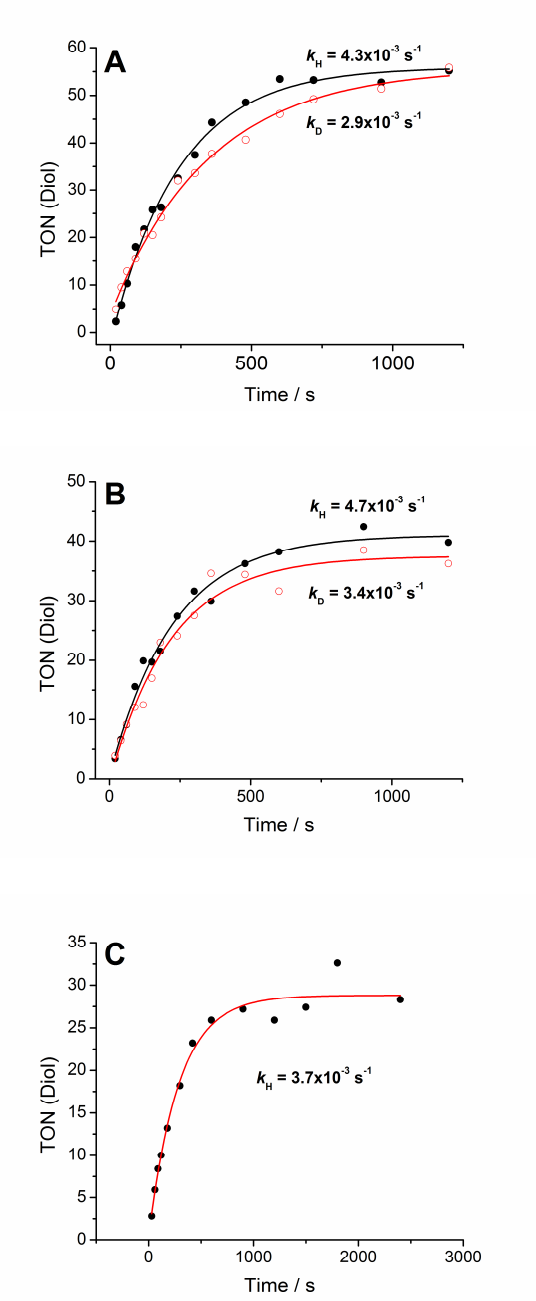

Figure 4.23: The kinetics of **1**/H_2O_2 (1/300)-catalyzed oxidation of (A) 200 equiv and (B) 100 equiv of dimethyl fumarate at -15 °C in either a 1/1 acetonitrile/acetic acid (●) or a 1/1 acetonitrile/acetic acid-d_1 (○).

Scheme 4.3: Possible rate limiting steps in **1**/H_2O_2-catalyzed olefin oxidation.

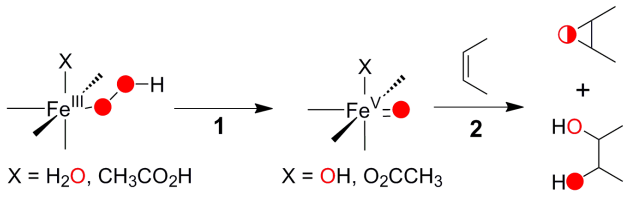

Scheme 4.4 depicts the entire landscape of **1**/H_2O_2-catalyzed olefin oxidation. The reported **1**/H_2O_2-catalyzed competitive olefin oxidation and *ipso*-hydroxylation further point out that the diverse oxidation transformations observed stem from a similar mechanistic pathway.[190] The most important step in this entire landscape is the water- and/or acid-assisted O–O bond cleavage. The proton (supplied from water or acid) attacks the distal O atom of the hydroperoxo species and facilitates the cleavage of the O–O bond. A kinetic isotope effect of ~2 observed in all reactions (Table 4.3) supports this hypothesis.

Scheme 4.4: Mechanistic landscape of **1**/H_2O_2-catalyzed oxidation reactions in acetonitrile.

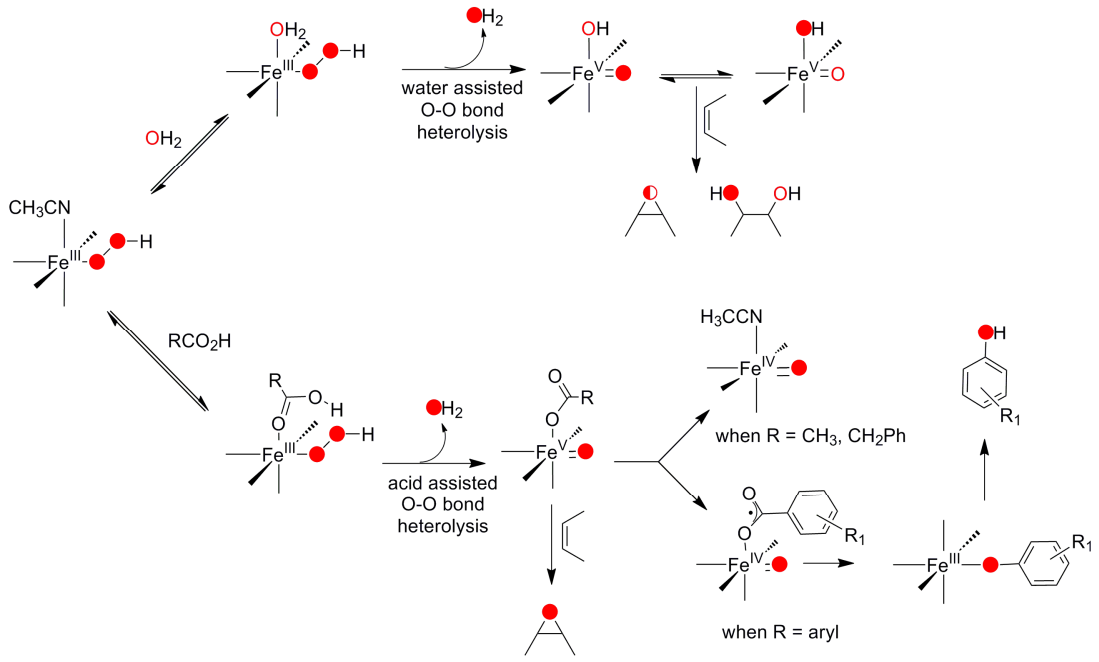

4.3.3 Reactivity of the Iron(III)-peroxo Species in Acetone

Complex **1** was also reported to react with H_2O_2 in acetone to generate an iron(III)-peroxo intermediate that was different from intermediate **1a**.[132] **1** with H_2O_2 as the oxidant was also shown to effect the oxidation of both cyclohexane and *cis*-cyclooctene in acetone. However, the effect of acetic acid on the iron(III)-peroxy-acetone intermediate was not investigated. It would thus be interesting to study the kinetics of olefin oxidation in acetone under identical conditions as in acetonitrile and compare the results.

Complex **1** reacted with H_2O_2 in acetone at -90 °C to generate an iron(III) peroxy-acetone intermediate, ($[Fe^{III}(TPA)(\kappa^2\text{-}OOC(CH_3)_2OH)]^{2+}$, **1c**) ($\lambda_{max}$ = 523 nm) (Figure 4.24),[132] which has been characterized in detail by EPR and resonance Raman spectroscopies. Intermediate **1c** is stable at least for 3 hours at -90 °C but underwent self-decay over 25 min at -50 °C to form $[Fe^{IV}(O)(TPA)]^{2+}$ via O–O bond homolysis. This self-decay was accelerated by the addition of 12 equivalents of pyridine *N*-oxide (PyO) and could be monitored at -90 °C. The $[Fe^{IV}(O)(TPA)]^{2+}$ product showed a shift of its λ_{max} from 724 nm in acetonitrile to 738 nm (Figure 4.24 inset) in the presence of PyO, suggesting the binding of PyO to the oxo iron(IV) center.[132]

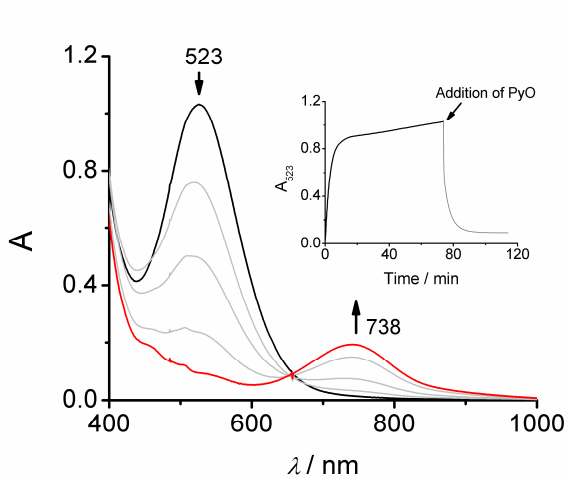

Figure 4.24: UV-vis spectra of the reaction of **1** (1 mM) with 10 equiv of H_2O_2 in acetone at -90 °C. The black spectrum depicts the iron(III)-acetone-peroxo intermediate (λ_{max} = 523 nm), the decay of which leads to the formation of the Fe^{IV}=O species (red spectrum). In the inset, it is shown that the addition of 12 equiv of pyridine *N*-oxide leads to the immediate decay of the mentioned peroxo intermediate.

The self-decay of the $[Fe^{III}(TPA)(\kappa^2\text{-}OOC(CH_3)_2OH)]^{2+}$ species at -50 °C allowed us to monitor its kinetics (Figure 4.25A) and observe the effect of PyO on the rate of its decay. Interestingly, PyO-induced decay of **1c** at -90 °C (Figure 4.26A) was one order of magnitude faster than the self-decay rate at -50 °C (Table 4.5). Also, by comparing the rates of decay of **1c** in the presence of H_2O_2 to D_2O_2, kinetic isotopic effect (k_H/k_D) values were determined. Both for the self- and PyO-induced decays of **1c**, k_H/k_D values of 0.8 were obtained (Table 4.5). The experimental KIE values of ~1 in these cases suggested, unlike the O–O bond heterolysis, no proton was involved in the rate limiting step.

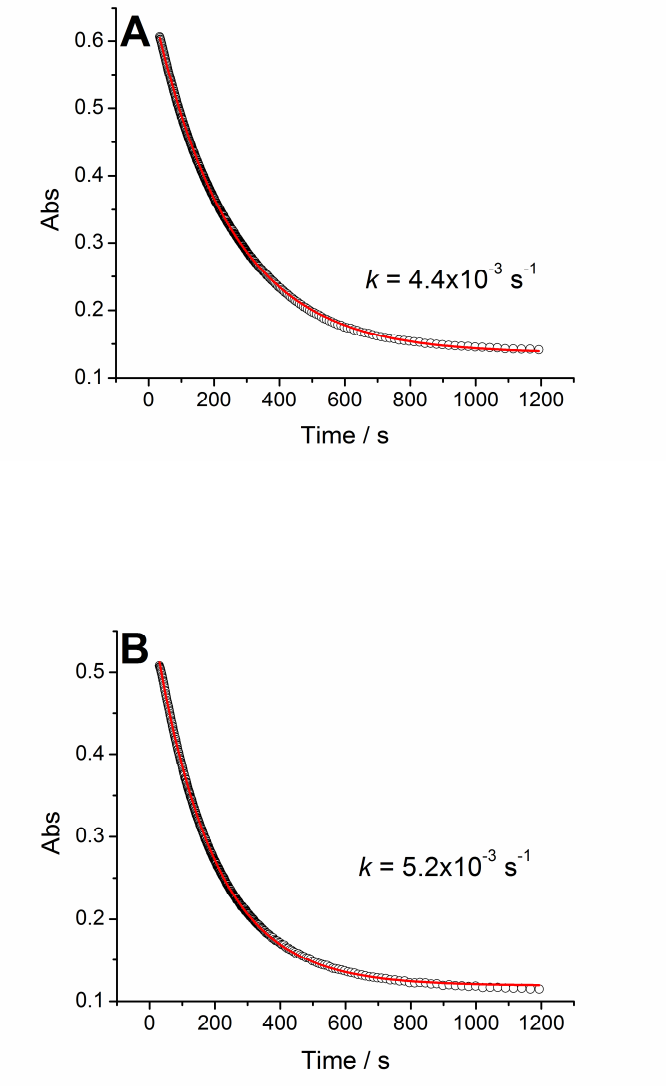

Figure 4.25: The kinetics of self-decay of intermediate **1c**, generated with **1** (1 mM) and 10 equivalents of (A) H_2O_2 and (B) D_2O_2 in acetone at -50 °C.

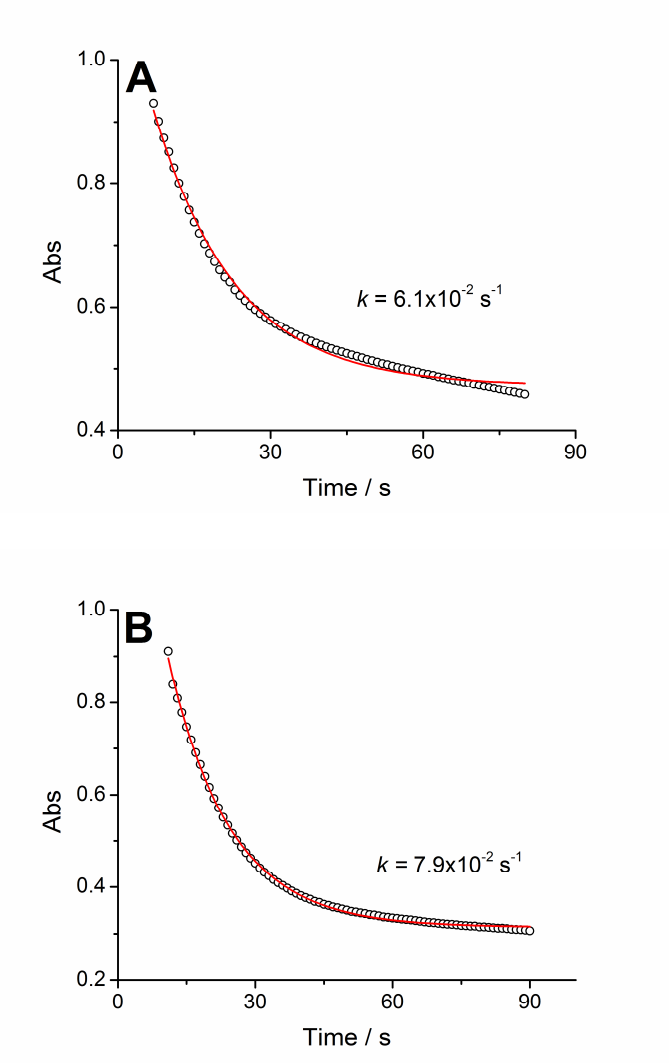

Figure 4.26: The kinetics of decay of intermediate **1c** in acetone, generated with **1** (1 mM) and 10 equivalents of (A) H_2O_2 and (B) D_2O_2 upon addition of 12 equiv of PyO at -90 °C.

Table 4.5: Comparison of the rate constants of the decay of intermediate **1c** at different conditions

Decay of **1c**	k_H (sec^{-1})	k_D (sec^{-1})	k_H/k_D
Self-decay at -50 °C	$4.4(3)\times10^{-3}$	$5.2(4)\times10^{-3}$	0.8
PyO-induced decay at -90 °C	$6.1(1)\times10^{-2}$	$7.9(5)\times10^{-2}$	0.8

1/H_2O_2 in acetone was also reported to effect the oxidation of *cis*-cyclooctene, although to a lower extent than in acetonitrile.[132] However, the kinetics experiments with 1-octene in pure acetone – where H_2O_2 was added all at once without syringe pumping – yielded only 1% of the oxidation products. However, a considerable amount of epoxide and *cis*-diol (combined yield of ~30%) could be obtained in a 1/1 mixture of acetone and acetic acid, allowing us to perform kinetic studies. This observation further underscored the importance of acetic acid in minimizing the disproportionation of H_2O_2.

UV-visible spectroscopic experiments were also performed to check the effect of the added AcOH in the catalytic system. Interestingly, it was observed that the addition of only one equivalent of AcOH led to the formation of the $[Fe^{III}_2(TPA)_2(\mu\text{-}O)(\mu\text{-}O_2CCH_3)]^{3+}$ species (Figure 4.27). However, the decay of the intermediate **1c** was quite complicated in the presence of acetic acid and could be fitted with multiple exponentials suggesting the involvement of more than one step before the formation of μ-oxo-diiron(III) species.

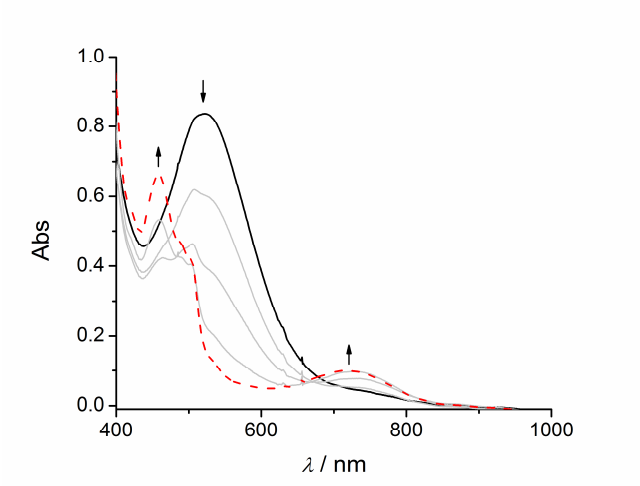

Figure 4.27: The effect of one equivalent of acetic acid upon intermediate **1c**, generated with 1 mM **1** and 10 equiv of H_2O_2, at -50 °C in acetone. Black solid line depicted the maximum formation of **1c**. The addition of acetic acid to the preformed **1c** led to the decay of the chromophore that led to the formation of $[Fe^{III}_2(TPA)_2(\mu\text{-}O)(\mu\text{-}O_2CCH_3)]^{3+}$ species (red-dashed line).

The olefin oxidation kinetics, however, were performed under identical conditions as in acetonitrile at -15 °C for the sake of comparison. The kinetics data in acetone suggested that – as in acetonitrile – the rates of olefin epoxidation and *cis*-dihydroxylation were comparable (Figure 4.28A). The yields of the oxidation products, however, were lower in acetone than in acetonitrile. The similar rates of formation of epoxide and *cis*-diol bolstered the hypothesis that they were generated through the same rate limiting step,

presumably the O–O bond cleavage. Interestingly, the rates of olefin oxidation in acetone were about one order of magnitude slower than those in acetonitrile.

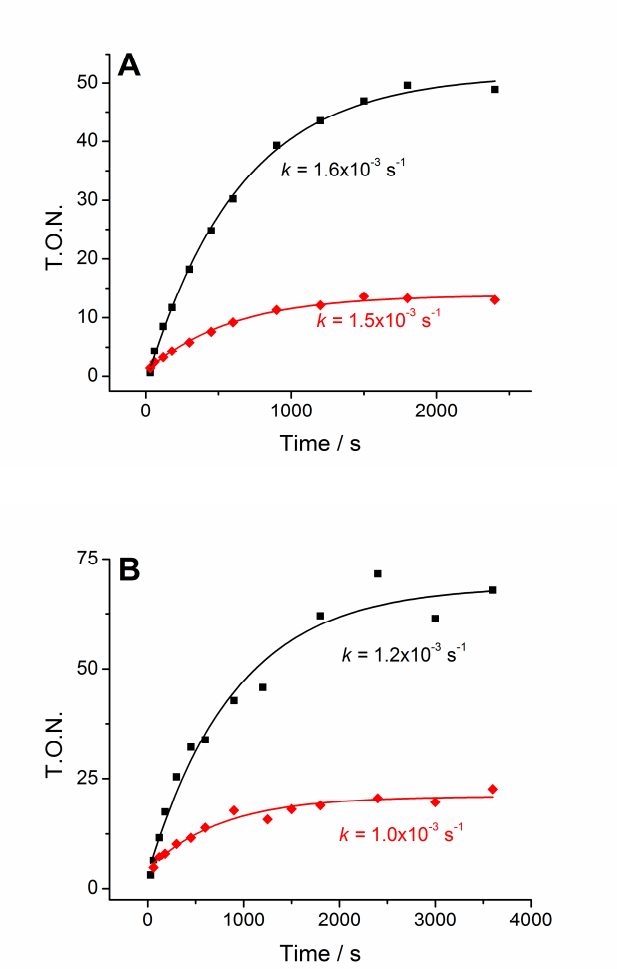

Figure 4.28: Epoxidation (■) and *cis*-dihydroxylation (◆) kinetics of 1-octene oxidation catalyzed by 0.5 mol% **1** and H_2O_2 (300 equiv) in either a 1/1 acetone/acetic acid (A) or a 1/1 acetone/acetic acid-d_1 (B) solvent at -15 °C.

The kinetic isotopic effect value was also determined in the **1**/H_2O_2-catalyzed oxidation of 1-octene in acetone by comparing the reaction rates in the presence of AcOH and AcOD (Figure 4.28). KIE values of 1.3 and 1.5 were determined for epoxidation and *cis*-dihydroxylation, respectively. These KIE values were similar to those obtained in the case of **1**/H_2O_2-catalyzed olefin oxidations in acetonitrile. The observation of catalytic conversions of olefin to epoxide and *cis*-diol combined with KIE values of >1 suggested that a proton-assisted cleavage of the O–O bond of the iron(III)-peroxo species to the high-valent iron(V)-oxo species was the rate limiting step. These observations further suggested a shift in the mode of the O–O bond cleavage to heterolysis in the presence of acid and at elevated temperature (-15 °C) from homolysis at lower temperature (-50 °C and below). Interestingly, the observation of O–O bond heterolysis in the presence of acetic acid was previously reported in the literature in the case of FeBPMEN[62,200] and FeTPA complexes.[59]

Labeling experiments with $H_2{}^{18}O_2$ in acetone were done in the catalytic oxidation of 1-octene by **1**. The identification of the oxidation products in GC-MS suggested a 72% incorporation of ^{18}O into epoxide, while 90% of the *cis*-diol was singly labeled (Table 4.6). Interestingly, in the case of a 1/1 acetone/acetic acid, the ^{18}O-label incorporation in epoxide increased to 93%, while the labeling pattern in *cis*-diol remained almost unperturbed. This pattern of increased ^{18}O-incorporation into epoxide from $H_2{}^{18}O_2$ in the presence of acetic acid was also observed in the case of perfluorobenzoic acid in acetonitrile.[190] These two sets of data in acetone and in acetonitrile further suggested the

involvement of an acid-assisted pathway in the olefin oxidation (see the discussion below). Furthermore, the comparison of the labeling patterns of epoxide in acetone and acetonitrile also suggested an increased incorporation of ^{16}O (from water) in acetone than acetonitrile. The increased O-atom incorporation into epoxide from water in acetone could be rationalized by the slower rate of reaction compared to acetonitrile (by 1 order of magnitude in the 1-octene oxidation at -15 °C), which could allow an increased exchange of water with the oxidant that led to the 10% increase (28% from 18%) in the ^{16}O-label incorporation from water into epoxide. All of the kinetics and labeling studies performed in this section helped us to better understand the reaction landscape of **1**/H_2O_2 in acetone.

Table 4.6: Labeling studies in the oxidation of 1-octene (1 M) by **1** (1 mM) and 10 equiv of $H_2{}^{18}O_2$ at room temperature to study the effect of solvent

Solvent	*1,2-epoxyoctane*		*1,2-octanediol*			*Ref*
	^{16}O	^{18}O	$^{16}O^{16}O$	$^{16}O^{18}O$	$^{18}O^{18}O$	
Acetonitrile	18	82	5	92	3	190
$C_6F_5CO_2H$[a]	8	92	5	93	2	34
Acetone	28	72	8	90	2	[b]
Acetone/AcOH	7	93	6	94	-	[b]

[a]25 equivalents of perfluorobenzoic acid was added to the acetonitrile solution. [b] This work.

Scheme 4.5 describes the current understanding of the reactivity of **1**/H_2O_2 system in acetone. The observation of the formation of the Fe^{IV}=O species (**O3**) from **P1** with an isosbestic point at 650 nm suggested that this is a homolytic cleavage of the O–O bond[132] (Pathway A in Scheme 4.5). A concomitant C–C bond cleavage after O–O bond homolysis leads to the formation of $CH_3CO_2^{\cdot}$, which then finally reacts with Fe^{IV}=O species (**O3**) and one molecule of **1** to generate **D1** (Pathway A_1).

O–O bond of **P1** could undergo a heterolysis leading to the formation of Fe^{V}(O)(OH) oxidant at elevated temperatures (Pathway B in Scheme 4.5). The observation of epoxide and *cis*-diol products in the oxidation of 1-octene along with the 28% of ^{16}O incorporation (from water) into epoxide and 90% of the singly labeled *cis*-diol in the $H_2{}^{18}O_2$ labeling studies (Table 4.6) suggest the involvement of a high-valent iron-oxo center, where the exchange can take place. The proposed oxidant Fe^{V}(O)(OH) can be generated from Fe^{III}-OOH via water-assisted O–O bond heterolysis.

In the presence of acetic acid, the reaction may follow Pathway C (Scheme 4.5). This pathway can be split further in two parts and one of them (Pathway C_1) leads to the formation of the oxidant **O2** via AcOH-assisted O–O bond heterolysis. The formation of **O2** can account for the increased yields of epoxide in the **1**/H_2O_2-catalyzed 1-octene oxidation in a 1/1 acetone/acetic acid solvent, which resembles the study done in a 1/1 acetonitrile/acetic acid. In the labeling experiments with $H_2{}^{18}O_2$, the increased ^{18}O incorporation into epoxide in the presence of AcOH (93% compared to 72% in Table 4.6) further supports the involvement of Pathway C_1. The almost identical labeling pattern for

cis-diol in acetone with or without acetic acid together with our previous observations with perfluorobenzoic acid[190] suggests that **O2** is not involved in *cis*-dihydroxylation.

The intermediate **P2** can also follow Pathway C_2 towards the formation of **D1**, considered as the thermodynamic sink in this reaction landscape. The lower yield of the olefin oxidation products in acetone could be rationalized by the formation of **D1**. This hypothesis of the acetic acid-assisted generation of **D1** is proved by its formation upon addition of acetic acid to the pre-generated **P1** (Figure 4.27). **D1** also could be generated from the acetic acid via Pathway A_1 as discussed above.

Scheme 4.5: The evolution of iron(III)(TPA)-peroxo intermediate in acetone.

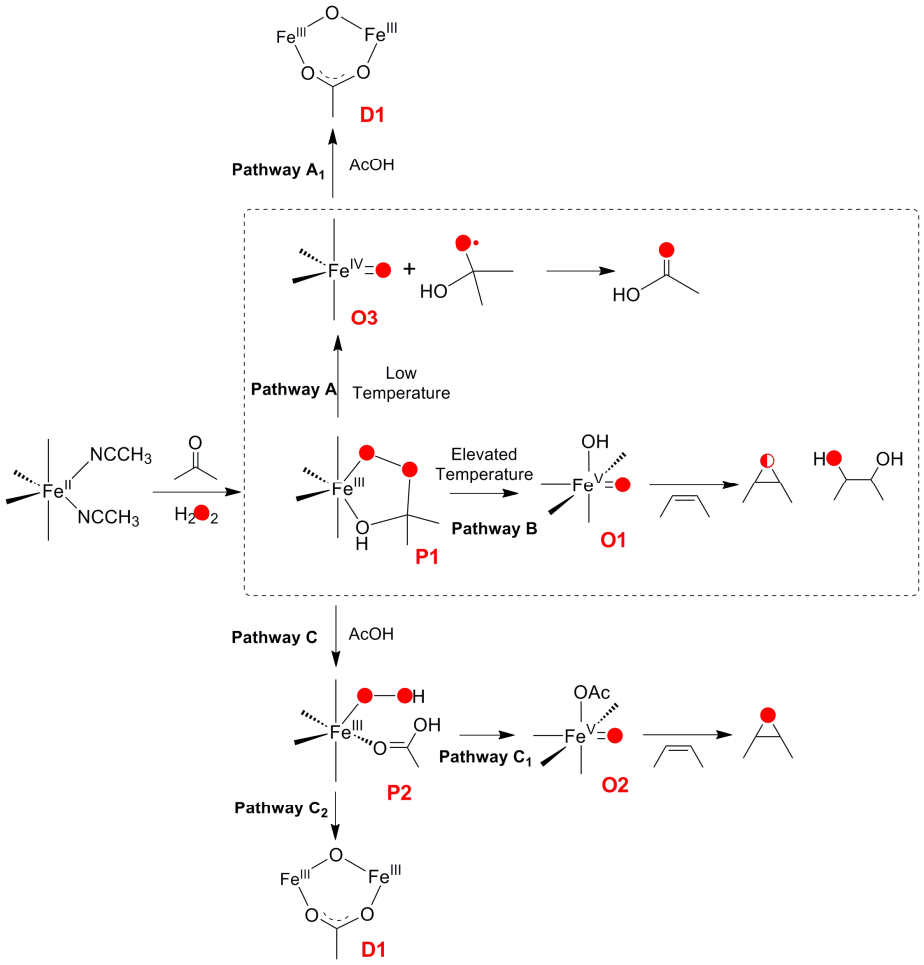

4.4 Conclusions

The common theme in the several oxidative transformations catalyzed by **1**/H_2O_2 discussed in this chapter is the cleavage of the O–O bond. O–O bond heterolysis has been proposed as the rate limiting step in the case of olefin oxidation[59] and for aromatic *ortho*- and *ipso*-hydroxylation,[62,140,190] while rate limiting O–O bond homolysis was observed in the case of the iron(III)-peroxo intermediate in acetone at lower temperature.[132] An understanding of the energetics of these O–O bond cleavage reactions may shed some light into these processes. To determine whether it is possible to differentiate between the two modes of O–O bond cleavage, activation parameters were measured for various reactions (Table 4.). It was found that the activation parameters for both homo- and heterolysis of the O–O bond were similar and could not be used to distinguish between these two types of cleavages. In the case of heme complexes as well, there was no difference in the activation parameters in O–O bond homo- and heterolysis.[188] However, a pattern has emerged from measurements of the H/D kinetic isotope effects for these transformations. In the case of **1**/H_2O_2-catalyzed oxidation of *cis*-cyclooctene, a KIE value of 2.4 was obtained in the case of epoxidation, while a KIE value of 2.1 was obtained for *cis*-dihydroxylation. For 1-octene, the KIE numbers were 1.9 and 1.7 for epoxidation and *cis*-dihydroxylation, respectively. Interestingly, KIE values in the range of 1.5-2.3 were obtained for *ipso*-hydroxylation. Epoxidation and *cis*-dihydroxylation in acetone also yielded KIE values of 1.3 and 1.5, respectively. Similar KIE values in the range of 2 for the O–O bond cleavage were also reported in the literature.[59,175,199,201] In contrast, KIE values for O–O bond homolysis were found to be ~ 1 as no involvement of

a proton in the rate determining step was expected. These observations further point out that determining the kinetic isotope effect, and not the activation parameters, would be a better way to identify the type of the O–O bond cleavage. To our knowledge, this is the first detailed study on differentiating O–O bond homo- and heterolysis in iron-peroxo systems.

Acknowledgement. This work was supported by a grant from the U.S. Department of Energy (FFG02-03ER15455 to L.Q.).

Chapter 5

The ‘Push-pull’ Phenomenon in Non-heme Iron-Catalyzed O–O Bond Cleavage

5.1 Introduction

In Nature, heme and non-heme iron oxygenases activate dioxygen and perform diverse oxidation reactions, namely epoxidation, hydroxylation, desaturation, and halogenation. The cleavage of the O–O bond is a very important step in these oxidative transformations. In the case of heme enzymes (e.g. horseradish peroxidase, cytochrome P450, catalase, NO synthase, and NO reductase),[202-206] [207-211] the O–O bond is cleaved heterolytically in a rate limiting step that converts the iron(III)-hydroperoxo species to the iron(IV)-oxo porphyrin π cation radical (Cpd I).[8] In the case of synthetic iron-porphyrin complexes as well, it was shown the O–O bond of the iron(III)-peroxo species was cleaved in a rate limiting step to generate Cpd I.[184,185,188] Interestingly, the cleavage of the O–O bond is an important step in the case of non-heme α-ketoglutarate (α-KG)-dependent dioxygenases, (e.g. Taurine/ α–ketoglutarate dioxygenase, Deacetoxycephalosporin C synthase, prolyl-4-hydroxylase, AlkB),[11] that converts an iron(IV)-peroxo species to an Fe(IV)-oxo(carboxylato) species.[12]

It was also shown in both heme enzymes and in synthetic iron porphyrin complexes that the replacement of the proximal ligand with more electron donating ones enhanced the electron donation at the iron center that in turn increased the rate of the O–O bond cleavage.[188] It was proposed that axial ligands like cysteines or histidines provide electron density to the anti-bonding orbital of the O–O bond through the iron center (push). The electronic push effect was also observed in a mutant (L358P) of cytochrome

$P450_{cam}$.[212] The replacement of leucine by proline (L358P) near the axial thiolate ligand, removed one of the conserved amide protons that were proposed to neutralize the negative charge of the thiolate sulfur and increased the anionic character of the axial ligand. The increased push effect of the thiolate in L358P was evidenced by the lower reduction potential of the heme and also by the up-field and down-field shifts of the ν(Fe-CO) and ν(C-O), respectively, in the carbonmonoxy L358P mutant.[212] In the case of reengineered myoglobin, the replacement of the proximal histidine with a cysteine or with the exogenous substituted-imidazoles increased electron donation to the iron center and consequently increased the rate of the O–O bond cleavage.[177] Similarly, in the case of synthetic iron-porphyrin complexes as well, the introduction of the electron-donating groups at the *meso* positions of the porphyrin ring increased the electron donation to the iron center and consequently increased the rate of the heterolytic cleavage of the O–O bond of iron(III)-acylperoxo complex towards the formation of Cpd I.[188] The further introduction of the electron donating imidazoles to the iron(III)-acylperoxo species increased the rate of heterolytic O–O bond scissions. The homolysis of the O-O bond of the iron(III)-acylperoxo species towards the formation of oxo-ferryl species was also accelerated – to a lesser extent than heterolysis – by enhanced electronic donation from the added imidazoles. Recently, it was also shown in the case of water soluble Mn porphyrin complex, a partially deprotonated axial (proximal) hydroxide ligand helped cleave the O–O bond in a rate limiting step via an increased electronic donation.[189]

The distal residues of the heme and porphyrin systems, on the other hand, regulate the proton delivery to the terminal O atom of the hydroperoxo ligand, creating a better leaving group (pull). In the case of cytochrome *c* peroxidase, it was shown that the histidine and arginine residues in the distal pocket were essential for the acid-base catalysis and for charge stabilization.[213] The importance of the distal histidine residue in the acid-base catalysis towards the cleavage of the O–O bond was further shown in the horseradish peroxidase (hHRP), where the mutation of histidine with either alanine (H42A) or valine (H42V) led to the decrease in the rate of both Cpd I formation and peroxidative catalysis.[214] Furthermore, the presence of glutamic acid residue (in the place of histidine in the distal pocket) in the crystal structure of chloroperoxidase from *Caldariomyces fumago*[215] and the increased rate of Cpd I formation in the horseradish peroxidase mutant H42E[216] underscored the role of a carboxylic acid in cleaving the O–O bond via a 'pull' effect.

Although the 'push-pull' phenomenon was observed for heme and porphyrin systems (Figure 5.1),[174,189] there was no demonstration of both of these effects in a single non-heme iron system. Goldberg and co-workers, however, demonstrated that increasing the electronic donation from the *trans* thiolate ligand by introducing electron donating substituents at the attached phenyl ring of the low-spin $[Fe^{III}([15]aneN4)(SAr)(OOR)]^{+}$ (where, [15]aneN4 = 1,4,8,12-tetraazacyclopentadecane and R = cumenyl or *tert*-butyl) species, lowered the ν(Fe–O) in the resonance Raman spectroscopy[217] and slightly

increased the Fe–O bond distance in the Extended X-ray Absorption Fine Structure (EXAFS) spectroscopy.[218] Interestingly, it was also reported recently that synthetic non-heme iron complex $[Fe^{II}(TMC)]^{2+}$ (TMC = 1,4,8,11-Tetramethyl-1,4,8,11-tetraaza-cyclotetradecane) was converted to $[Fe^{IV}(TMC)(O)]^{2+}$ in a near quantitative yield using H_2O_2 and 2,6-lutidine.[195] It was proposed that 2,6-lutidine helped in deprotonating H_2O_2 and then acted as an acid in protonating the distal O atom that helped the heterolytic scission of the O–O bond (Pull effect). Herein, we show that tuning the ligand electronics, by introducing different substituents in the backbone, can exert an electronic 'push' effect that enhance the rate of the O–O bond cleavage of the iron(III)-peroxo species and improve the yields of the catalytic oxidation products. We also demonstrate that the addition of exogenous acids in the same reaction platform also increase the catalytic yields of oxidation products, presumably by facilitating the cleavage of the O–O bond in an acid-assisted 'pull' effect.

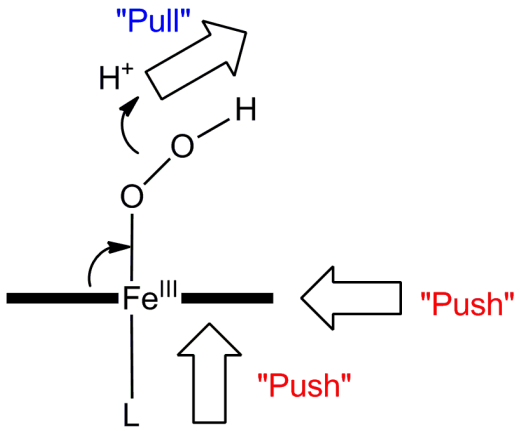

Figure 5.1: Schematic depiction of 'push–pull' effect in heme and iron-porphyrin systems.

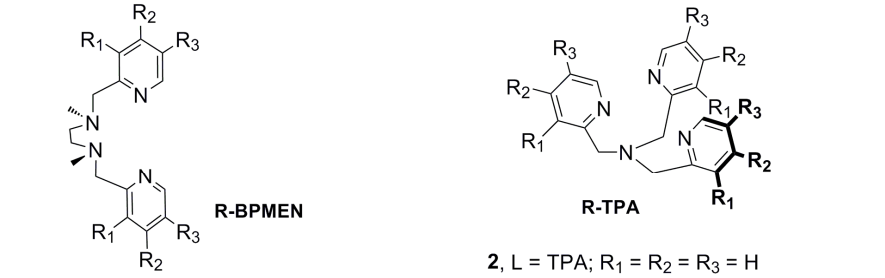

1, L = BPMEN; $R_1 = R_2 = R_3 = H$

4, L = SR-BPMEN; $R_1 = R_3 = Me$, $R_2 = OMe$

2, L = TPA; $R_1 = R_2 = R_3 = H$

3, L = SR-TPA; $R_1 = R_3 = Me$, $R_2 = OMe$

5, L = EW-TPA; $R_1 = R_2 = H$, $R_3 = CO_2Me$

Figure 5.2: Ligands used in this study and the corresponding iron complexes (represented by numbers).

5.2 Experimental Section

5.2.1 Materials and Synthesis

All chemicals and solvents were purchased from Aldrich and were used without additional purification unless otherwise noted. CH_3CN solvent was dried over CaH_2 before use. All hydrocarbon (alkane and olefin) substrates were passed over basic alumina immediately prior to use. The syntheses of the ligands BPMEN (N,N′-bis-(2-pyridylmethyl)-N,N′-dimethyl-1,2-ethylenediamine),[219] TPA (tris-(pyridyl-2-methyl)amine),[89] and SR-TPA (tris(4-methoxy-3,5-dimethylpyridyl-2-methyl)amine)[220] (Figure 5.2) and their corresponding iron complexes have been reported previously.

5.2.2 Synthesis of *N,N′*-bis(4-methoxy-3,5-dimethylpyridyl-2-methyl)-*N,N′*-dimethyl-1,2-diaminoethane (SR-BPMEN)

To a solution of 3,5-dimethyl-4-methoxy-2-chloromethylpyridine (3.07 gm, 13 mmol) in 20-22 mL of methanol, added was *N,N′*-di(methyl)ethylenediamine (6.9 mmol) with stirring. Aqueous potassium hydroxide solution (4.74 gm, 84.5 mmol) was added drop wise to this stirred solution using an additional funnel. The reaction was then stirred at room temperature for 48 hours. After the stirring a white solid was separated at the bottom of the reaction flask with a supernatant liquid. The solid was filtered out and the liquid was extracted with methylene chloride. The extract was dried over sodium sulfate and filtered. The filtrate was concentrated to yield light yellow oil. Yield: 2.04 gm (41%).

ESI-MS: 387 $(M+H)^+$. ^1H NMR ($CDCl_3$, 300 MHz): δ 2.14 (4H, s, bridged-CH_2), 2.24 (6H, s, CH_3), 2.55 (2H, s, py-H5), 3.37 (2H, s, py-H3), 3.53 (4H, s, CH_2), 3.69 (6H, s, OCH_3), 8.11 (2H, s, py-H6).

5.2.3 Synthesis of Methyl 6-(bromomethyl)nicotinate

Methyl 6-(bromomethyl)nicotinate was synthesized by bromination of Methyl 6-methylnicotinate using *N*-bromosuccinimide/benzoyl peroxide according to the published procedure.[221,222] The product was isolated as a dark red solid. Yield: 2.5 gm (50 %). ESI-MS: 231 $(M+H)^+$. ^1H NMR ($CDCl_3$, 500 MHz): δ 3.95 (3H, s, CH_3), 4.57 (2H, s, CH_2), 7.52 (1H, d, J = 8 Hz, py-H3), 8.28 (1H, dd, J = 8.5 Hz, 2.5 Hz, py-H4), 9.14 (1H, d, J = 2.0 Hz, py-H6).

5.2.4 Synthesis of Tris-(5-methoxycarbonylpyridyl-2-methyl)amine (5-$(O_2CMe)_3$-TPA aka EW-TPA)

To a solution of methyl(6-bromomethyl)nicotinate (1.058 gm, 4.6 mmol) in a 10 mL tetrahydrofuran (THF) solution at room temperature added were four equal portions of aqueous ammonia (6.1 mmol in total) over a period of four days. The reaction did not change color initially but turned into an orange solution over the next day and a white solid was separated out. The reaction mixture was stirred at room temperature over seven days. After filtering out the white solid, the filtrate was evaporated to dryness and dissolved in methylene chloride and dried over magnesium sulfate. After filtration, the

solution was evaporated to dryness to yield a brownish-yellow solid. Yield: 1.2 gm (60 %). ESI-MS: $(M+H)^+$ 465. ^1H NMR ($CDCl_3$, 300 MHz): δ 3.95 (9H, s, CH_3), 4.00 (6H, s, CH_2), 7.63 (3H, d, J = 9 Hz, py-H3), 8.26 (3H, dd, J = 8.1 Hz, 2.1 Hz, py-H4), 9.14 (3H, d, J = 3.0 Hz, py-H6).

5.2.5 Syntheses of $[Fe^{II}(SR\text{-}TPA)](OTf)_2$ (3), $[Fe^{II}(SR\text{-}BPMEN)](OTf)_2$ (4), and $[Fe^{II}(EW\text{-}TPA)](OTf)_2$ (5)

In a N_2-containing glovebox, a mixture of the R-TPA ligand (1.0 mmol) and $Fe^{II}(OTf)_2 \cdot 2NCCH_3$ (1.0 mmol) was stirred for 1 hour in 5 mL of CH_3CN. In all cases, dark red solutions were formed upon stirring. For **3** and **5**, direct addition of Et_2O into this solution at room temperature and storing at -20 °C resulted in the formation of purified **2** after 2 days as deep purple crystals in a 62% yield. Complex **5** was crystallized out after 2 days as dark yellow-brown crystals in a 53% yield. The formed complexes were recrystallized by dissolving in minimum amount of acetonitrile and adding diethyl ether to that solution. For SR-BPMEN ligand, a mixture of the SR-BPMEN ligand (1.0 mmol) and $Fe^{II}(OTf)_2 \cdot 2NCCH_3$ (1.0 mmol) was stirred for 1 h in 5 mL of tetrahydrofuran (THF) solution. **4** was isolated as a white solid in 60% yield that settled at the bottom of the reaction vessel and was filtered using a glass frit and washed with cold THF solution. Characterization of **3**: ESI-MS *m/z* 669 ($[Fe(SR\text{-}TPA)(OTf)]^+$), 555 ($[Fe(SR\text{-}TPA)(Cl)]^+$), 260 ($[Fe(SR\text{-}TPA)]^{2+}$). Anal. Calcd (found) for $[Fe(SR\text{-}TPA)](OTf)_2 \bullet H_2O \bullet 0.5CH_3CN$ ($C_{30}H_{39.5}F_6FeN_{4.5}O_{10}S_2$): C, 42.04 (41.94); H, 4.65 (4.59); N, 7.35 (7.72). Characterization of **4**: ESI-MS *m/z* 591 ($[Fe(SR\text{-}BPMEN)(OTf)]^+$), 221 ([Fe(SR-

BPMEN)]$^{2+}$). Anal. Calcd (found) for [Fe(SR-BPMEN)](OTf)$_2$•H$_2$O ($C_{24}H_{36}F_6FeN_4O_9S_2$): C, 38.00 (37.83); H, 4.78 (4.41); N, 7.39 (7.31). Characterization of **5**: ESI-MS *m*/*z* 669 ([Fe(EW-TPA)(OTf)]$^+$), 260 [Fe(EW-TPA)]$^{2+}$). Anal. Calcd (found) for [Fe(EW-TPA)](OTf)$_2$•3H$_2$O ($C_{26}H_{30}F_6FeN_4O_{15}S_2$): C, 35.79 (35.97); H, 3.47 (3.14); N, 6.42 (6.62).

5.2.6 Instrumentation

UV-vis spectra were acquired on a Hewlett-Packard (Agilent) 8452 diode array spectrophotometer over a range of 190-1100 nm. In kinetic experiments, quartz cuvettes were cooled to the desired temperature in a liquid nitrogen cryostat by Unisoku Co. Ltd. (Osaka, Japan). ESI-MS spectra were recorded on a Bruker Biotof-II mass spectrometer under conditions of a spray chamber voltage of 4000 Volt and a dry gas temperature of 200 °C. Product analyses of catalysis reactions were performed on a Perkin-Elmer Sigma 3 gas chromatograph (AT-1701 column, 30 m) with a flame ionization detector. GC-MS experiments were carried using an HP 6890 gas chromatograph (HP-5 column, 30 m) with an Agilent 5973 mass detector. GC-MS experiments were carried out using an HP 6890 gas chromatograph (HP-5 column, 30m) with an Agilent 5973 mass detector.

5.2.7 Spectroscopic Studies

Spectroscopic experiments of *ipso*-hydroxylation of various aromatic acids in the presence of **2**, **3** and **5** were performed in acetonitrile by adding 20 equivalents of substituted benzoic acid to the pre-formed Fe^{III}-OOH species (1 mM, generated with 10 equiv of hydrogen peroxide) in a 1-cm quartz cuvette precooled at -40 °C. $[Fe^{IV}(TPA)(O)]^{2+}$ species was generated at 25 °C by adding 0.03 mL of 0.07 M (1 equiv) CH_3CO_3H solution in acetonitrile to the 1 mM solution of **2**, **3** or **5** in acetonitrile.

5.2.8 Catalytic Studies

Catalytic studies were performed by using 0.2 mL of a 10-mM solution of **1**-**5** along with 0.287 mL of a 70-mM solution of H_2O_2 (10 equiv) at room temperature in acetonitrile where the final concentration of the iron in the solution was 1 mM. H_2O_2 was added using a syringe pump over 25 minutes with an additional 5 min of stirring. For *ipso*-hydroxylation catalysis, 25 equivalents (relative to iron complexes) of perfluoro-, 2-nitro-, and 2-chlorobenzoic acid were added in various experiments. For cyclohexane oxidation, 0.216 mL of neat substrate (1000 equiv compared to iron complex) was added for various trials. For olefin oxidation, either a 0.031 mL (100 equiv) or a 0.31 mL (1000 equiv) of 1-octene and a 0.29 mL (1000 equiv) of *tert*-butyl acrylate were added. For higher equivalents of H_2O_2 addition, oxidant was added over a longer period of time by

maintaining same number of moles of oxidant added per minute (48 μmoles/min). Each catalytic result reported represented an average of at least three experiments.

5.3 Results and Discussion

5.3.1 Electronic 'Push' Effect

Complex **2** in acetonitrile was shown to generate a low-spin iron(III)-hydroperoxo intermediate upon addition of H_2O_2 at -40 °C. This intermediate was characterized in detail by UV-vis, EPR, and resonance Raman spectroscopy.[79,86,132] Another iron(III)-peroxo intermediate was also reported and characterized in detail in the case of **2** and *tert*-butyl hydroperoxide.[223] $[Fe^{III}(TPA)(OO^tBu)]^{2+}$ (λ_{max} = 594 nm) could be generated by reacting **2** (1 mM) and 10 equivalents of *tert*-butyl hydroperoxide at -40 °C. Upon introduction of substituents on the pyridine rings of the TPA ligand, the λ_{max}'s of both the $[Fe^{III}(OOH)]^{2+}$ and the $[Fe^{III}(OO^tBu)]^{2+}$ species shifted from the parent species. In the case of complex **5**, both of the intermediates were red-shifted relative to their counterparts generated with **2** (Figure 5.3). In the case of complex **3**, on the contrary, the introduction of the electron donating groups shifted the chromophores to the higher energy (blue-shift) (Table 5.1). The observed shifts of the chromophores were consistent with their assignment as ligand-to-metal charge-transfer bands, as the replacement of the ester group with hydrogen and then with electron donating methyl and methoxy groups would lead to the higher energy acceptor orbitals on the iron center.

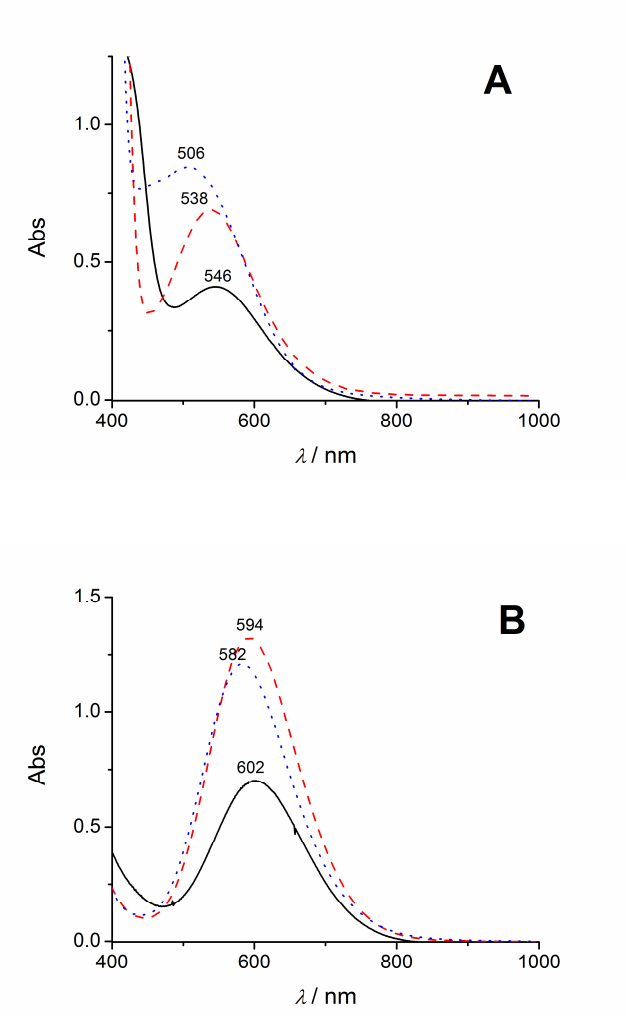

Figure 5.3: UV-vis spectra of the (A) $[Fe^{III}(OOH)]^{2+}$ and (B) $[Fe^{III}(OO^{t}Bu)]^{2+}$ species at -40 °C, generated upon addition of each of 10 equivalents of hydrogen peroxide and *tert*-butyl hydroperoxide, respectively to $[Fe(TPA)]^{2+}$, $[Fe(SR\text{-}TPA)]^{2+}$, and $[Fe(EW\text{-}TPA)]^{2+}$ complexes. Black solid line: $[Fe(EW\text{-}TPA)]^{2+}$; red dashed line: $[Fe(TPA)]^{2+}$ and blue dotted line: $[Fe(SR\text{-}TPA)]^{2+}$.

Table 5.1: Properties of the $[Fe^{III}\text{-}OOH]^{2+}$, $[Fe^{III}\text{-}OO^{t}Bu]^{2+}$, and $[Fe^{IV}{=}O]^{2+}$ species generated upon reacting 1 mM of each of **2**, **3**, and **5** in acetonitrile with H_2O_2, *tert*-butyl hydroperoxide and peracetic acid, respectively.[a]

Ligand (L)	λ_{max} of $[LFe^{III}\text{-}OOH]^{2+}$ (nm)	λ_{max} of $[LFe^{III}\text{-}OO^{t}Bu]^{2+}$ (nm)	k_{decay} of $[LFe^{III}\text{-}OOH)]^{2+}$ at -40 °C (s^{-1})	$t_{1/2}$ of $[LFe^{IV}{=}O]^{2+}$ at 25 °C (min)
EW-TPA	546	602	$5.9(1)\times10^{-6}$	2
TPA	538	594	$2.4(4)\times10^{-4}$	4
SR-TPA	506	582	$1.3(2)\times10^{-2}$	7

[a] See Experimental Section

Figure 5.4 and Table 5.1 compare the self-decay rates of the $[Fe^{III}(OOH)]^{2+}$ intermediates of complexes **2**, **3**, and **5**. The rate of self-decay of $[Fe^{III}(SR\text{-}TPA)(OOH)]^{2+}$ was found to be 50 times faster than that of $[Fe^{III}(TPA)(OOH)]^{2+}$ at -40 °C, which was in turn 40 times faster than that of $[Fe^{III}(EW\text{-}TPA)(OOH)]^{2+}$. The data suggested that the rate of self-decay of the iron(III)-hydroperoxo species with the most electron donating ligands was about 2000 times faster than that of the most electron-withdrawing one. The faster rate of self-decay of the iron(III)-hydroperoxo species of **3** can be explained by the increased electronic donation or a 'push' effect from the ligand backbone to the iron center (Scheme 5.1), which facilitated decay of the $[Fe^{III}(OOH)]^{2+}$ species. Unfortunately, the rate of decay of the $[Fe^{III}(OO^{t}Bu)]^{2+}$ species was complicated and involved more than one exponential.

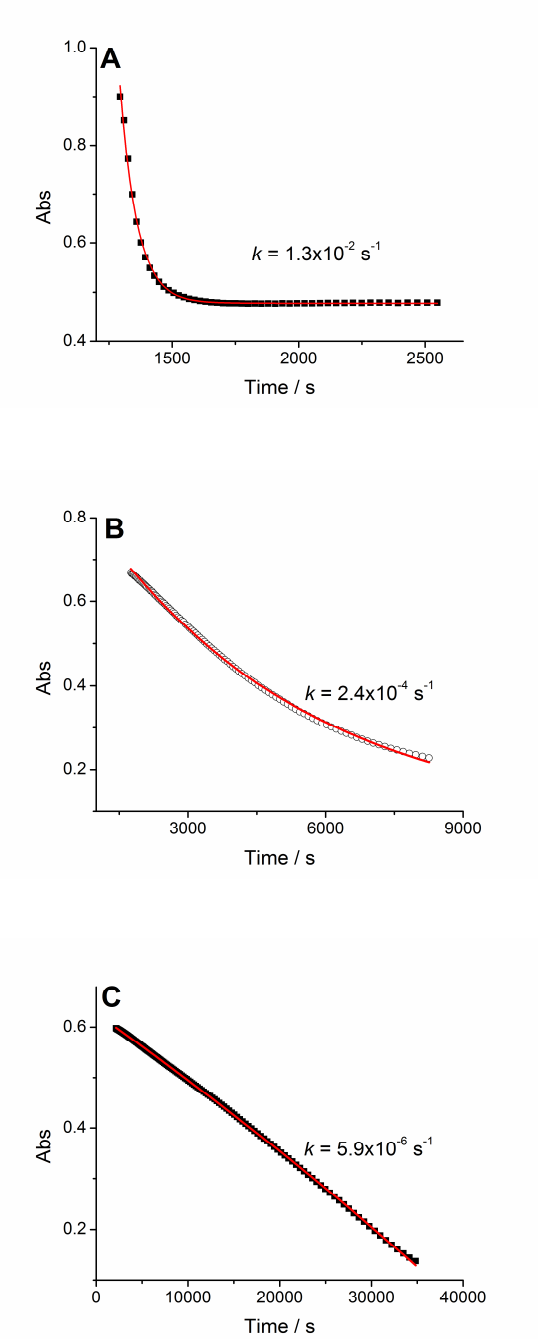

Figure 5.4: Kinetics of self-decay of the iron(III)-hydroperoxo species, generated by 1 mM (A) $[Fe^{II}(SR\text{-}TPA)]^{2+}$, (B) $[Fe^{II}(TPA)]^{2+}$ and (C) $[Fe^{II}(EW\text{-}TPA)]^{2+}$ and 10 equivalents of H_2O_2 at -40 °C.

The effect of electron-donating substituents on the reaction rates can also be monitored in the case of *ipso*-hydroxylation of the benzoates involving **2**/H_2O_2. The kinetics were monitored in acetonitrile by following the generation of the phenolate-to-iron(III) charge transfer chromophore upon addition of the substituted benzoic acids to the preformed iron(III)-hydroperoxo species at -40 °C. Unfortunately, addition of substituted benzoic acids to the $[Fe^{III}(EW\text{-}TPA)(OOH)]^{2+}$ intermediate did not generate any chromophore, unlike in **2** and **3**. Hence, only complexes **2** and **3** could be used in the comparison of the rates of *ipso*-hydroxylation. The first order fitting of the data (with 20 mM added acid) reflected the rate limiting conversion of the iron(III)-hydroperoxo species to the iron(V)-oxo species en route to the formation of the iron(III)-phenolate products (Figure 5.5). Interestingly, an enhancement of the reaction rate (by 4 times) was observed in the case of perfluorobenzoic acid upon moving from $[Fe(TPA)]^{2+}$ to $[Fe(SR\text{-}TPA)]^{2+}$. Similar enhancements of the reaction rates were also observed upon switching from **2** to **3** in the case of 2-chloro-6-nitro- and 2-nitrobenzoic acids (Figures 5.6 and 5.7, Table 5.2). The low temperature kinetics studies demonstrated that electron donation from ligand to the iron center also modulated the rate of reaction, presumably by a 'push' effect. Apart from enhancing the rates of reactions, electron donation from the supporting ligand backbone could potentially stabilize the high-valent oxidation states of iron.

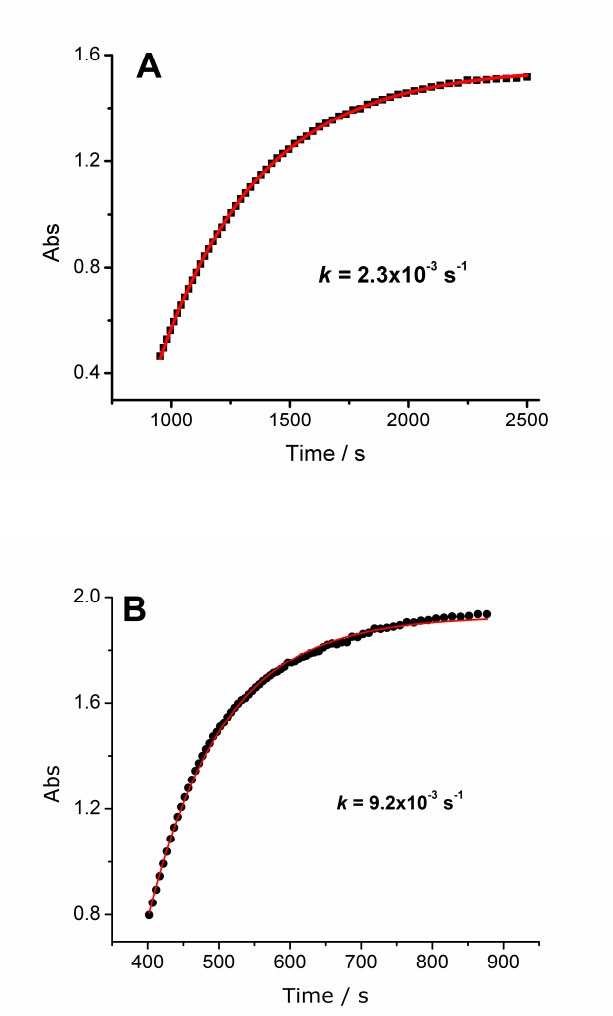

Figure 5.5: Rate limiting conversion of the Fe^{III}-OOH species to the Fe^{V}=O species in the *ipso*-hydroxylation of perfluorobenzoic acid (20 mM) using 1 mM (A) $[Fe(TPA)]^{2+}$ and (B) $[Fe(SR\text{-}TPA)]^{2+}$ in acetonitrile at -40 °C.

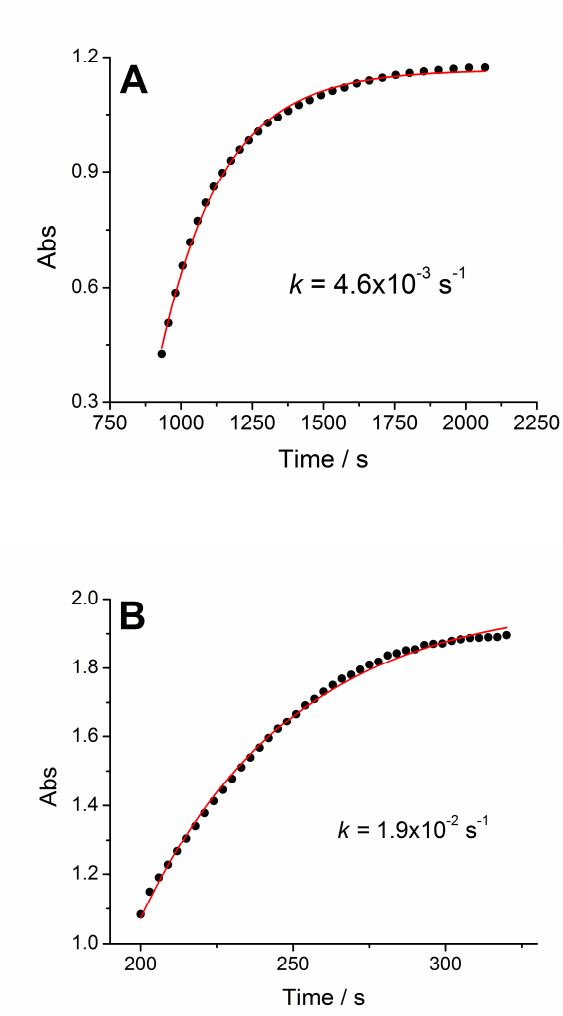

Figure 5.6: Rate limiting conversion of the Fe^{III}-OOH species to the Fe^{V}=O species in the *ipso*-hydroxylation of 2-chloro-6-nitrobenzoic acid (20 mM) using 1 mM (A) $[Fe(TPA)]^{2+}$ and (B) $[Fe(SR\text{-}TPA)]^{2+}$ in acetonitrile at -40 °C.

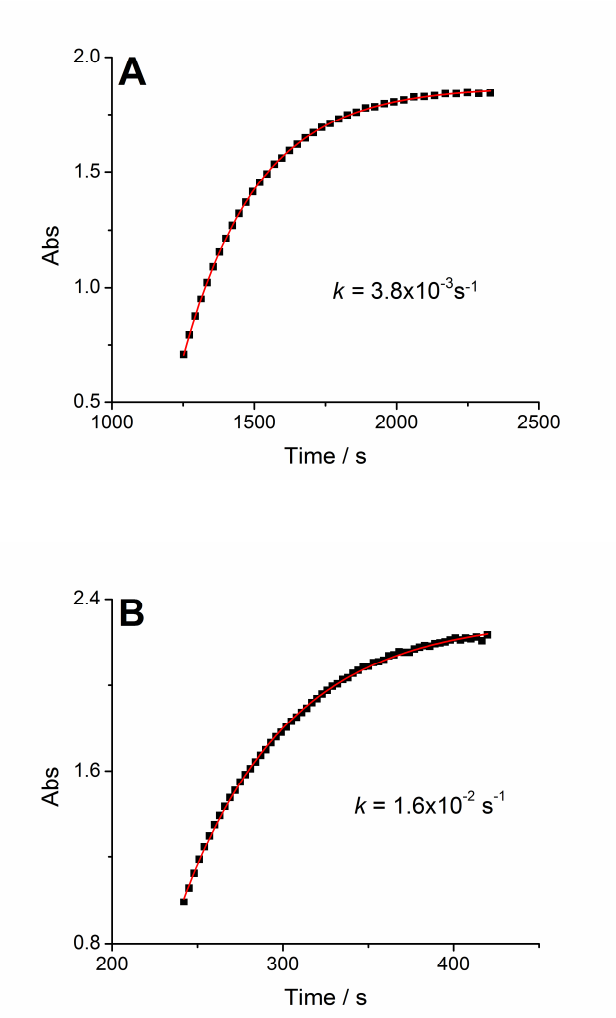

Figure 5.7: Rate limiting conversion of the Fe^{III}-OOH species to the Fe^{V}=O species in the *ipso*-hydroxylation of 2-nitrobenzoic acid (20 mM) using 1 mM (A) $[Fe(TPA)]^{2+}$ and (B) $[Fe(SR\text{-}TPA)]^{2+}$ in acetonitrile at -40 °C.

Table 5.2: Comparison of rate constants of conversion of the Fe^{III}-OOH species to the Fe^{V}=O species by $[Fe(TPA)]^{2+}$ and $[Fe(SR\text{-}TPA)]^{2+}$ in acetonitrile at -40 °C

Benzoic acid	$[Fe(TPA)]^{2+}$	$[Fe(SR\text{-}TPA)]^{2+}$
Perfluoro	$2.3(2) \times 10^{-3}$ s^{-1}	$9.2(4) \times 10^{-3}$ s^{-1}
2-Nitro	$3.8(4) \times 10^{-3}$ s^{-1}	$1.6(1) \times 10^{-2}$ s^{-1}
2-Chloro-6-nitro	$4.6(3) \times 10^{-3}$ s^{-1}	$1.9(3) \times 10^{-2}$ s^{-1}

The differences in electron donating ability of the three TPA ligands were also reflected in the relative lifetimes of the Fe^{IV}=O species generated with these ligands. Table 5.1 compares the half-lives of the Fe^{IV}=O species at 25 °C generated with either complex **2, 3** or **5** and one equiv of CH_3CO_3H. The $[Fe^{IV}(SR\text{-}TPA)(O)]^{2+}$ had the longest half-life of 7 minutes at room temperature followed by $[Fe^{IV}(TPA)(O)]^{2+}$ ($t_{½}$ = 4 min) and $[Fe^{IV}(EW\text{-}TPA)(O)]^{2+}$($t_{½}$ = 2 min). Greater electron donation from the SR-TPA ligand to the iron center in **3** helped in stabilizing the high-valent iron-oxo unit, while the destabilizing effects of electron withdrawing ester groups in **5** led to a shorter lifetime of the iron-oxo species (Scheme 5.1). This study thus further pointed out the usefulness of the electron donating ligands in stabilizing high-valent oxidation states of iron.

Scheme 5.1: Schematic depiction of electronic 'push' effect in the intermediates of non-heme iron complex **2** and H_2O_2.

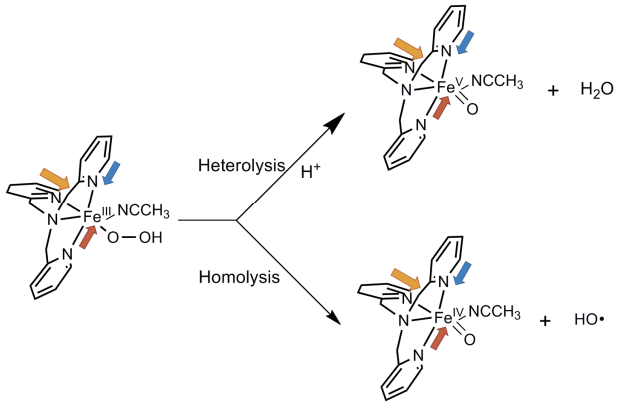

5.3.2 Catalytic *ipso*-Hydroxylation

The increased rate of conversion of the iron(III)-peroxo species to the iron(V)-oxo species with electron donating substituents at -40 °C was also reflected in the catalytic *ipso*-hydroxylation reactions at room temperature. The yield of phenol formation was increased with the $[Fe(SR\text{-}TPA)]^{2+}$ complex compared to that of $[Fe(TPA)]^{2+}$ (Figure 5.8 and Table 5.3). Interestingly, the lowest yield of phenol product was observed with $[Fe(EW\text{-}TPA)]^{2+}$. These results could be explained by invoking the idea of increased electron donation from the ligand backbone to the iron center in the rate limiting conversion of the iron(III)-peroxo species to the iron(V)-oxo species. The electronic 'push' effect in the heterolytic cleavage of the O–O bond – also demonstrated by an increased rate of reaction in the case of **3** (Table 5.2) – resulted in the improved yields in

the catalytic oxidation reactions. Conversely, the ester groups of **5** made the iron center electron deficient (compared to **2** and **3**) and consequently the rate limiting O–O bond cleavage step was slower.

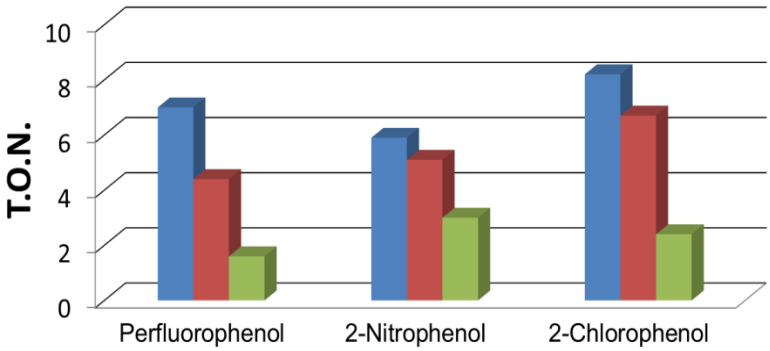

Figure 5.8: Catalytic conversion of benzoic acid to phenol using iron complexes and H_2O_2 in a ratio of FeL/Benzoic acid/H_2O_2 = 1/25/10 at room temperature. The concentration of iron in the reaction is 1 mM. Blue, red and green bars indicate [Fe(SR-TPA)]$^{2+}$, [Fe(TPA)]$^{2+}$, and [Fe(EW-TPA)]$^{2+}$, respectively. T.O.N. (Turn over number) was calculated as moles of product / mole of the catalyst.

Table 5.3: *ipso*-Hydroxylation of benzoic acid by iron(II) complexes of the TPA series of ligands and H_2O_2 at room temperature[a]

Complex	Perfluorophenol	2-Nitrophenol	2-Chlorophenol
$[Fe(EW\text{-}TPA)]^{2+}$	1.6 (3)	3.0 (4)	2.4 (3)
$[Fe(TPA)]^{2+}$	4.4 (1)	5.1 (1)	6.7 (4)
$[Fe(SR\text{-}TPA)]^{2+}$	7.0 (2)	5.9 (3)	8.2 (3)

[a] Reaction conditions: FeL (1 mM) / benzoic acid / H_2O_2 = 1 / 25 / 10 at room temperature. H_2O_2 was added using a syringe pump over 30 minutes

5.3.3 Catalytic Olefin Oxidation

Complexes **1** and **2** are two of the first reported non-heme iron complexes in the literature to carry out the olefin *cis*-dihydroxylation along with epoxidation using H_2O_2 as an oxidant.[53] To test the relative abilities of the new series of iron complexes to effect olefin oxidations, reactions were tried with 1-octene. The results showed that the olefin oxidation was best carried with the $[Fe(SR\text{-}TPA)]^{2+}$, followed by the $[Fe(TPA)]^{2+}$and $[Fe(EW\text{-}TPA)]^{2+}$ (Figure 5.9A). To test whether this hypothesis was also valid in the case of electron withdrawing olefins such as *tert*-butyl acrylate, we quantified the oxidation products with the TPA series of iron complexes and H_2O_2. The results suggested that the changing the nature of the olefin did not perturb the observed trend of increased oxidation products with the iron complexes of electron-rich ligands (Figure 5.9B).

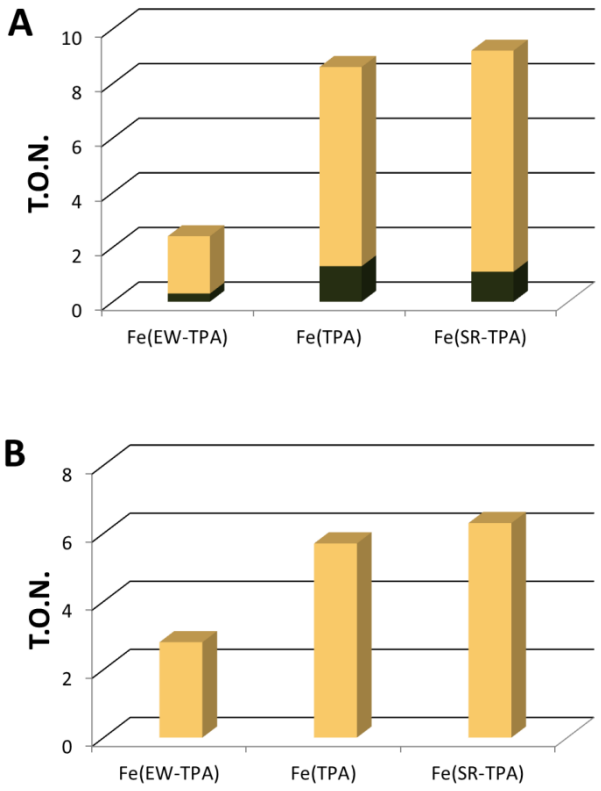

Figure 5.9: Catalytic oxidation of (A) 1-octene and (B) *tert*-butyl acrylate using iron complexes and H_2O_2 in a ratio of FeL/olefin/H_2O_2 = 1/1000/10 at room temperature. The concentration of iron in the reaction solution is 1 mM. Black and yellow bars indicate epoxide and *cis*-diol, respectively.

Table 5.4: Hydrocarbon (alkane and olefin) oxidation catalyzed by iron complexes of the TPA series of ligands using the reaction conditions FeL/substrate/H_2O_2 = 1/1000/10 at room temperature

Complex	1,2-Epoxyoctane	1,2-Octanediol	*tert*-Butyl acrylate diol	Cyclohexanol	Cyclohexanone
$[Fe(EW\text{-}TPA)]^{2+}$	0.3 (3)	2.1 (3)	2.8 (1)	1.5 (7)	0.5 (1)
$[Fe(TPA)]^{2+}$	1.3 (3)	7.3 (9)	5.7 (4)	2.5 (2)	0.2 (1)
$[Fe(SR\text{-}TPA)]^{2+}$	1.1 (1)	8.1 (2)	6.3 (5)	4.6 (3)	0.5 (2)
$[Fe(BPMEN)]^{2+}$	6.4 (1)	1.6 (1)	-	5.6 (5)	0.6 (2)
$[Fe(SR\text{-}BPMEN)]^{2+}$	6.4 (1)	2.9 (3)	-	6.6 (6)	0.8 (2)

5.3.4 Catalytic Alkane oxidation

Complexes **1** and **2** were also shown to catalyze the oxidation of cyclohexane to cyclohexanol and cyclohexanone.[52,57] Iron complexes of the TPA (**2**, **3**, and **5**) and the BPMEN (**1** and **4**) families have been investigated in the oxidation of cyclohexane using H_2O_2 as an oxidant at room temperature (Figure 5.10 and Table 5.4). The effect of ligand electronics was more prominent in the case of $[Fe(R\text{-}TPA)]^{2+}$-catalyzed oxidation of cyclohexane. The yield of cyclohexanol was about 2 times higher in the case of **3** than that of **2**, while the yield was the lowest in **5** (Figure 5.10). The iron complexes of the BPMEN family also showed a similar trend where the iron complex with a more electron donating ligand (**4**) showed slightly increased reactivity towards cyclohexane oxidation than **1** (Figure 5.10).

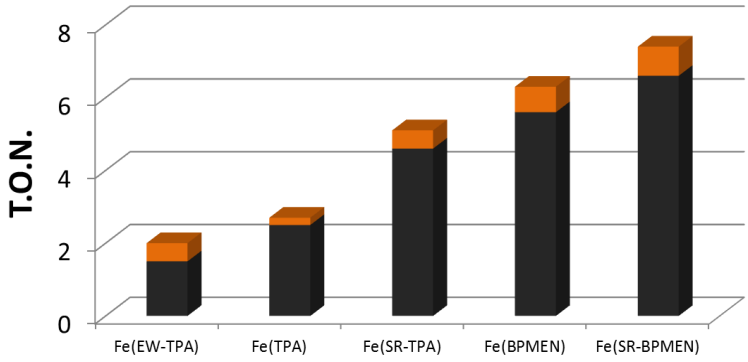

Figure 5.10: Catalytic oxidation of cyclohexane by the FeTPA family and FeBPMEN family of complexes and H_2O_2 in a ratio of FeL/cyclohexane/H_2O_2 = 1/1000/10 at room temperature. The concentrations of iron in the reactions are 1 mM. Black and saffron bars indicate cyclohexanol and cyclohexanone, respectively.

Figure 5.11 suggests that iron complexes of super-rich ligands were still more effective than the unsubstituted ones with increased amount of H_2O_2. It turned out that upon addition of 20 equivalents of H_2O_2 (with a similar rate of addition as of 10 equivalents, 48 μmoles/min), **3** was a better catalyst compared to **2** in both olefin and alkane oxidations (Figure 5.11). A similar trend was also observed in the case of the BPMEN series of iron complexes. However, this effect was more prominent in the $[Fe^{II}$(R-TPA)$]^{2+}$-catalyzed alkane oxidations.

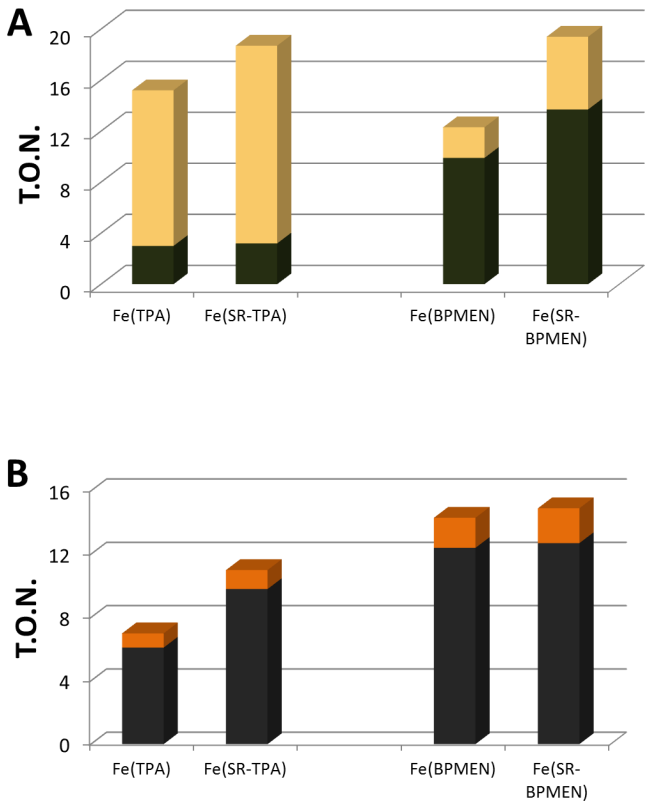

Figure 5.11: Comparison of the yields of oxidation products of (A) 1-octene (1 M) and (B) cyclohexane (1 M), catalyzed by FeTPA and FeBPMEN complexes (1 mM) and their super-rich counterparts in the presence of 20 equivalents of H_2O_2 in acetonitrile at room temperature. Epoxide and *cis*-diol products of 1-octene are indicated by deep-green and beige bars, respectively. Cyclohexanol and cyclohexanone are indicated by black and saffron bars, respectively.

5.4 Acid-assisted 'Pull' Effect

The discovery of the electronic 'push' effect in model non-heme iron chemistry also led us to investigate whether there was any involvement of the acid-assisted 'pull' effect. To understand the effects of acid in our oxidative chemistry, we have focused on **1**, the most reactive non-heme iron complex reported in the literature thus far.[52,53,57] It is important to mention at this point that we have shown that in the case of complex **2**, the addition of benzoic acids could lead to the hydroxylation of the arene ring and the aromatic ring oxidation was in competition with olefin oxidation.[190] We thus avoided benzoic acids to gauge the acid effect in our hydrocarbon oxidation studies, although Feringa and co-workers have used substituted benzoic acids in their Mn-catalyzed olefin oxidation reactions.[224,225]

5.4.1 Acid Effect in Alkane Oxidation

The beneficial effect of acetic acid in the highly selective oxidations of tertiary and secondary C–H bonds of alkanes was shown by Chen and White using a small molecule iron-catalyst [Fe(*S,S*-PDP)$(CH_3CN)_2$]$(SbF_6)_2$ (PDP = 2-(((S)-2-[(S)-1-(pyridin-2-ylmethyl)pyrrolidin-2-yl]pyrrolidin-1-yl)methyl)pyridine) and H_2O_2.[155,226] Interestingly, the addition of aliphatic acids was also found to be beneficial towards cyclohexane oxidation in the case of a related non-heme iron complex **1** using H_2O_2 as the oxidant (injected via a syringe pump). Acetic acid turned out to be the best additive in terms of

the maximum yield of cyclohexanol. As little as 2 equiv of added acetic acid was accounted for the 85% conversion of the oxidant into cyclohexanol (Figure 5.12). Pivalic and trifluoroacetic acid also increased the yields of cyclohexanol in a similar way (Table 5.5). The addition of aliphatic acids led us to check whether we really needed the syringe pumping of H_2O_2. When H_2O_2 (10 mM) was added directly to the reaction mixture in the presence of 2 equiv AcOH, it turned out that 80% conversion of the oxidant to the cyclohexanol took place within 5 minutes. The increased reaction time, however, did not improve the product yields of the reaction (Figure 5.13).

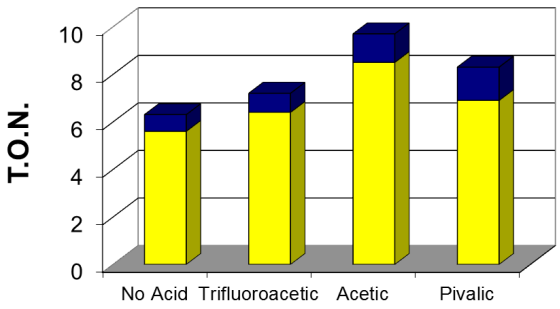

Figure 5.12: **1**/H_2O_2-catalyzed oxidation of cyclohexane at room temperature in the presence of substituted acetic acid additives in a ratio of **1**/acetic acid/cyclohexane/H_2O_2 = 1/2/1000/10. H_2O_2 was added using a syringe pump over 30 minutes. The yellow and blue bars indicate cyclohexanol and cyclohexanone, respectively.

Table 5.5: The effect of added acids in the **1** (1 mM)-catalyzed oxidation of cyclohexane (1 M) and 1-octene (0.1 M) in the presence of 2 equiv of additive and 10 equiv of H_2O_2 at room temperature

Additive	Cyclohexanol	Cyclohexanone	1,2-Epoxyoctane	1,2-Octanediol
No Acid	5.6 (7)	0.7 (2)	4.5 (2)	1.0 (1)
Trifluoroacetic acid	6.4 (3)	0.8 (1)	4.4 (6)	1.2 (1)
Dichloroacetic acid	-	-	5.4 (8)	0.5 (1)
Acetic acid	8.5 (4)	1.2 (1)	5.6 (6)	1.3 (1)
Pivalic acid	6.9 (2)	1.4 (1)	8.7 (6)	-

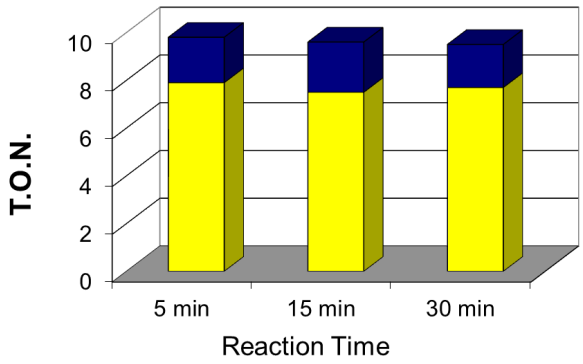

Figure 5.13: Cyclohexane oxidation over several time courses in the presence of 2 equiv of AcOH. H_2O_2 (10 equiv compared to **1**) was added all-at-once to **1**/substrate (1/1000) at room temperature. The yellow and blue bars indicate cyclohexanol and cyclohexanone, respectively.

The high yield of cyclohexane oxidation products in 5 minutes by the direct addition of H_2O_2 in the presence of acetic acid was reminiscent to the AcOH-assisted olefin oxidation study reported by Mas-Ballesté and Que,[59] where they showed the quantitative conversion of *cis*-cyclooctene to the *cis*-cyclooctene oxide in one minute at 0 °C. The observation that the reported olefin oxidation could be done under limiting substrate conditions led us to examine the effect of substrate concentration in alkane oxidation in the presence of AcOH. Figure 5.14 shows the substrate concentration dependence in the acetic acid-assisted oxidation of cyclohexane. However, it turned out that a huge excess (1000 equiv compared to **1**) of substrate was required to achieve appreciable yields of cyclohexanol. Cutting the amounts of the substrate each time by a factor of 10 reduced the cyclohexanol yields by 50%.

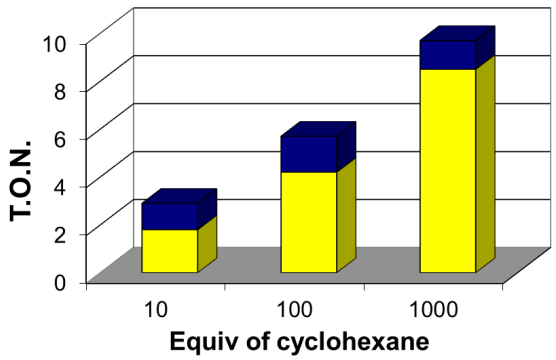

Figure 5.14: Substrate concentration dependence for **1**/H_2O_2–catalyzed cyclohexane oxidation in the presence of AcOH using the conditions described in Figure 5.12.

To check whether the yields of the alkane oxidation could be increased in the presence of excess acetic acid – like the one in the case of olefin oxidation[59] – we varied the amounts of added acetic acid in our alkane oxidation study. However, contrary to the observations with the olefin oxidation, the addition of increasing amounts of acetic acid led to the decrease in the yields of cyclohexanol (Figure 5.15).

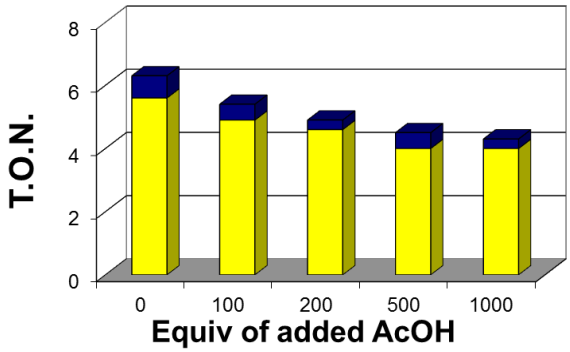

Figure 5.15: Cyclohexane oxidation by **1**/H_2O_2 in the presence of varied amounts of acetic acid using the conditions mentioned in Figure 5.12.

5.4.2 Acid Effect in Olefin Oxidation

Complex **1** was also reported as an effective catalyst using H_2O_2 as an oxidant, for the oxidation of terminal olefins to the corresponding epoxides in the presence of acetic acid as an additive.[129] Addition of 10 equivalents of acetic acid to **1** (3 mol %) and olefin (2.0 mmol) and H_2O_2 (3.0 mmol) led to ~80-90% observed yields of the epoxide products in

most of the cases. Interestingly, Mas-Balléste and Que reported that complexes **1** and **2** (0.5 mol %) could quantitatively catalyze the oxidation of *cis*-cyclooctene to its epoxide in one minute at 0 °C in the presence of a huge excess of acetic acid.[59] An $[Fe^{V}(O)(OAc)]^{2+}$ (generated via AcOH-assisted O–O bond cleavage of the iron(III)-hydroperoxo species) was proposed as the active oxidant responsible for the exclusive epoxidation. Interestingly, Feringa and co-workers also showed that the addition of different carboxylic acids in the oxidation of *cis*-cyclooctene by $[Mn^{IV}_2O_3(tmtacn)_2]^{2+}$ (tmtacn = *N*,*N*′,*N*″-trimethyl-1,4,7-triazacyclononane) and H_2O_2 could modulate the outcome of the oxidation products: trichloroacetic acid favored the epoxidation (in a 7:1 ratio over *cis*-dihydroxylation) and salicylic acid preferred *cis*-dihydroxylation (in a 11:1 ratio over epoxidation).[224] To gain further understanding of the role of the added acid in the non-heme iron-catalyzed olefin oxidations, reactions were performed with the substituted acetic acids. The points of interest were how the substitution at the acid affected the outcome of the reaction and modulated the epoxide-to-diol ratio. In general, this study would further enhance our understanding of the acid-effect in the olefin oxidation.

Figure 5.16 shows the effect of the substituted acetic acids in the **1**-catalyzed oxidation of 1-octene using H_2O_2 as the oxidant. Similar to the alkane oxidation study, two equivalents of substituted acetic acid were added in the reaction mixture. Interestingly, it was found that the weakest of all the acids added, pivalic acid, showed the highest yield

(~9 turnovers, 90% with respect to the added oxidants) of the epoxide product with no *cis*-diol formed (Table 5.5). Interestingly, increasing the acidity of the added acid led to a decrease in the epoxide yields with a concomitant increase in the yields of *cis*-diol.

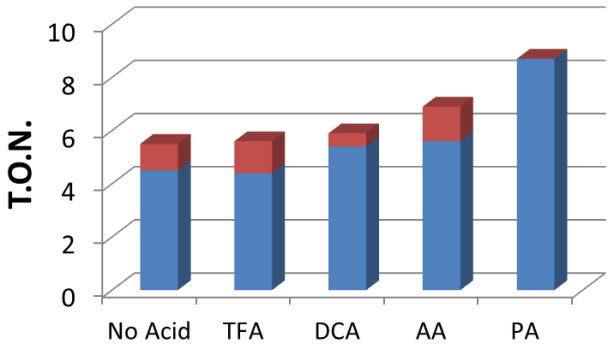

Figure 5.16: 1-catalyzed oxidation of 1-octene in the presence of 2 equivalents of acetic acid and its derivatives. 10 equivalents of H_2O_2 were introduced by using a syringe pump to **1** (1 mM) and 1-octene (0.1 M) at room temperature. TFA, DCA, AA, and PA stand for trifluoroacetic acid, dichloroacetic acid, acetic acid, and pivalic acid, respectively. Blue and red bars indicate epoxide and *cis*-diol, respectively.

5.5 Mechanistic Discussion

Scheme 5.2 describes our current understanding of the reaction landscape of **1**- and **2**-catalyzed oxidative transformations using H_2O_2 as an oxidant. It is proposed that hydrocarbon oxidation (olefin epoxidation and *cis*-dihydroxylation and alkane C–H bond hydroxylation) and *ipso*-hydroxylation are carried out on the same reaction platform. The $[Fe^{III}\text{-}OOH]^{2+}$ intermediates in both **1** and **2** serve as the common starting point in the mechanistic discussion.[62,79,132] It is proposed that cleavage of the O–O bond of the iron(III)-peroxo species towards the generation of the high-valent iron-oxo species is the rate limiting step in these oxidative transformations.[140,190] Thus, any alteration of this step would be reflected in the rate of the reaction. The increased rates of reactions (both self-decay of the iron(III)-hydroperoxo species and *ipso*-hydroxylation of benzoates) with iron complexes of electron donating ligands suggest that increasing the basicity of the pyridine ligands (Scheme 5.1) enhance the rate of the O–O bond cleavage. Interestingly, the beneficial effect of the electron donating substituents is also observed in the yields of catalytic oxidation products. The electron donating ligands also stabilize the high-valent iron-oxo species as evidenced by an increase in the half-life time (Table 5.1).

The aliphatic acid additives, on the other hand, help cleave the O–O bond of the $[Fe^{III}\text{-}OOH]^{2+}$ species by an acid-assisted pathway that leads to the formation of the $[Fe^{V}(O)(O_2CR)]^{2+}$ species.[59,190] AcOH-assisted heterolytic scission of the O–O bond of the iron(III)-peroxo species was also demonstrated by the formation of 2-methyl-1-phenyl-2-propanol in the reaction of **1**, acetic acid and 2-methyl-1-phenyl-2-propyl

hydroperoxide.[62] The presence of catalytic amounts of acids helps generate the $[Fe^{V}(O)(O_2CR)]^{2+}$ species that acts as the key oxidant in the aliphatic C–H bond hydroxylation. Varying the substituents at the acetic acid can also modulate the stability of the $[Fe^{V}(O)(O_2CR)]^{2+}$ oxidant. It is, however, not clear why acetic acid, and not any of its other siblings, yields maximum amounts of products in the cyclohexane oxidation. The effect of acid in the iron-catalyzed O–O bond cleavage landscape is better understood in the case of olefin oxidation. The *cis*-diol formation could take place in the water-assisted pathway via an $[Fe^{V}(O)(OH)]^{2+}$ oxidant, while the epoxide could be formed via both the $[Fe^{V}(O)(OH)]^{2+}$ and the $[Fe^{V}(O)(O_2CR)]^{2+}$ species (Scheme 5.2). The relative amounts of the formed epoxide and *cis*-diol along with the relative incorporations of the ^{18}O atom in the labeling experiments with $H_2{}^{18}O_2$ in the presence or absence of acids can help us gain further insight into the reaction landscape. Lowering the acidity of the substituted acetic acids upon incorporating electron donating substituents increases the basicity of the conjugate base that can help stabilize the $[Fe^{V}(O)(O_2CR)]^{2+}$ species and consequently the acid-assisted pathway is favored. The possibility of the increased formation of the $[(\mu\text{-}O)(\mu\text{-}O_2CR)Fe^{III}{}_2(TPA)_2]^{3+}$ species (Scheme 5.2) – usually considered as the thermodynamic sink in non-heme iron-based catalyst systems[227] – upon lowering the pK_a of the acid (due to the increased concentration of free anions in solution) may explain the lower yields of the oxidation products in the case of stronger acids. Formation of such bridged-dinuclear species were observed in the case of $[Mn^{IV}{}_2O_3(tmtacn)_2]^{2+}$ and trichloroacetic- and pivalic acid and several other substituted benzoic acids.[224,225] Although, unlike iron, the dinuclear manganese species were

proposed as the active catalyst in the oxidation reactions. The important question that needs to be addressed is why the yields of the cyclohexane oxidation products go down in the presence of a huge excess of acetic acid while *cis*-cyclooctene was quantitatively converted to its epoxide.

Scheme 5.2: Complete reaction landscape of hydrocarbon and aromatic oxidation by tetradentate iron complexes and H_2O_2.

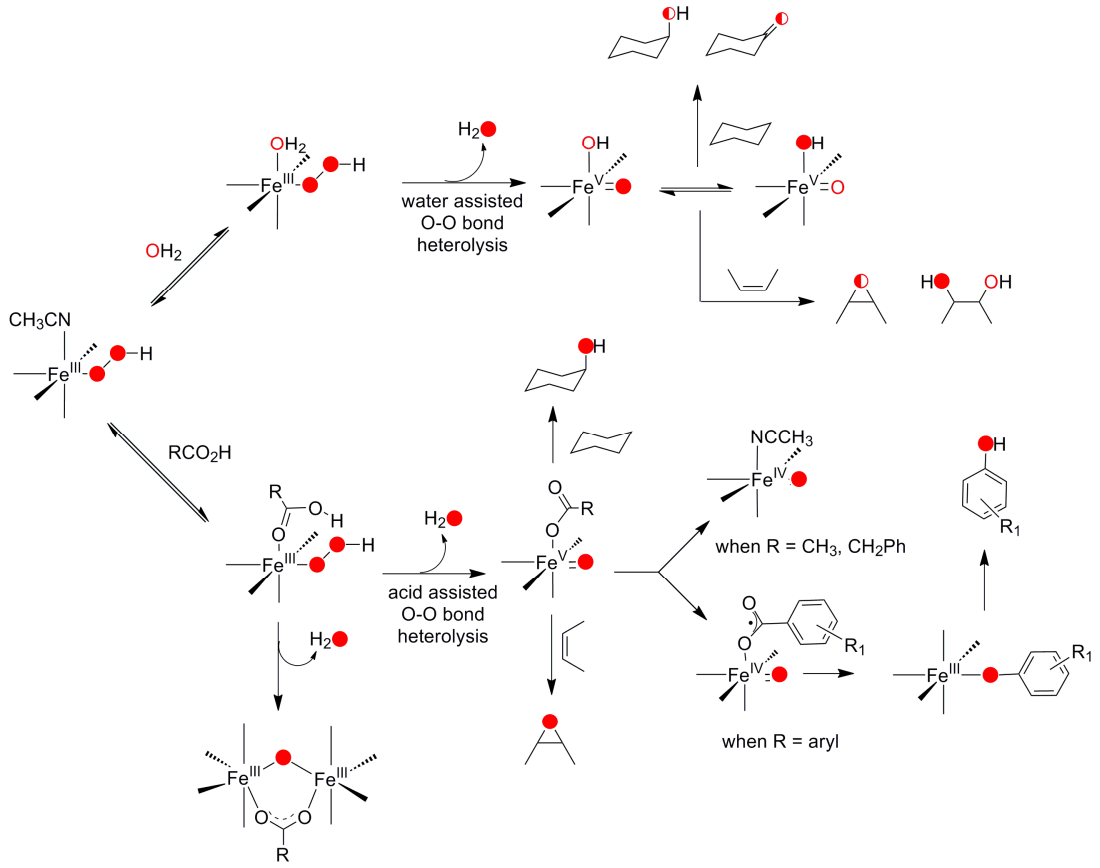

In summary, it is shown in this chapter that substituents at the ligand backbone can influence the metal center electronically and can modulate its reactivity. It is also shown electron donating ligands have a beneficial effect in stabilizing high-valent iron oxidation states. This is one of the first demonstrations of an electronic push effect in the non-heme iron systems. We have also demonstrated that the addition of aliphatic acids increases the yields of both alkane and olefin oxidation products. This serves as an example of the acid-assisted cleavage of the O–O bond or a 'pull' effect in the non-heme iron-catalyzed oxidative chemistry. Taken together, this chapter demonstrates the 'push-pull' effect in the cleavage of the O–O the bond in model non-heme iron systems.

References:

(1) Abu-Omar, M. M.; Loaiza, A.; Hontzeas, N. *Chem. Rev.* **2005**, *105*, 2227-2252.

(2) Denisov, I. G.; Makris, T. M.; Sligar, S. G.; Schlichting, I. *Chem. Rev.* **2005**, *105*, 2253-2278.

(3) Bruijnincx, P. C. A.; Koten, G. v.; Gebbink, R. J. M. K. *Chem. Soc. Rev.* **2008**, *37*, 2716-2744.

(4) Kovaleva, E. G.; Lipscomb, J. D. *Nat. Chem. Biol.* **2008**, *4*, 186-193.

(5) Solomon, E. I.; Brunold, T. C.; Davis, M. I.; Kemsley, J. N.; Lee, S.-K.; Lehnert, N.; Neese, F.; Skulan, A. J.; Yang, Y.-S.; Zhou, J. *Chem. Rev.* **2000**, *100*, 235-349.

(6) Hayaishi, O.; Katagiri, M.; Rothberg, S. *J. Am. Chem. Soc.* **1955**, *77*, 5450-5451.

(7) Solomon, E. I.; Chen, P.; Metz, M.; Lee, S.-K.; Palmer, A. E. *Angew. Chem., Int. Ed.* **2001**, *40*, 4570-4590.

(8) Ortiz de Montellano, P. R. *Chem. Rev.* **2009**, *110*, 932-948.

(9) Wallar, B. J.; Lipscomb, J. D. *Chem. Rev.* **1996**, *96*, 2625-2658.

(10) Tshuva, E. Y.; Lippard, S. J. *Chem. Rev.* **2004**, *104*, 987-1012.

(11) Hausinger, R. P. *Crit. Rev. Biochem. Mol. Biol.* **2004**, *39*, 21-68.

(12) Costas, M.; Mehn, M. P.; Jensen, M. P.; Que, L., Jr. *Chem. Rev.* **2004**, *104*, 939-986.

(13) Hegg, E. L.; Que, L., Jr. *Eur. J. Biochem.* **1997**, *250*, 625-629.

(14) Que, L., Jr. *Nat. Struct. Biol.* **2000**, *7*, 182-184.

(15) Karlsson, A.; Parales, J. V.; Parales, R. E.; Gibson, D. T.; Eklund, H.; Ramaswamy, S. *Science* **2003**, *299*, 1039-1042.

(16) *Microbial Degradation of Organic Compounds*; Gibson, D. T., Ed.; Marcel Dekker: New York, 1984.

(17) Gibson, D. T.; Parales, R. E. *Curr. Opin. Biotechnol.* **2000**, *11*, 236-243.

(18) Price, J. C.; Barr, E. W.; Glass, T. E.; Krebs, C.; Bollinger, J. M., Jr. *J. Am. Chem. Soc.* **2003**, *125*, 13008-13009.

(19) Price, J. C.; Barr, E. W.; Tirupati, B.; Bollinger, J. M., Jr.; Krebs, C. *Biochemistry* **2003**, *42*, 7497-7508.

(20) Riggs-Gelasco, P. J.; Price, J. C.; Guyer, R. B.; Brehm, J. H.; Barr, E. W.; Bollinger, J. M., Jr.; Krebs, C. *J. Am. Chem. Soc.* **2004**, *126*, 8108-8109.

(21) Price, J. C.; Barr, E. W.; Hoffart, L. M.; Krebs, C.; Bollinger, J. M., Jr. *Biochemistry* **2005**, *44*, 8138-8147.

(22) Proshlyakov, D. A.; Henshaw, T. F.; Monterosso, G. R.; Ryle, M. J.; Hausinger, R. P. *J. Am. Chem. Soc.* **2004**, *126*, 1022-1023.

(23) Grzyska, P. K.; Ryle, M. J.; Monterosso, G. R.; Liu, J.; Ballou, D. P.; Hausinger, R. P. *Biochemistry* **2005**, *44*, 3845-3855.

(24) Grzyska, P. K.; Appelman, E. H.; Hausinger, R. P.; Proshlyakov, D. A. *Proc. Natl. Acad. Sci. U. S. A.* **2010**, *107*, 3982-3987.

(25) Tuderman, L.; Myllylä, R.; Kivirikko, K. I. *Eur. J. Biochem.* **1977**, *80*, 341-348.

(26) Myllylä, R.; Tuderman, L.; Kivirikko, K. I. *Eur. J. Biochem.* **1977**, *80*, 349-357.

(27) Trewick, S. C.; Henshaw, T. F.; Hausinger, R. P.; Lindahl, T.; Sedgwick, B. *Nature* **2002**, *419*, 174-178.

(28) Falnes, P. Ø.; Johansen, R. F.; Seeberg, E. *Nature* **2002**, *419*, 178-182.

(29) Aas, P. A.; Otterlei, M.; Falnes, P. Ø.; Vågbø, C. B.; Skorpen, F.; Akbari, M.; Sundheim, O.; Bjørås, M.; Slupphaug, G.; Seeberg, E.; Krokan, H. E. *Nature* **2003**, *421*, 859-796.

(30) Vaillancourt, F. H.; Yeh, E.; Vosburg, D. A.; Garneau-Tsodikova, S.; Walsh, C. T. *Chem. Rev.* **2006**, *106*, 3364-3378.

(31) Blasiak, L. C.; Vaillancourt, F. H.; Walsh, C. T.; Drennan, C. L. *Nature* **2006**, *440*, 368-371.

(32) Galonic, D. P.; Barr, E. W.; Walsh, C. T.; Bollinger, J. M., Jr.; Krebs, C. *Nat. Chem. Biol.* **2007**, *3*, 113-116.

(33) Galonic Fujimori, D.; Barr, E. W.; Matthews, M. L.; Koch, G. M.; Yonce, J. R.; Walsh, C. T.; Bollinger, J. M., Jr.; Krebs, C.; Riggs-Gelasco, P. J. *J. Am. Chem. Soc.* **2007**, *129*, 13408-13409.

(34) Vaillancourt, F. H.; Yeh, E.; Vosburg, D. A.; O'Connor, S. E.; Walsh, C. T. *Nature* **2005**, *436*, 1191-1194.

(35) Vaillancourt, F. H.; Vosburg, D. A.; Walsh, C. T. *ChemBioChem* **2006**, *7*, 748-752.

(36) Sinnecker, S.; Svensen, N.; Barr, E. W.; Ye, S.; Bollinger, J. M., Jr.; Neese, F.; Krebs, C. *J. Am. Chem. Soc.* **2007**, *129*, 6168-6179.

(37) Hoffart, L. M.; Barr, E. W.; Guyer, R. B.; Bollinger, J. M., Jr.; Krebs, C. *Proc. Natl. Acad. Sci. U.S.A.* **2006**, *103*, 14738-14743.

(38) Kappock, T. J.; Caradonna, J. P. *Chem. Rev.* **1996**, *96*, 2659-2756.

(39) Fitzpatrick, P. F. *Annu. Rev. Biochem.* **1999**, *68*, 355-381.

(40) Klinman, J. P. *J. Biol. Inorg. Chem.* **2001**, *6*, 1-13.

(41) Eser, B. E.; Barr, E. W.; Frantom, P. A.; Saleh, L.; Bollinger, J. M.; Krebs, C.; Fitzpatrick, P. F. *J. Am. Chem. Soc.* **2007**, *129*, 11334-11335.

(42) Fusetti, F.; Erlandsen, H.; Flatmark, T.; Stevens, R. C. *J. Biol. Chem.* **1998**, *273*, 16962-16967.

(43) Kobe, B.; Jennings, I. G.; House, C. M.; Michell, B. J.; Goodwill, K. E.; Santarsiero, B. D.; Stevens, R. C.; Cotton, R. G. H.; Kemp, B. E. *Nat. Struct. Biol.* **1999**, *6*, 442-448.

(44) Erlandsen, H.; Kim, J. Y.; Patch, M. G.; Han, A.; Volner, A.; Abu-Omar, M. M.; Stevens, R. C. *J. Mol. Biol.* **2002**, *320*, 645-661.

(45) Wang, L.; Erlandsen, H.; Haavik, J.; Knappskog, P. M.; Stevens, R. C. *Biochemistry* **2002**, *41*, 12569-12574.

(46) Goodwill, K. E.; Sabatier, C.; Marks, C.; Raag, R.; Fitzpatrick, P. F.; Stevens, R. C. *Nat. Struct. Biol.* **1997**, *4*, 578-585.

(47) Oldenburg, P. D.; Que, L., Jr. *Catal. Today* **2006**, *117*, 15-21.

(48) Que, L., Jr.; Tolman, W. B. *Nature* **2008**, *455*, 333-340.

(49) Enthaler, S.; Junge, K.; Beller, M. *Angew. Chem., Int. Ed.* **2008**, *47*, 3317-3321.

(50) Oldenburg, P. D.; Shteinman, A. A.; Que, L., Jr. *J. Am. Chem. Soc.* **2005**, *127*, 15672-15673.

(51) Oldenburg, P. D.; Feng, Y.; Pryjomska-Ray, I.; Ness, D.; Que, L. *J. Am. Chem. Soc.* **2010**, *132*, 17713-17723.

(52) Chen, K.; Que, L., Jr. *J. Am. Chem. Soc.* **2001**, *123*, 6327-6337.

(53) Chen, K.; Costas, M.; Kim, J.; Tipton, A. K.; Que, L., Jr. *J. Am. Chem. Soc.* **2002**, *124*, 3026-3035.

(54) Chen, K.; Costas, M.; Que, L., Jr. *J. Chem. Soc., Dalton Trans.* **2002**, 672-679.

(55) Ryu, J. Y.; Kim, J.; Costas, M.; Chen, K.; Nam, W.; Que, L., Jr. *Chem. Commun.* **2002**, 1288-1289.

(56) Company, A.; Gómez, L.; Fontrodona, X.; Ribas, X.; Costas, M. *Chem.--Eur. J.* **2008**, *14*, 5727-5731.

(57) Chen, K.; Que, L., Jr. *Chem. Commun.* **1999**, 1375-1376.

(58) Chen, K.; Que, L., Jr. *Angew. Chem., Int. Ed.* **1999**, *38*, 2227-2229.

(59) Mas-Ballesté, R.; Que, L., Jr. *J. Am. Chem. Soc.* **2007**, *129*, 15964-15972.

(60) Taktak, S.; Flook, M.; Foxman, B. M.; Que, L., Jr.; Rybak-Akimova, E. V. *Chem. Commun.* **2005**, 5301–5303.

(61) Oh, N. Y.; Seo, M. S.; Lim, M. H.; Consugar, M. B.; Park, M. J.; Rohde, J.-U.; Han, J.; Kim, K. M.; Kim, J.; Que, L., Jr.; Nam, W. *Chem. Commun.* **2005**, 5644-5646.

(62) Makhlynets, O. V.; Rybak-Akimova, E. V. *Chem.--Eur. J.* **2010**, *16*, 13995-14006.

(63) Fujita, M.; Costas, M.; Que, L., Jr. *J. Am. Chem. Soc.* **2003**, *125*, 9912-9913.

(64) Costas, M.; Chen, K.; Que, L., Jr. *Coord. Chem. Rev.* **2000**, *200-202*, 517-544.

(65) Walling, C. *Acc. Chem. Res.* **1975**, *8*, 125-131.

(66) Buxton, G. V.; Greenstock, C. L.; Helman, W. P.; Ross, A. B. *J. Phys. Chem. Ref. Data* **1988**, *17*, 513-886.

(67) Sono, M.; Roach, M. P.; Coulter, E. D.; Dawson, J. H. *Chem. Rev.* **1996**, *96*, 2841-2887.

(68) Nesheim, J. C.; Lipscomb, J. D. *Biochemistry* **1996**, *35*, 10240-10247.

(69) Kaizer, J.; Klinker, E. J.; Oh, N. Y.; Rohde, J.-U.; Song, W. J.; Stubna, A.; Kim, J.; Münck, E.; Nam, W.; Que, L., Jr. *J. Am. Chem. Soc.* **2004**, *126*, 472-473.

(70) Klinker, E. J.; Shaik, S.; Hirao, H.; Que, L., Jr *Angew. Chem., Int. Ed.* **2009**, *48*, 1291-1295.

(71) Trotman-Dickenson, A. F. *Adv. Free Radical Chem.* **1965**, *1*, 1-38.

(72) Miyajima, S.; Simamura, O. *Bull. Chem. Soc. Jpn.* **1975**, *48*, 526-530.

(73) Ingold, K. U.; MacFaul, P. A. In *Biomimetic Oxidations Catalyzed by Transition Metal Complexes*; Meunier, B., Ed.; Imperial College Press: London, 2000, p 45-89.

(74) Russell, G. A. *J. Am. Chem. Soc.* **1957**, *79*, 3871-3877.

(75) Groves, J. T.; Nemo, T. E.; Myers, R. S. *J. Am. Chem. Soc.* **1979**, *101*, 1032-1033.

(76) England, J.; Gondhia, R.; Bigorra-Lopez, L.; Petersen, A. R.; White, A. J. P.; Britovsek, G. J. P. *Dalton Trans.* **2009**, 5319-5334.

(77) Tanase, S.; Marques-Gallego, P.; Browne, W. R.; Hage, R.; Bouwman, E.; Feringa, B. L.; Reedijk, J. *Dalton Trans.* **2008**, 2026-2033.

(78) Bilis, G.; Christoforidis, K. C.; Deligiannakis, Y.; Louloudi, M. *Catal. Today* **2010**, *157*, 101-106.

(79) Kim, C.; Chen, K.; Kim, J.; Que, L., Jr. *J. Am. Chem. Soc.* **1997**, *119*, 5964-5965.

(80) England, J.; Davies, C. R.; Banaru, M.; White, A. J. P.; Britovsek, G. J. P. *Adv. Synth. Catal.* **2008**, *350*, 883-897.

(81) Roelfes, G.; Lubben, M.; Hage, R.; Que, L., Jr.; Feringa, B. L. *Chem.--Eur. J.* **2000**, *6*, 2152-2159.

(82) Groves, J. T.; Nemo, T. E. *J. Am. Chem. Soc.* **1983**, *105*, 6243-6248.

(83) Khenkin, A. M.; Shilov, A. E. *New J. Chem.* **1989**, *13*, 659-667.

(84) das Dores Assis, M.; R. Lindsay Smith, J. *J. Chem. Soc. Perkin Trans. 2* **1998**, 2221-2226.

(85) Sorokin, A. B.; Khenkin, A. M. *New J. Chem.* **1990**, *14*, 63-67.

(86) Ho, R. Y. N.; Roelfes, G.; Feringa, B. L.; Que, L., Jr. *J. Am. Chem. Soc.* **1999**, *121*, 264-265.

(87) Lange, S. J.; Miyake, H.; Que, L., Jr. *J. Am. Chem. Soc.* **1999**, *121*, 6330-6331.

(88) Jensen, M. P.; Lange, S. J.; Mehn, M. P.; Que, E. L.; Que, L., Jr. *J. Am. Chem. Soc.* **2003**, *125*, 2113-2128.

(89) Zang, Y.; Kim, J.; Dong, Y.; Wilkinson, E. C.; Appelman, E. H.; Que, L., Jr. *J. Am. Chem. Soc.* **1997**, *119*, 4197-4205.

(90) Kim, J.; Larka, E.; Wilkinson, E. C.; Que, L., Jr. *Angew. Chem., Int. Ed.* **1995**, *34*, 2048-2049.

(91) Kim, J.; Zang, Y.; Costas, M.; Harrison, R. G.; Wilkinson, E. C.; Que, L., Jr *J. Biol. Inorg. Chem.* **2001**, *6*, 275-284.

(92) Ménage, S.; Wilkinson, E. C.; Que, L., Jr.; Fontecave, M. *Angew. Chem., Int. Ed.* **1995**, *34*, 203-205.

(93) Moran, G. R.; Derecskei-Kovacs, A.; Hillas, P. J.; Fitzpatrick, P. F. *J. Am. Chem. Soc.* **2000**, *122*, 4535-4541.

(94) Guroff, G.; Daly, J. W.; Jerina, D. M.; Renson, J.; Witkop, B.; Udenfriend, S. *Science* **1967**, *157*, 1524-1530.

(95) Mekmouche, Y.; Ménage, S.; Toia-Duboc, C.; Fontecave, M.; Galey, J.-B.; Lebrun, C.; Pecaut, J. *Angew. Chem., Int. Ed.* **2001**, *40*, 949-952.

(96) Mehn, M. P.; Fujisawa, K.; Hegg, E. L.; Que, L., Jr. *J. Am. Chem. Soc.* **2003**, *125*, 7828-7842.

(97) Flatmark, T.; Stevens, R. C. *Chem. Rev.* **1999**, *99*, 2137-2160.

(98) Fitzpatrick, P. F. *Biochemistry* **2003**, *42*, 14083-14091.

(99) Foster, T. L.; Caradonna, J. P. *Comprehensive Coordination Chemistry II* **2004**, *8*, 343-368.

(100) Fishman, A.; Tao, Y.; Rui, L. Y.; Wood, T. K. *J. Biol. Chem.* **2005**, *280*, 506-514.

(101) Sazinsky, M. H.; Bard, J.; Donato, A. D.; Lippard, S. J. *J. Biol. Chem.* **2004**, *279*, 30600-30610.

(102) Mitchell, K. H.; Rogge, C. E.; Gierahn, T.; Fox, B. G. *Proc. Natl. Acad. Sci. U.S.A.* **2003**, *100*, 3784-3789.

(103) Murray, L. J.; Lippard, S. J. *Acc. Chem. Res.* **2007**, *40*, 466-474.

(104) Krebs, C.; Galonić Fujimori, D.; Walsh, C. T.; Bollinger, J. M., Jr. *Acc. Chem. Res.* **2007**, *40*, 484-492.

(105) Bollinger, J. M., Jr.; Krebs, C. *J. Inorg. Biochem.* **2006**, *100*, 586-605.

(106) Liu, A.; Jin, Y.; Zhang, J.; Brazeau, B. J.; Lipscomb, J. D. *Biochem. Biophys. Res. Commun.* **2005**, *338*, 254-261.

(107) Lee, S.-K.; Nesheim, J. C.; Lipscomb, J. D. *J. Biol. Chem.* **1993**, *268*, 21569-21577.

(108) Lee, S.-K.; Fox, B. G.; Froland, W. A.; Lipscomb, J. D.; Münck, E. *J. Am. Chem. Soc.* **1993**, *115*, 6450-6451.

(109) Walling, C. J., R. A. *J. Am. Chem. Soc.* **1975**, *97*, 363-367.

(110) Kurata, T.; Watanabe, Y.; Katoh, M.; Sawaki, Y. *J. Am. Chem. Soc.* **1988**, *110*, 7472-7478.

(111) Sawyer, D. T.; Sobkowiak, A.; Matsushita, T. *Acc. Chem. Res.* **1996**, *29*, 409-416.

(112) Udenfriend, S.; Clark, C. T.; Axelrod, J.; Brodie, B. B. *J. Biol. Chem.* **1954**, *208*, 731-739.

(113) Hage, J. P.; Powell, J. A.; Sawyer, D. T. *J. Am. Chem. Soc.* **1995**, *117*, 12897-12898.

(114) Tezuka, T.; Narita, N.; Ando, W.; Oae, S. *J. Am. Chem. Soc.* **1981**, *103*, 3045-3049.

(115) Mathieu, D.; Frapart, Y.-M.; Bartoli, J. F.; Boucher, J.-L.; Battioni, P.; Mansuy, D. *Chem. Commun.* **2004**, 54-55.

(116) Balland, V.; Charlot, M.-F.; Banse, F.; Girerd, J.-J.; Mattioli, T. A.; Bill, E.; Bartoli, J.-F.; Battioni, P.; Mansuy, D. *Eur. J. Inorg. Chem.* **2004**, 301-308.

(117) Bartoli, J.-F.; Lambert, F.; Morgenstern-Badarau, I.; Battioni, P.; Mansuy, D. *C. R. Chim.* **2002**, *5*, 263-266.

(118) Bianchi, D.; Bertoli, M.; Tassinari, R.; Ricci, M.; Vignola, R. *J. Mol. Catal. A: Chem.* **2003**, *204-205*, 419-424.

(119) Hamilton, G. A.; Hanifin, J. W.; Friedman, J. P. *J. Am. Chem. Soc.* **1966**, *88*, 5269-5272.

(120) de Visser, S. P.; Oh, K.; Han, A.-R.; Nam, W. *Inorg. Chem.* **2007**, *46*, 4632-4641.

(121) Ménage, S.; Galey, J.-B.; Dumats, J.; Hussler, G.; Seité, M.; Luneau, I. G.; Chottard, G.; Fontecave, M. *J. Am. Chem. Soc.* **1998**, *120*, 13370-13382.

(122) Furutachi, H.; Murayama, M.; Shiohara, A.; Yamazaki, S.; Fujinami, S.; Uehara, A.; Suzuki, M.; Ogo, S.; Watanabec, Y.; Maeda, Y. *Chem Commun.* **2003**, 1900-1901.

(123) Avenier, F.; Dubois, L.; Latour, J.-M. *New J. Chem.* **2004**, 782-784.

(124) Nielsen, A.; Larsen, F. B.; Bond, A. D.; McKenzie, C. J. *Angew. Chem., Int. Ed.* **2006**, *45*, 1602-1606.

(125) Yamashita, M.; Furutachi, H.; Tosha, T.; Fujinami, S.; Saito, W.; Maeda, Y.; Takahashi, K.; Tanaka, K.; Kitagawa, T.; Suzuki, M. *J. Am. Chem. Soc.* **2007**, *129*, 2-3.

(126) Kitajima, N.; Ito, M.; Fukui, H.; Moro-oka, Y. *J. Am. Chem. Soc.* **1993**, *115*, 9335-9336.

(127) Tanase, S.; Bouwman, E. *Adv. Inorg. Chem.* **2006**, *58*, 29-75.

(128) Kryatov, S. V.; Rybak-Akimova, E. V.; Schindler, S. *Chem. Rev.* **2005**, *105*, 2175-2226.

(129) White, M. C.; Doyle, A. G.; Jacobsen, E. N. *J. Am. Chem. Soc.* **2001**, *123*, 7194-7195.

(130) Duban, E. A.; Bryliakov, K. P.; Talsi, E. P. *Mendeleev Commun.* **2005**, *15*, 12-14.

(131) Duban, E. A.; Bryliakov, K. P.; Talsi, E. P. *Eur. J. Inorg. Chem.* **2007**, 852-857.

(132) Mairata i Payeras, A.; Ho, R. Y. N.; Fujita, M.; Que, L., Jr. *Chem.--Eur. J.* **2004**, *10*, 4944 – 4953.

(133) Lehnert, N.; Ho, R. Y. N.; Que Jr., L.; Solomon, E. I. *J. Am. Chem. Soc.* **2001**, *123*, 8271-8290.

(134) Lim, M. H.; Rohde, J.-U.; Stubna, A.; Bukowski, M. R.; Costas, M.; Ho, R. Y. N.; Münck, E.; Nam, W.; Que, L., Jr. *Proc. Natl. Acad. Sci. U.S.A.* **2003**, *100*, 3665-3670.

(135) SMART V5.054; Bruker Analytical X-ray Systems: Madison, WI, 2001.

(136) Blessing, R. H. *Acta Cryst. A* **1995**, *51*, 33-38.

(137) SAINT+ V6.45; Bruker Analytical X-Ray Systems: Madison, WI, 2003.

(138) SHELXTL V6.14; Bruker Analytical X-Ray Systems: Madison, WI, 2000.

(139) Korendovych, I. V.; Kryatov, S. V.; Rybak-Akimova, E. V. *Acc. Chem. Res.* **2007**, *40*, 510-521.

(140) Makhlynets, O. V.; Das, P.; Taktak, S.; Flook, M.; Mas-Ballesté, R.; Rybak-Akimova, E. V.; Que, L., Jr. *Chem.-- Eur. J.* **2009**, *15*, 13171-13180.

(141) Korzekwa, K. R.; Swinney, D. C.; Trager, W. F. *Biochemistry* **1989**, *28*, 9019-9027.

(142) Kang, M.-J.; Song, W. J.; Han, A.-R.; Choi, Y. S.; Jang, H. G.; Nam, W. *J. Org. Chem.* **2007**, *72*, 6301-6304.

(143) de Visser, S. P.; Shaik, S. *J. Am. Chem. Soc.* **2003**, *125*, 7413-7424.

(144) Sorokin, A.; Meunier, B. *Eur. J. Inorg. Chem.* **1998**, *1998*, 1269-1281.

(145) Nam, W. *Acc. Chem. Res.* **2007**, *40*, 522–531.

(146) Que, L., Jr. *Acc. Chem. Res.* **2007**, *40*, 493-500.

(147) Klein, G. W.; Bhatia, K.; Madhavan, V.; Schuler, R. H. *J. Phys. Chem.* **1975**, *79*, 1767-1774.

(148) Bassan, A.; Blomberg, M. R. A.; Siegbahn, P. E. M.; Que, L., Jr. *Chem.--Eur. J.* **2005**, *11*, 692-705.

(149) Park, M. J.; Lee, J.; Suh, Y.; Kim, J.; Nam, W. *J. Am. Chem. Soc.* **2006**, *128*, 2630-2634.

(150) Yoon, J.; Wilson, S. A.; Jang, Y. K.; Seo, M. S.; Nehru, K.; Hedman, B.; Hodgson, K. O.; Bill, E.; Solomon, E. I.; Nam, W. *Angew. Chem., Int. Ed.* **2009**, *48*, 1257-1260.

(151) de Oliveira, F. T.; Chanda, A.; Banerjee, D.; Shan, X.; Mondal, S.; Que Jr., L.; Bominaar, E. L.; Münck, E.; Collins, T. J. *Science* **2007**, *315*, 835-838.

(152) Lee, S. H.; Han, J. H.; Kwak, H.; Lee, S. J.; Lee, E. Y.; Kim, H. J.; Lee, J. H.; Bae, C.; Lee, S. N.; Kim, Y.; Kim, C. *Chem.--Eur. J.* **2007**, *13*, 9393 – 9398.

(153) Lyakin, O. Y.; Bryliakov, K. P.; Britovsek, G. J. P.; Talsi, E. P. *J. Am. Chem. Soc.* **2009**, *131*, 10798-10799.

(154) Feng, Y.; Ke, C.-y.; Xue, G.; Que, L., Jr. *Chem. Commun.* **2009**, 50-52.

(155) Chen, M. S.; White, M. C. *Science* **2007**, *318*, 783-787.

(156) Wang, J.; Itoh, H.; Tsuchiya, M.; Tokumaru, K.; Sakuragi, H. *Tetrahedron* **1995**, *51*, 11967-11978.

(157) Kauppi, B.; Lee, K.; Carredano, E.; Parales, R. E.; Gibson, D. T.; Eklund, H.; Ramaswamy, S. *Structure* **1998**, *6*, 571-586.

(158) Wolfe, M. D.; Lipscomb, J. D. *J. Biol. Chem.* **2003**, *278*, 829-835.

(159) Company, A.; Gomez, L.; Guell, M.; Ribas, X.; Luis, J. M.; Que, L., Jr.; Costas, M. *J. Am. Chem. Soc.* **2007**, *129*, 15766-15767.

(160) Britovsek, G. J. P.; England, J.; White, A. J. P. *Inorg. Chem* **2005**, *44*, 8125-8134.

(161) Britovsek, G. J. P.; England, J.; White, A. J. P. *Dalton Trans.* **2006**, 1399-1408.

(162) Britovsek, G. J. P.; England, J.; Spitzmesser, S. K.; White, A. J. P.; Williams, D. J. *Dalton Trans.* **2005**, 945-955.

(163) Mas-Ballesté, R.; Costas, M.; Berg, T. v. d.; Que, L. J. *Chem.--Eur. J.* **2006**, *12*, 7489-7500.

(164) Company, A.; Feng, Y.; Güell, M.; Ribas, X.; Luis, J. M.; Que, L., Jr.; Costas, M. *Chem.--Eur. J.* **2009**, *15*, 3359-3362.

(165) Bruijnincx, P. C. A.; Buurmans, I. L. C.; Gosiewska, S.; Moelands, M. A. H.; Lutz, M.; Spek, A. L.; Koten, G. v.; Klein Gebbink, R. J. M. *Chem.--Eur. J.* **2008**, *14*, 1228-1237.

(166) Alonso, D. A.; Nájera, C.; Pastor, I. M.; Yus, M. *Chem.--Eur. J.* **2010**, *16*, 5274-5284.

(167) Mas-Ballesté, R.; Fujita, M.; Hemmila, C.; Que, L., Jr. *J. Mol. Catal. A: Chem.* **2006**, *251*, 49-53.

(168) Quiñonero, D.; Morokuma, K.; Musaev, D. G.; Mas-Balleste, R.; Que, L., Jr. *J. Am. Chem. Soc.* **2005**, *127*, 6548-6549.

(169) Mas-Ballesté, R.; Fujita, M.; Que, L., Jr. *Dalton Trans.* **2008**, 1828-1830.

(170) Rittle, J.; Green, M. T. *Science* **2010**, *330*, 933-937.

(171) Gumiero, A.; Metcalfe, C. L.; Pearson, A. R.; Raven, E. L.; Moody, P. C. E. *J. Biol. Chem.* **2011**, *286*, 1260-1268.

(172) *Cytochrome P-450. Structure, Mechanism and Biochemistry*; 3rd ed.; Ortiz de Montellano, P. R., Ed.; Kluwer Academic/Plenum Publishers: New York, 2005.

(173) Meunier, B.; de Visser, S. P.; Shaik, S. *Chem. Rev.* **2004**, *104*, 3947-3980.

(174) Dawson, J. H. *Science* **1988**, *240*, 433-439.

(175) Dunford, H. B.; Hewson, W. D.; Steiner, H. *Can. J. Chem.* **1978**, *56*, 2844–2852.

(176) Makris, T. M.; Koenig, K. v.; Schlichting, I.; Sligar, S. G. *J. Inorg. Biochem.* **2006**, *100*, 507-518.

(177) Ozaki, S.-i.; Roach, M. P.; Matsui, T.; Watanabe, Y. *Acc. Chem. Res.* **2001**, *34*, 818-825.

(178) Hessenauer-Ilicheva, N.; Franke, A.; Meyer, D.; Woggon, W.-D.; van Eldik, R. *Chem.--Eur. J.* **2009**, *15*, 2941-2959.

(179) Groves, J. T.; Haushalter, R. C.; Nakamura, M.; Nemo, T. E.; Evans, B. J. *J. Am. Chem. Soc.* **1981**, *103*, 2884-2886.

(180) Fujii, H. *Coord. Chem. Rev.* **2002**, *226*, 51-60.

(181) Kang, M.-J.; Song, W. J.; Han, A.-R.; Choi, Y. S.; Jang, H. G.; Nam, W. *J. Org. Chem.* **2007**, *72*, 6301-6304.

(182) Neumann, C. S.; Walsh, C. T.; Kay, R. R. *Proc. Natl. Acad. Sci. U.S.A.* **2010**, *107*, 5798-5803.

(183) Higuchi, T.; Shimada, K.; Maruyama, N.; Hirobe, M. *J. Am. Chem. Soc.* **1993**, *115*, 7551-7552.

(184) Liu, S. Y.; Soper, J. D.; Yang, J. Y.; Rybak-Akimova, E. V.; Nocera, D. G. *Inorg. Chem.* **2006**, *45*, 7572-7574.

(185) Soper, J. D.; Kryatov, S. V.; Rybak-Akimova, E. V.; Nocera, D. G. *J. Am. Chem. Soc.* **2007**, *129*, 5069-5075.

(186) Roelfes, G.; Lubben, M.; Chen, K.; Ho, R. Y. N.; Meetsma, A.; Genseberger, S.; Hermant, R. M.; Hage, R.; Mandal, S. K.; Young, V. G., Jr.; Zang, Y.; Kooijman, H.; Spek, A. L.; Que, L., Jr.; Feringa, B. L. *Inorg. Chem.* **1999**, *38*, 1929-1936.

(187) Lubben, M.; Meetsma, A.; Wilkinson, E. C.; Feringa, B.; Que, L., Jr. *Angew. Chem., Int. Ed.* **1995**, *34*, 1512-1514.

(188) Yamaguchi, K.; Watanabe, Y.; Morishima, I. *J. Am. Chem. Soc.* **1993**, *115*, 4058-4065.

(189) Jin, N.; Lahaye, D. E.; Groves, J. T. *Inorg. Chem.* **2010**, *49*, 11516-11524.

(190) Das, P.; Que, L., Jr. *Inorg. Chem.* **2010**, *49*, 9479-9485.

(191) Carrano, C. L. C., M. W.; Sharma, K.; Backes, G.; Sanders-Loehr, J. *Inorg. chem.* **1990**, *29*, 1865-1870.

(192) Shongwe, M. S.; Al-Rashdi, B. A.; Adams, H.; Morris, M. J.; Mikuriya, M.; Hearne, G. R. *Inorg. Chem.* **2007**, *46*, 9558-9568.

(193) Norman, R. E.; Yan, S.; Que, L., Jr.; Sanders-Loehr, J.; Backes, G.; Ling, J.; Zhang, J. H.; O'Connor, C. J. *J. Am. Chem. Soc.* **1990**, *112*, 1554-1562.

(194) Bautz, J.; Bukowski, M. R.; Kerscher, M.; Stubna, A.; Comba, P.; Lienke, A.; Münck, E.; Que, L., Jr., *Angew. Chem., Int. Ed.* **2006**, *45*, 5681–5684.

(195) Li, F.; England, J.; Que, L. *J. Am. Chem. Soc.* **2010**, *132*, 2134-2135.

(196) Li, F.; Meier, K. K.; Cranswick, M. A.; Chakrabarti, M.; Van Heuvelen, K. M.; Münck, E.; Que, L., Jr. *J. Am. Chem. Soc.* **2011**, *133*, 7256-7259.

(197) Kaizer, J.; Costas, M.; Que, L., Jr. *Angew. Chem., Int. Ed.* **2003**, *42*, 3671-3673.

(198) Balch, A. L. *Inorg. Chim. Acta* **1992**, *198-200*, 297-307.

(199) Traylor, T. g.; Xu, F. *J. Am. Chem. Soc.* **1990**, *112*, 178-186.

(200) Lyakin, O. Y.; Bryliakov, K. P.; Talsi, E. P. *Inorg. Chem.* **2011**, *50*, 5526-5538.

(201) Tinberg, C. E.; Lippard, S. J. *Biochemistry* **2010**, *49*, 7902-7912.

(202) *Peroxidases in Chemistry and Biology*; Everse, J.; Everse, K. E.; Grisham, M. B., Eds.; CRC Press: Boca Raton, 1991.

(203) *Cytochrome P-450. Structure, Mechanism and Biochemistry*; 2nd ed.; Ortiz de Montellano, P. R., Ed.; Plenum Press: New York, 1995.

(204) Isaac, I. S.; Dawson, J. H. *Essays Biochem.* **1999**, *34*, 51–69.

(205) Beyer, W. F. J.; Fridovich, I. *Basic Life Sci.* **1988**, *49*, 651-661.

(206) Jouve, H. M.; Andreoletti, P.; Gouet, P.; Hajdu, J.; Gagnon, J. *Biochimie* **1997**, *79*, 667-671.

(207) Park, S.-Y.; Shimizu, H.; Adachi, S.-i.; Nakagawa, A.; Tanaka, I.; Nakahara, K.; Shoun, H.; Obayashi, E.; Nakamura, H.; lizuka, T.; Shiro, Y. *Nat. Struct. Mol. Biol.* **1997**, *4*, 827-832.

(208) Nakahara, K.; Tanimoto, T.; Hatano, K.; Usuda, K.; Shoun, H. *J. Biol. Chem.* **1993**, *268*, 8350-8355.

(209) Griffith, O. W.; Stuehr, D. J. *Annu. Rev. Physiol* **1995**, *57*, 707-734.

(210) Deisseroth, A.; Dounce, A. L. *Physiol. Rev.* **1970**, *50*, 319-375.

(211) Shoun, H.; Tanimoto, T. *J. Biol. Chem.* **1991**, *266*, 11078-11082.

(212) Yoshioka, S.; Takahashi, S.; Ishimori, K.; Morishima, I. *J. Inorg. Biochem.* **2000**, *81*, 141-151.

(213) Poulos, T. L.; Kraut, J. *J. Biol. Chem.* **1980**, *255*, 8199-8205.

(214) Newmyer, S. L.; de Montellano, P. R. O. *J. Biol. Chem.* **1995**, *270*, 19430-19438.

(215) Sundaramoorthy, M.; Terner, J.; Poulos, T. L. *Structure* **1995**, *3*, 1367-1378.

(216) Tanaka, M.; Ishimori, K.; Mukai, M.; Kitagawa, T.; Morishima, I. *Biochemistry* **1997**, *36*, 9889-9898.

(217) Namuswe, F.; Kasper, G. D.; Sarjeant, A. A. N.; Hayashi, T.; Krest, C. M.; Green, M. T.; Moënne-Loccoz, P.; Goldberg, D. P. *J. Am. Chem. Soc.* **2008**, *130*, 14189-14200.

(218) Stasser, J.; Namuswe, F.; Kasper, G. D.; Jiang, Y.; Krest, C. M.; Green, M. T.; Penner-Hahn, J.; Goldberg, D. P. *Inorg. Chem.* **2010**, *49*, 9178-9190.

(219) Toftlund, H.; Pedersen, E.; Yde-Andersen, S. *Acta Chem. Scand. A* **1984**, *38*, 693-697.

(220) Xue, G.; Wang, D.; De Hont, R.; Fiedler, A. T.; Shan, X.; Münck, E.; Que, L., Jr. *Proc. Natl. Acad. Sci. U.S.A.* **2007**, *104*, 20713-20718.

(221) Yamaguchi, M.; Kousaka, H.; Izawa, S.; Ichii, Y.; Kumano, T.; Masui, D.; Yamagishi, T. *Inorg. Chem.* **2006**, *45*, 8342-8354.

(222) Tyeklár, Z.; Jacobson, R. R.; Wei, N.; Murthy, N. N.; Zubieta, J.; Karlin, K. D. *J. Am. Chem. Soc.* **1993**, *115*, 2677-2689.

(223) Lehnert, N.; Ho, R. Y. N.; Que, L., Jr.; Solomon, E. I. *J. Am. Chem. Soc.* **2001**, *123*, 8271-8290.

(224) de Boer, J. W.; Brinksma, J.; Browne, W. R.; Meetsma, A.; Alsters, P. L.; Hage, R.; Feringa, B. L. *J. Am. Chem. Soc.* **2005**, *127*, 7990-7991.

(225) de Boer, J. W.; Browne, W. R.; Brinksma, J.; Alsters, P. L.; Hage, R.; Feringa, B. L. *Inorg. Chem.* **2007**, *46*, 6353-6372.

(226) Chen, M. S.; White, M. C. *Science* **2010**, *327*, 566-571.

(227) Taktak, S.; Kryatov, S. V.; Haas, T. E.; Rybak-Akimova, E. V. *J. Mol. Catal. A: Chem.* **2006**, *259*, 24-34.

Appendix

Publications and Presentations

Publications

- **Parthapratim Das**, Lawrence Que Jr. "Iron Catalyzed Competitive Olefin Oxidation and *ipso*-Hydroxylation of Arenes. Further Evidence for a Fe^{V}=O Oxidant" – *Inorg. Chem.* **2010**, *49*, 9479–9485

- Olga V. Makhlynets, **Parthapratim Das**, Sonia Taktak, Margaret Flook, Rubén Mas-ballesté, Elena V. Rybak-Akimova, Lawrence Que Jr. "Iron-Promoted *ortho*- and/or *ipso*-Hydroxylation of Benzoic Acids with H_2O_2" *Chem.--Eur. J.* **2009**, *15*, 13171-13180

Presentations

- **Parthapratim Das**, Lawrence Que Jr. "Electronic "push effect" in the cleavage of the O–O bond of the nonheme Fe(III)-OOH intermediate in Fe(TPA)-catalyzed oxidations", presented at 241st ACS National Meeting, Anaheim, CA, March 27-31, 2011. (Oral)

- **Parthapratim Das**, Olga V. Makhlynets, Elena V. Rybak-Akimova, Lawrence Que Jr. "Regioselective *ortho*- and *ipso*-Hydroxylation of Benzoates by Non-heme Iron Complexes", presented at 239th ACS National Meeting, San Francisco, CA, March 21-25, 2010. (Oral)

- **Parthapratim Das**, Lawrence Que Jr. "Differentiating between Homo- and Heterolytic O–O Bond Cleavage in a Non-Heme Iron Center", presented 239th ACS National Meeting, San Francisco, CA, March 21-25, 2010. (Poster, Sci-Mix)

- **Parthapratim Das**, Olga Makhlynets, Elena Rybak-Akimova, Lawrence Que Jr. "Substituent effect in directing *ortho* and *ipso* hydroxylation of benzoates by non-heme iron complexes", presented at the NIH Chemistry-Biology Interface Training Grant Symposium, University of Minnesota St. Paul, MN, May 28, 2008. (Poster)

- **Parthapratim Das**, Lawrence Que Jr. "*ortho*-Hydroxylation of Benzoates by Model Non-heme Iron Complexes", presented at 235th ACS National Meeting, New Orleans, LA, April 6-10, 2008. (Poster)